RAINFALL INDUCED DISTRESS IN LOW VOLUME PAVEMENTS

by

MAHSA HEDAYATI

Presented to the Faculty of the Graduate School of

The University of Texas at Arlington in Partial Fulfillment

of the Requirements

for the Degree of

DOCTOR OF PHILOSOPHY

THE UNIVERSITY OF TEXAS AT ARLINGTON

August 2014

Acknowledgements

I'd like to express my appreciation to my adviser, Dr. Sahadat Hossain, for his invaluable supervision, support and confidence. This dissertation would not have been possible without time and care that Dr. Hossain provided. I'd also like to acknowledge the help and thoughts of Dr. Romansochi, Dr. Yu and Dr. Adnan, who helped me with their constructive comments and guidance. For their cooperation, I'd like to extend my appreciation to my colleagues and friends who helped me during all stages of the research.

I'd also like to thank the Texas Department of Transportation for providing the required funding for this research. The appreciation especially goes to Abbas Mehdibeigi, Boon Thian and Al Aramoon from TxDOT Dallas district, for their involvement and impact during all stages of this process.

I'm extremely grateful for my supportive family; my dear husband Reza whose considerations and understanding provided the strength I needed the entire time; my parents, who sent their encouragement and love continuously and my brother, who has kept me motivated and revived for many years. I am also in debt and grateful for all other family members whose contribution is much to share whiles their absence is too hard to fill. Finally, I wish to thank the almighty lord, for his continuous blessing and inspiration.

25th June 2014

Abstract

REAL TIME VOLUME CHANGE INDUCED DISTRESS

IN LOW-VOLUME PAVEMENTS

Mahsa Hedayati, PhD

University of Texas at Arlington

Supervising Professor: Dr. Sahadat Hossain

Annual expenses of distresses caused by volume change of expansive soils induce significant financial burden on maintenance authorities. The problems occur as the expansive soils within the unsaturated zone of the soil experience variation in moisture content. Swelling and shrinkage of the soils causes structural cracks, malfunction of piping and irrigation systems and loss of support for ground slabs. Due to their low stiffness, light loading and extensive construction, pavements are particularly vulnerable to the effects of expansive soils. Accurate understanding of behavior of expansive subgrade, interaction of subgrade pavement structure and incorporation of the results in design processes can improve the pavement service life significantly.

The objective of this research was to; 1) study the behavior of expansive soils and their constitutive performance; 2) determine the real time pattern of subgrade moisture and temperature variation in the entire depth of active zone; 3) determine the pattern of real time pavement deformation in response to the site's moisture balance; 4) provide a comprehensive data analysis on the collected data; 5) determine the vertical deformation of the site using soil's constitutive relations; 6) model the real time moisture variation and volume change of the expansive soil; 7) determine the interaction of subgrade volume change and hot mix asphalt pavement distress; 8) determine the

possible service life of the pavement under normal loading and mix design and 9) provide conclusions and recommendations for future study.

A selected farm to market pavement site was selected for monitoring and field instrumentation and investigated through resistivity imaging and in-situ modulus measurement. Samples were collected and tested in the laboratory to determine the soil's properties. The site was instrumented with moisture/temperature sensors, rain gauge and inclinometers casings. The monitoring activities included regular data acquisition, horizontal profiling and topographical surveying. A comparison was drawn between the observed field volume change, current Texas Department of Transportation (TxDOT) method and soil's constitutive relations. The collected data were later analyzed to determine the possible trend of moisture and temperature variation and pavement deformation. Finite element was used to model transient moisture variation and volumetric deformation of the soil. In addition, the direct effect of volume change on pavement distress development was studied under three different surface temperatures.

Results indicated that the in-situ soil is classified as CH and possesses high swelling potential. Both moisture variations extend to 4.5m depth, which exceed the current estimations of active zone. Trend of moisture variation was best described as a combination of seasonal and temporary variation. The seasonal trend consisted of sinusoidal fluctuation as a function of site's moisture balance, while the temporary increase happened in response to rainfall and dissipated rapidly. The temperature was recorded as a first degree Fourier series at all depths. Although the average temperature was roughly constant, the domain of temperature variation and lag time varied with soil depth. The pavement deformation was a mixed function of seasonal variation and excessive swelling and shrinkage in response to the available moisture infiltration. Comparing the observed variation with predictive methods, it was determined the current

TxDOT method provides inaccurate measurements and can be considered effective only for under special conditions. However, estimation of swell and shrink of the soil can be acceptably done through soil constitutive modeling. The transient analysis of site's moisture and deformation analysis indicated that excessive deformation occur in the site that may not be captured by surveying, mainly because surveying is a discrete data acquisition method which misses data records between survey intervals. Excessive movement can accelerate pavement deterioration, which was confirmed with direct analysis of coupled swell/distress analysis. Provided the stress strain behavior of asphalt and volumetric deformation of the subgrade soil, it was determined that the initial cracks are most possible to occur within two years of pavement construction. Increase of asphalt stiffness did not improve pavement's lifetime; therefore, controlling the subgrade swelling potential may be more effective in pavement distress prevention.

Table of Contents

List of Figures

List of Tables

Chapter 1

Introduction

1.1. Introduction

Expansive soils cover more than 25% of the total area of the United States. Major deposits of these soils are distributed in the states of Colorado, California, Nevada, Arizona and Texas (Buhler and Cerato, 2007). Stability and performance of the structures constructed on expansive soils are affected as the soil experiences volumetric deformation. The impacts may include construction damages to residential buildings, cracks in the structures, malfunction of piping and irrigation systems and loss of support for ground slabs. Annual financial losses are estimated to be $15 billion, which is higher than all other natural disasters combined (Jones and Jefferson, 2012).

Expansive subgrade soils can induce major deterioration on pavements including surficial distresses, edge cracks, shoulder drop-offs and shrinkage cracks. In Texas, 25% of the annual expenditures of the Texas Department of Transportation (TxDOT) are assigned to maintenance and repair of damaged pavements (Sebesta, 2002). The destructions are more visible in low volume hot mix asphalt pavements, which comprise a significant portion of Texas transportation system. These roads have light loading and traffic (<0.01 ESALs); therefore, premature failure usually occurs as a result of environmental factors (Wanyan et al., 2010). Post construction damages can be significantly reduced if this issue is addressed during the design stage. Therefore, an accurate understanding of soil behavior and the potential effect on pavement performance is necessary.

Behavior of expansive soils is mostly governed by the moisture balance of the system. Current methods suggest rough estimations of moisture content in the subgrade, such as equilibrium moisture content and seasonal variation (Zheng and Zhang, 2013;

Zapata and Houston, 2008; Wang et al., 2014). Even so, results of several in-situ studies suggest sensitivity of moisture content to environmental factors especially infiltration and evaporation (Nguyen et al., 2010; Manosuthikij, 2008; Wolfe et al., 2010).

Methods of evaluating total volumetric deformation of expansive soils are grouped into three categories: oedometer tests, suction- based methods and empirical relations. Oedometer tests use the consolidation theory in reverse and measure the maximum swelling under a constant seating pressure, as the soil absorbs moisture freely (ASTM, 2008). Different oedometer techniques have been studied, including constant pressure, constant volume and 3D swelling methods (Rao et al., 1988; Fredlund et al., 2012; Puppala et al., 2014). However, this method is considered sensitive to disturbance and conservative (Lytton et al., 2005; Houston et al., 2011; Nelson and Miller, 1992; Fityus et al., 2005). Suction-based methods use the theory of unsaturated soil mechanics to explain volume changes in expansive soil. Although an increasing number of researchers use suction-based methods as part of their approach (Ng et al., 2000; Puppala, et al., 2006), suction measurements are subject to errors that can be substantial. In addition, their complexity and unavailability has been a disadvantage among practicing engineers (Zapata et al., 2000).

Empirical approaches express a relationship between field measurements and laboratory-determined soil parameters (i.e. LL and PI) and are common for estimating possible volumetric deformations (Houston, et al., 2011; Osman and Sharief, 1987). The reliability of these methods increase with better estimations of moisture variations, swell properties of soil and suction variation profile of the soil. Based on a research performed by McDowell (1956), TxDOT recommends using an empirical approach, Potential Vertical Rise –PVR, for considering heave problems in pavement design. The method is

conservative and the assumptions made as part of it may result in significant errors (Lytton et al., 2005).

Recently, numerical approaches have been introduced and developed to provide additional information on volumetric deformation and unsaturated soil behavior. Limited literature is available on numerical modeling of volumetric deformation. Abed (2007) conducted a 2D analysis of swelling and shrinkage of an expansive soil in Sudan using Barcelona Basic model in PLAXISFLOW-PLAXIS environment. The author concluded that FE modeling can be used to replicate field measurements and estimate future field performance. Puppala et al (2014) ran a static 3D analysis using Abaqus to evaluate the in-situ swelling of an expansive subgrade soil. Both authors studied the static infiltration while effects of cyclic wetting and drying (due to real time rainfall and evaporation) are yet to be studied. The accuracy of numerical approaches will increase if they are combined with long term in-situ monitoring.

1.2. Problem Statement

Volumetric deformation of unsaturated expansive subgrade is governed by moisture variation. Based on existing literature, current assumptions for pavement design such as equilibrium moisture content and seasonal moisture variations may lead into inaccurate design. In addition, current methods do not reflect actual moisture balance of the subgrade. Pavement design procedure serviceability can be enhanced through further study of exact moisture variations in subgrade soils using in-situ installation and monitoring.

Interaction of the transient moisture variation can be reflected in repetitive volume changes of expansive soil, which in turn will affect the stability and deterioration of pavement. Thorough study of this process will provide deep insights and provide

engineers with better understanding of climatic-structural interaction of the pavement system.

Due to the sophisticated nature of coupled stress/pore pressure behavior of unsaturated soil, swelling/shrinkage of the soil has not been numerically analyzed. Abaqus finite elements (FE) software has the strong capability of performing such analysis in transient mode and providing graphical output that will benefit future researchers. FE analysis can also be effectively used to observe the effect of volume change in strain development in pavement structure and determine zones of stress concentration that will be most likely to fail. Results of FE parametric study could be used as a design guide for practicing engineers. However, currently no such guide is available.

1.3. Research Objectives

The objectives of the current research are to study and analyze real time moisture variation and pavement volumetric deformation and their contributions to pavement performance. The objectives can be listed as below.

a. Determine the zone of moisture variation for low volume rural pavement systems
b. Determine the pattern of moisture and temperature variation in expansive subgrade soils
c. Determine the long term effects of climatic variations on performance of pavement
d. Provide design guides based on results of numerical modeling and in-situ monitoring
e. Provide recommendations for future studies

To address the mentioned tasks, a field instrumentation program was developed. A 2-lane, low volume asphalt concrete pavement site constructed on expansive subgrade

soils was considered for in-situ monitoring. An experimental program was developed to study the properties of soil and obtain more information on the soil characteristics. Temperature and moisture sensors were installed and monitored to determine the in-situ moisture/temperature variation. Vertical movement of the pavement was also surveyed. Results from laboratory testing and field instrumentation were combined with numerical modeling to study the coupled effect of stress-pore water and to model the effect of rainfall on long term performance of pavement. The specific tasks to achieve the mentioned goals are:

1. Site investigation and sample collection from the case study site
2. Determination of basic soil properties
3. Determination of zone of moisture variation and capture in-situ data through extensive in-situ instrumentation and monitoring
4. Study the infiltration/exfiltration behavior of rainfall/evaporation into the pavement system
5. Parametric study of pavement performance through a detailed numerical analysis in Abaqus environment
6. Determine the swelling threshold of the asphalt concrete pavement and provide remedial suggestions for future study.

1.4. Thesis Organization

This dissertation is divided into eight chapters as summarized below:

Chapter 1 provides general insights and information about the topic. Problem statement, research objectives and thesis organization are also addressed.

Chapter 2 presents a complete literature review of the subject. Current methods of addressing moisture infiltration into the unsaturated subgrade soils are discussed and fundamental concepts of swelling of expansive soils are covered. Current design

methods to consider this problem in pavement design procedures are reviewed, as is a summary of current research on field instrumentation. In addition, a brief description of fracture mechanics and possible damages caused to asphalt concrete due to swelling and shrinkage of expansive subgrade is presented.

Chapter 3 describes, in detail, the tasks performed during this research. Site investigation, sample collection and field instrumentation are explained. Laboratory testing and geophysical investigation using resistivity imaging were performed to obtain more information on subsurface conditions. The periodic monitoring schedule of the instrumented site is explained. Volumetric deformation parameters of the soil were extracted from the samples and modeled in finite element environment. In addition, the steps of a developed numerical study are explained to analyze the real time deformation and damage development of pavement due to climatic conditions. Calibration process is explained and a comparison is drawn between the field recordings and numerical modeling. Based on the results of systematic numerical modeling, steps taken towards developing an accurate design guide are explained.

Chapter 4 presents the results of field instrumentation followed by discussion and comparison with existing literature. This chapter also encloses the design guide developed based on the results of the systematic numerical modeling. The design guide considers several coupled nonlinear material behavior to describe the coupled analysis of stress/pore water pressure and deformation of the soil as a result of moisture infiltration. Later, the computed volumetric strain is compared against failure criteria in fracture mechanics to estimate the acceptable service life of the pavement. The design guide is shown in charts for ease of use.

Chapter 5 summarizes the conclusions of this research and provides recommendations for future studies.

Chapter 2

Literature Review

2.1. Expansive Soils

Expansive soils are widely found in semi-arid and arid regions of the world and cover approximately 25% of the area of the United States. Engineering properties of these soils are highly sensitive to changes of water content in the active zone. Volumetric deformation of expansive soils damages ground-bearing structures such as foundation slabs, bridges, residential homes, pipelines and roadways. In the US, financial losses caused by expansive soil are estimated to be more than 15 billion dollars annually (Table 2. 1), higher than all other natural disasters combined (Jones and Jefferson, 2012). Due to their low stiffness, light loading and extended presence over the country, pavements are particularly vulnerable to damage. Continuous destruction caused by expansive subgrade soils increases the pavement's roughness and reduces its serviceability gradually. Therefore, understanding the causes of pavement distress and the behavior of expansive subgrades are critical in acceptable pavement performance and design (Sebesta, 2002).

Table 2. 1: Global-wide damages of expansive soils (Adem and Vanapalli, 2013)

Region	Damage/year	Reference
USA	$15 Billion	Jones and Jefferson (2012)
UK	£ 400 million	Driscoll and Crilly (2000)
France	€ 3.3 billion	Johnson (1973)
Saudi Arabia	$ 300 million	Ruwaih (1987)
China	¥ 100 million	Ng et al (2003)
Australia	$ 150 million	Osman et al (2005)

2.1.1. Swelling Mechanism

Swelling capability is mostly observed in clays from smectite family, including vermiculite and montmorillonite (Young, 2012). Factors controlling the pattern and extent of volumetric deformation include the type of clay mineral, overburden and confining pressure, initial moisture content, initial dry density and most importantly, presence of free water content (Chen, 2012). Although all factors contribute to volumetric deformation, water content is considered to be the most critical.

In micro scale, swelling occurs as water molecules infiltrate between clay sheets and interact with the clay mineral surface via hydrogen bonding. As illustrated in Figure 2. 1 hydration increases interlayer distance and causes swelling in macro scale (Hensen and Smit, 2002). On the other hand, exfiltration of water molecules from the matrix brings clay sheets closer and results in overall shrinkage of the soil. Possible sources of water dynamics include precipitation, thawing, irrigation, pumping, load application and evapotranspiration. Reaching full saturation from a relatively dry state can cause swelling up to 20%.

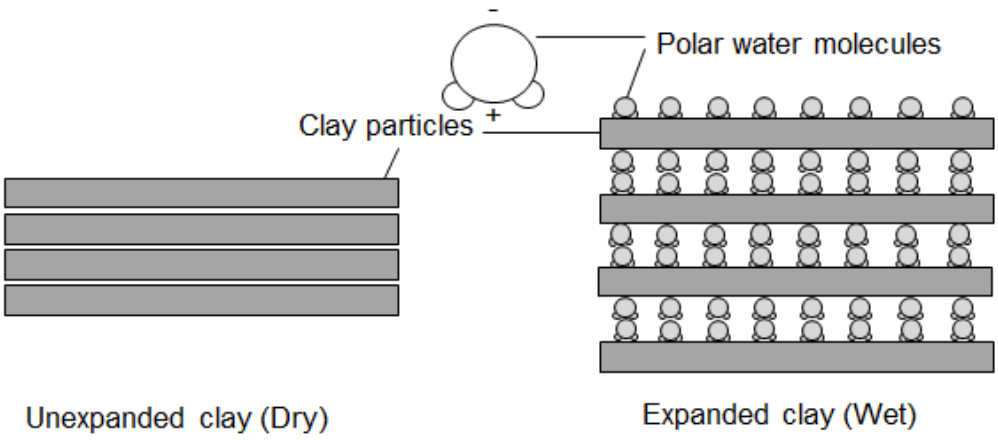

Figure 2. 1: Infiltration of water molecules between clay sheets (Hensen and Smit, 2002)

2.1.2. Pavements and Expansive Subgrade

In a survey research, Wanyan et al (2010) reported that 18 out of 52 Texas Department of Transportation (TxDOT) districts routinely face expansive soil problems. Continuous maintenance of pavement distresses accounts for approximately 25% of TxDOT construction and maintenance budget. Although the roadway surface is regularly treated, destructive expansive subgrade is rarely addressed as the source of distresses. Therefore, roughness reoccurs within a short timeframe of 6 months and 2 years after patching.

It is suggested that flexible pavements, including farm to market (FM) roads, perform better than rigid pavements due to their flexibility and displacement tolerance (Dafalla and Shamrani, 2012). AASHTO (2002) classifies FM roads as low-volume pavements which are lightly loaded and have an average daily traffic (ADT) of less than 400 vehicles. Although FM roads are flexible, low structural elastici modulus can intensify destructions of expansive subgrade. Regular pavement and slab distresses are caused from two sources, as shown in Figure 2. 2 (Fredlund, et al., 2006):

1. Differential movement between edge and center of the slabs: Since the soil outside the slab is more exposed, moisture variation amplifies with distance from the center. Slabs will distort into either a center lift (long term) or an edge lift (seasonal) mode. Center lift (edge drop) occurs when soil beneath the slab gains excessive moisture as a result of capillary action. Conversely, edge lift happens as the perimeter soil becomes wetter than the soil beneath the slab. The differential movement increases stress concentration inside the structure and initiates the crack, which propagates with time and load repetitions.
2. Loss of support: As the soil shrinks, the slab's edge might separate from the supporting soil. The amount of slab support provided by the foundation soil is defined as

the support index “C”, which itself is related to the climatic rating and plasticity index of the soil. Generally, the higher the climate index, the more stable the moisture balance is. Separation of the slab increases stress concentration in the slab and causes the slab to develop top down cracking, as frequently observed by area engineers (Luo, 2007).

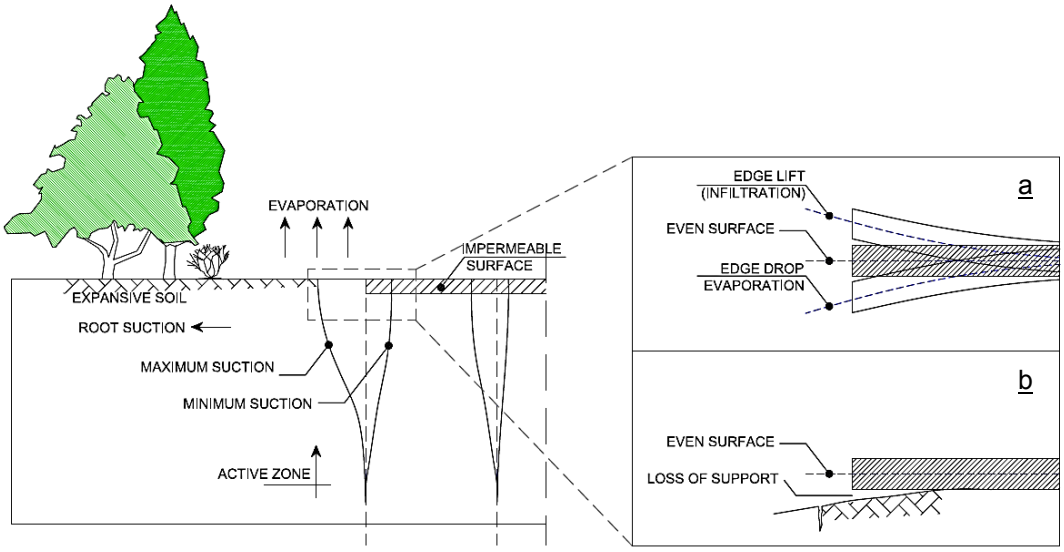

Figure 2. 2: Suction/moisture content variation under pavement and possible damages: a. excessive movement, b. loss of support

Combination of the mentioned phenomenon causes pavement surficial distresses such as edge cracks/drop off, longitudinal or transverse cracking, reflection cracking and upheaval or swelling, which are frequently observed and reported by area engineers (Oh, et al., 2012; Buhler and Cerato, 2007). The distresses and common causes are:

2.1.2.1. Edge Drop-offs

Pavement longitudinal edge cracks happen within 0.3 to 0.6 m of the outer edge of the pavement (Figure 2. 3) due to excessive differential movement, lack of lateral (shoulder) support, base weakness frost action, inadequate drainage, groundwater and soil

moisture variation in soils (Hearn, et al., 2008) and weak cohesive soils (Heath et al., 1990). Excessive moisture variation under the pavement shoulder and considerable swell shrink movement intensify the cracking. Due to tensile strains, cracks are developed in the region where the moisture front advancing reaches its maximum penetration under the pavement (Zornberg and Gupta, 2009).

Figure 2. 3: Edge drop

2.1.2.2. Longitudinal/Transverse Cracking

Longitudinal cracks occur due to differential heave and are a common consequence of expansive subgrade soil (Figure 2. 4). In North Texas, cracking is observed in almost all low volume pavements constructed on expansive soils. Cracking begins as single or multiple longitudinal cracks which progress with time to a pattern resembling alligator cracking. It usually initiates when differential heave is maximum and grows with drying highly plastic subgrade toward the end of dry seasons (Zornberg and Gupta, 2009; Sebesta, 2002)

Transverse cracks occur across the pavement centerline or laydown direction (Figure 2. 4) and are caused as a result of asphalt hardening and/or thermal contraction of the surfacing layer. Swelling subgrade is usually associated with deterioration of existing cracks and occurrence of secondary ones under traffic action.

Figure 2. 4: Longitudinal (left) and transverse (right) cracking

2.1.2.3. Reflection Cracking

Reflection cracking in a flexible overlay is usually the result of propagation over existing cracks/joint due to differential movement across the layers (Figure 2. 5). Cracking in the highly plastic subgrade reflects through the pavement structure, creating an inlet for water into the pavement. Reflection cracking is generally not load initiated; however loading can speed up the deterioration process (AASHTO 2004).

Figure 2. 5: Reflection cracking

2.1.2.4. Upheaving/ Waves in Profile

This phenomenon occurs as the expansion properties of the subgrade soil vary along the road profile (Figure 2. 6). Dynamic loads circulating on distorted pavements can contribute to deterioration of the surface profile and increase of roughness. The

distress is described as pavement roughness and is computed as a function of vertical differences between an ideal surface profile and the actual surface profile. Typical roughness indices are satisfaction measures of users traveling on the road.

Figure 2. 6: Uneven profile

2.1.3. Treatment of Swelling Soil

When expansive soils are encountered along a project in environments and areas where significant moisture fluctuations in the subgrade are expected, consideration should be given to the following alternatives to minimize future volume change potential of the expansive soil (MEPDG, 2004):

- Soil removal and replacement: If the expansive layer is relatively thin, removal and replacement is economically justified.
- Moisture control: Increasing the width of pavement with shoulder (MEPDG, 2004), underseal (Estakhri and Ramakrishnan, 2006) and moisture barriers (Jayatilaka, 1999) can be used to decrease moisture variation under the main driving lane and reduce possible subgrade volume change.
- Scarification and prewetting: Water is injected into the upper portion of the expansive clay subgrade to nearly eliminate subgrade swell potential. The combined effect of moistened subgrade and moisture barriers can be very successful (Petry and Little, 2002).

- Recompaction and strengthening of subgrade and pavement section: Compaction at a moisture content slightly drier than optimum has been successfully used to control subgrade volume change (Petry and Little, 2002). If not sufficient, a stronger design of asphalt mix is suggested.
- Chemical treatment for base and subgrade with lime, cement, fly ash: Several research projects (e.g., Harris, 2008 and Freeman and Little, 2002) have shown that the subgrade condition improves with addition of stabilizers. Scullion et al. (2001) optimized cement content for adequate strength, durability, and economy. Experience has shown 2 to 3 percent Type I cement can reduce swelling of the soil significantly.

2.2. Swelling Measurement and Theory

Swelling problems caused to infrastructures have attracted wide attention during the last four decades. However, research on roads and pavements is ongoing (Dafalla and Shamrani, 2011). To interpret interactions of swelling clays and pavement performance, a good understanding of swelling mechanism and analysis procedures is crucial. In this part, current procedures of swell measurement and prediction along with theory of volume change are explained.

2.2.1. Measurement and Prediction Methods

Many agencies require swelling of clays to be predicted during design and considered in construction. Overall, prediction methods can be grouped into three categories: Oedometer tests, empirical relations and suction-based methods (Lytton, Aubeny and Bulut, 2005).

2.2.1.1. Oedometer Tests

The oedometer method uses the consolidation theory in reverse and measures the maximum possible swell under a constant seating pressure. An undisturbed sample is placed in the consolidation ring, submerged into water and allowed to swell freely as it

absorbs moisture (ASTM, 2008). The method is inexpensive and easy to follow, but sensitive to disturbance and operator skills. Simplifications have been suggested to facilitate and increase the accuracy of predictions (Fredlund et al., 2012; Rao et al., 1988). The general equation for swell prediction follows the same pattern as consolidation test, as shown in Eq.2.1.

$$\Delta H = C_s \frac{H}{1+e_0} \log\left(\frac{\sigma'_f}{\sigma'_s}\right) \quad \text{(Eq. 2. 1)}$$

Where:

ΔH = Overall vertical movement

C_s = Swelling index

H = Depth of swelling layer

e_0 = Initial void ratio

σ'_f = Final stress state

σ'_s = Swelling pressure

Different researchers have proposed variable interpretations of parameters in Eq.2.1, including Fredlund (1983), Dhowian (1990), Nelson and Miller (1992) and Nelson et al (2006).

2.2.1.2. Empirical Relations

Empirical or semi-empirical methods are based on a correlation between laboratory/field measurements and soil properties including mineralogy, soil water chemistry, standard/cone penetration tests, liquid limit and plasticity index. Environmental conditions such as water conditions (e.g. climate, drainage, vegetation, permeability, temperature) and stress conditions (e.g. history and in-situ conditions, loading and soil profile) can also affect the overall volume change. A summary of existing empirical relations is presented in Table 2. 2.

Table 2. 2: Summary of existing empirical relations

Method	Parameters
McDowell (1956)	Initial molding water content, bulk density, liquid limit and plasticity index
Nayak and Christensen (1970)	$\%Swell = \frac{0.00229{I_p}^{2.67}(1.45c)}{w_i} + 6.38$ SP = swell percent I_p= plasticity index c = clay content w_i= initial moisture content
Weston (1980)	$\%Swell = 0.00411LLw^{4.17}.\sigma_v^{-3.86}.{w_i}^{-2.33}$ LLw = weighted liquid limit
Clayton (1995)	CPT/SPT
Das et al. (2010)	Natural moisture content, dry density, liquid limit, plasticity index, and clay fraction
Berawala and Solanki (2010)	Liquid limit, plasticity Index
Nelson et al. (2010)	Extrapolation of surveying over time
Houston et al. (2011)	Site specific parameters

2.2.1.3. Suction Based Methods

Suction methods are based on unsaturated soil mechanics. Suction (ψ) is defined as negative pore water pressure and is used as a separate stress state variable in addition to effective stress (σ). Volumetric strain (ε_{vol}) is defined as a function of suction, water content and net normal stress (Figure 2. 7).

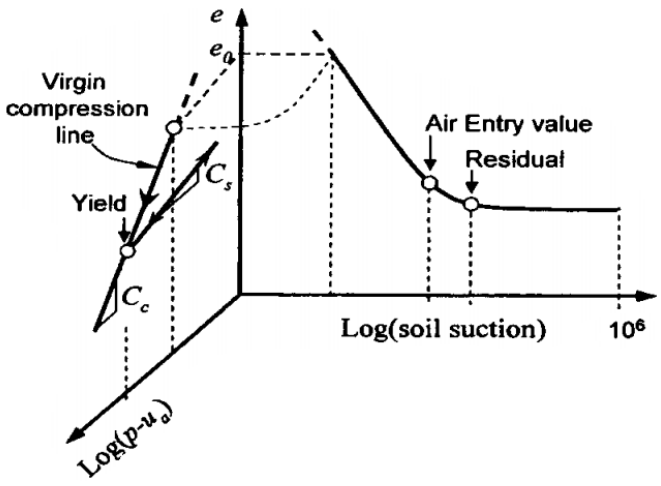

Figure 2. 7: $\boldsymbol{\varepsilon_{vol}}$ as a function of σ and ψ (Fredlund, 2006)

For small increments of volume change on the volume–mean principle stress-suction surface, ε_{vol} is linearly related to log(*σ)* and log(*ψ)*. The overall relation can be written as

$$\varepsilon_{\mathrm{vol}} = \frac{\Delta V}{V_0} = -\gamma_{\mathrm{h}} \log\left(\frac{\psi_{\mathrm{f}}}{\psi_{\mathrm{i}}}\right) - \gamma_{\sigma} \log\left(\frac{\sigma_{\mathrm{f}}}{\sigma_{\mathrm{i}}}\right) - \gamma_{\pi} \log\left(\frac{\pi_{\mathrm{f}}}{\pi_{\mathrm{i}}}\right) \qquad \text{(Eq. 2. 2)}$$

Where:

V_0 = Initial volume

ΔV = Change in volume

γ_{h} = Matric suction compression index

$\psi_{\mathrm{i}}, \psi_{\mathrm{f}}$ = Initial and the final values of matric suction

γ_{σ} = Mean principal stress compression index

$\sigma_{\mathrm{i}}, \sigma_{\mathrm{f}}$ = Initial and the final values of mean principal stress

γ_{π} = Osmotic suction compression index

$\pi_{\mathrm{i}}, \pi_{\mathrm{f}}$ = Initial and the final values of osmotic suction

As the osmothic suction is small, the above equation is usually rewritten as:

$$\varepsilon_{\mathrm{vol}} = \frac{\Delta V}{V_0} = -\gamma_{\mathrm{h}} \log\left(\frac{\psi_{\mathrm{f}}}{\psi_{\mathrm{i}}}\right) - \gamma_{\sigma} \log\left(\frac{\sigma_{\mathrm{f}}}{\sigma_{\mathrm{i}}}\right) \qquad \text{(Eq. 2. 3)}$$

The final heave is estimated by integrating volumetric strain through the active zone. Nelson et al., (2001) define this zone as “the zone of soil that is contributing to heave due to soil expansion at any particular time.” Usually, the depth of active zone varies between 1.5 and 3.2 m (Hossain, 2013):

$$\Delta H = \int_{i=1}^{H} \varepsilon_{\text{vol}} . dz_i \qquad \text{(Eq. 2. 4)}$$

Where:

ΔH = Vertical deformation

H = Depth of active zone

i = Increment number

Researchers have proposed a variety of suction-based methods. Examples can be found in Aitchison (1973), Lytton (1977), Hamberg and Nelson (1984), Fityus and Smith (1998) and Briaud et al. (2003) and Zapata et al. (2009).

2.2.1.4. Current Prediction Method in Texas

Currently, TxDOT recommends method TX-124E: Determination of Potential Vertical Rise, “PVR”, to determine the possible swelling of expansive soils based on a research performed by McDowell (1956). LL, PI, surcharge pressure and initial water content of soil layers are used to estimate potential heave from a family of curves. The initial water content is compared with maximum (0.47LL + 2) and minimum (0.2LL + 9) water contents to evaluate the percent volumetric change. The PVR of the site is equal to the sum of the *PVR* of the layers. If *PVR* of the site exceeds the recommended PVR values (Table 2. 3), subgrade properties should be modified so the criterion is met (TxDOT, 1999).

Table 2. 3: Maximum PVR values recommended by TxDOT (TxDOT, 1999)

Type of highway	Maximum allowed PVR (in)
IH/US	1
SH	1.5
FM	2

2.2.1.5. Evaluation of Current Methods

Selecting the most appropriate and accurate model for volume change prediction is vital in performance evaluation of pavement. A comparison of the existing methods would be helpful for researchers and practicing engineers.

One-dimensional consolidation methods are simple and inexpensive; however, they do not provide swelling with respect to water content or report final swelling at full saturation. Therefore, they may over predict the actual swelling at the field, as the soil usually experiences moisture variations within the unsaturated phase. Also, this method is only applicable when capillary water is available freely to saturate the soil, such as cases with shallow groundwater table which is not frequently observed in the field.

Empirically-based methods are common in geotechnical engineering (Houston, et al., 2011). Yet, the methods are confined to their locale of origin and have to rely on assumed moisture conditions. These limitations apply to both laboratory samples and field measurements. In addition, the relationships may be based on a small data set or use a specific test method at only a small number of sites (Jones and Jefferson, 2012). Uncertainties such as site conditions and variations of the test method would probably lead to considerable errors in correlations.

The PVR method is straight forward, simple to use and has been practiced over 30 years in Texas. Yet, it only provides the potential vertical swell of the soil from the current soil moisture without considering the potential vertical shrink, or the potential

vertical amplitude of movements (Zhang, 2004). Manosuthkij et al (2007) compared the PVR method with outputs of several recommended approaches and field measurements and concluded that the PVR method had the most difference with measured vertical deformation in the field. In addition, assumptions made during the method decrease its reliability. Lytton et al (2005) summarizes these assumptions as below:

Assumption 1: Soil at all depths has access to free capillary water: This hypothesis is only valid in cases where shallow ground water table exists in the field.

Assumption 2: Vertical deformation swelling strain (ε_{ver}) is one-third of the volume change strain (ε_{vol}): the ($\varepsilon_{ver}/\varepsilon_{vol}$) ratio increases as the confining pressure increases. At deep layers ε_{ver} can be as high as ε_{vol} (Lytton, Aubeny and Bulut, 2005).

Assumption 3: Remolded samples accurately represent in-situ soil: This assumption may be inaccurate, as volumetric deformation parameters are sensitive to disturbance.

Assumption 4: PVR equal to 0.5" (1.25cm) would produce unsatisfactory results: The PVR is an index of the maximum possible swelling in the field and cannot determine the serviceability of structure.

Assumption 5: Volume change can be predicted using the plasticity index alone: Volume change is a function of many parameters; using single parameters may reduce the reliability of the method.

Due to general assumptions in previous processes, more attention is drawn toward suction-based techniques. The method is based on strong theoretical background and limiting uncertainties from the following sources (Walsh, et al., 2009) can further improve the outputs:

(1) Determination of the depth of the active zone

(2) Estimation of swell properties of the soil

(3) Evaluation of soil suction profiles

Several potential disadvantages of suction-based methods, including limited range of linear relation between ε_{vol} and log (Ψ), dependence of suction compression index γ_h of multiple parameters and difficulty of measuring suction to use in the swell prediction methods. Yet, acceptable estimations of moisture/suction profile variations in the field along with revision of soil constitutive modeling in the soil can increase the efficiency of the design significantly. Chao et al (2006) developed a method to determine the final suction profile under residential areas based on the assumption of equilibrium moisture content. Lytton et al (2005) used Mitchell's equation to estimate cyclic variation of suction in pavement subgrade soils. Zhang (2010) used tracking of soil moisture content to estimate amplitude of vertical deformation in a site and concluded that "suction-based and water content-based methods have the same theoretical basis and can be interchanged with each other through the soil-water characteristic curve when numerical simulation is performed." However, no method was found to estimate actual variations in the field condition.

2.2.2. Theory of Volume Change for Expansive Soil

Since volume change of expansive soils is affected by both stress and suction, a coupled stress/pore water pressure analysis can provide the most accurate evaluation of soil's deformation. To perform such an analysis, accurate relations between soil water, stress and volume change should be understood and analytical assumptions need to be carefully stated.

It is usually assumed that expansive soils are elastic and have lost much of their structural plasticity due to multiple wetting and drying cycles. In addition, the expansive soil is assumed over consolidated and has experienced maximum pressure in the past while drying. Zhang and Briaud (2010) suggest that the above assumptions are

reasonable, especially in case of pavements and lightly loaded structures where the influence of the superstructure on soil yielding can be neglected. Also, the relations between stress state variables are considered unique which demonstrates that there is only one relationship between the deformation and stress state variables (Chao, 2007).

Coupled solution for unsaturated soils involves two criteria: soil mass equilibrium and the continuity of the pore-water, which is based on the general theory of consolidation for unsaturated soils (Hung et al., 2002).

The basic constitutive relationships can be written in three different forms using elasticity, compressibility or volume-mass parameters. The volume-mass form involves using void ratio, water content and/or degree of saturation (Vanapalli and Lu, 2012). A complete volume-mass characterization can be done by defining two of the variables, usually void ratio and water content, as below (Fredlund et al., 2012):

$$de = a_t d(\sigma_m - u_a) + a_m d(u_a - u_w) \quad \text{Eq. 2. 5}$$

$$dw = b_t d(\sigma_m - u_a) + b_m d(u_a - u_w) \quad \text{Eq. 2. 6}$$

Where

$\sigma_m - u_a$ = Mean net stress

$u_a - u_w$ = Matric suction

a_t = Coefficient of compressibility with respect to net normal stress

a_m = Coefficient of compressibility with respect to matric suction

b_t = Coefficient of moisture variation with respect to net normal stress

b_m = Coefficient of moisture variation with respect to matric suction

Having defined or measured the required parameters, the soil behavior can be explained with a constitutive surface as shown in Figure 2. 8.

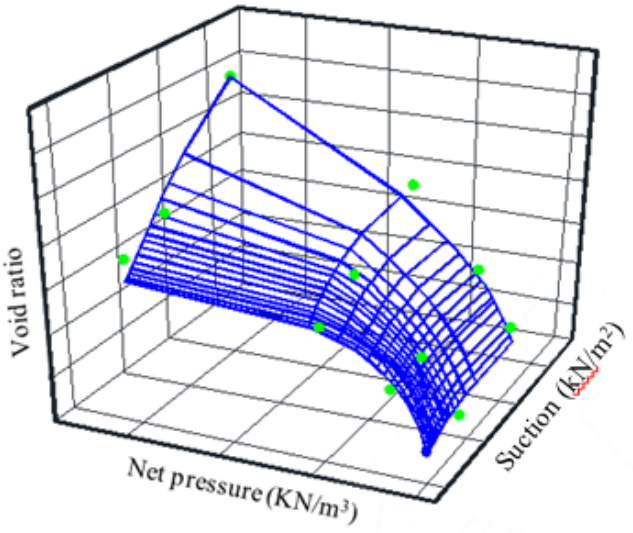

Figure 2. 8: Schematic void ratio constitutive surface

The constitutive surfaces express the soil state variables such as void ratio, water content and degree of saturation as a function of two independent stress state variables, matric suction and mechanical stress. Literature suggests that the constitutive surfaces will be unique if the soil is elastic (Zhang and Briaud, 2003; Zhang and Lytton, 2009). Individual effect of stress state variables on volume change can be evaluated under the six cases shown in Figure 2. 9. Fredlund et al, (2006) suggests analyzing the unsaturated soil using saturated state as a reference or starting point and evaluating the effect of unsaturation on soil behavior, as discussed in the following subsections.

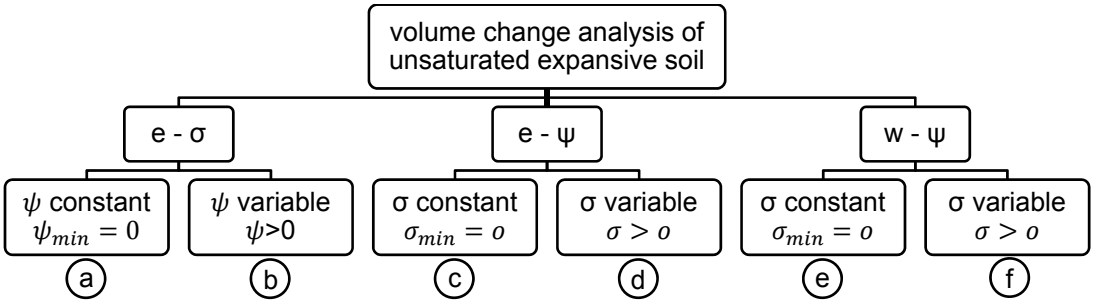

Figure 2. 9: Sequence of unsaturated modeling

2.2.2.1. Volume Change-Stress Relation under Zero or Constant Suction

Stress-deformation analysis under this condition can be explained using original Hooke's law, as:

$$(d\varepsilon_v)_\sigma = \frac{3(1-2\mu)}{E}\frac{[d(\sigma_x-u_a)+d(\sigma_y-u_a)+d(\sigma_z-u_a)]}{3} \quad \text{Eq. 2. 7}$$

Where:

ε_v = Volumetric strain

μ = Poisson ratio

E = Young's modulus of elasticity

σ_i = Normal stress in x, y or z direction

u_a = Pore air pressure

In terms of void ratio, the condition is the same as consolidation and can be measured by loading-unloading curve shown in Figure 2. 10-a. The volumetric deformation can be expressed as:

$$e_\sigma = \begin{cases} e_0 - C_s \log\left(\frac{\sigma}{\sigma_0}\right) & \sigma < \sigma' \\ e_0 - C_s \log\left(\frac{\sigma'}{\sigma_0}\right) - C_c \log\left(\frac{\sigma-\sigma'}{\sigma'}\right) & \sigma \geq \sigma' \end{cases} \quad \text{(Eq. 2. 8)}$$

Where:

e_σ = Void ratio under pressure σ

e_0 = Initial void ratio

C_s = Rebound coefficient

σ_0 = Initial pressure

σ = Pressure at any time

C_c = Compression index

Since expansive soils are assumed over consolidated, the first branch of the equation is usually used.

2.2.2.2. Volume Change-Stress Relation under Variable Suction

Matric suction variations will also cause the volume change-stress of unsaturated soils. Compression of samples under unsaturated conditions (constant suction) is similar to compression under saturated condition (Figure 2. 10-b). However, different normal pressures can affect the inflection point and the rate of volume change due to stress. Literature suggests that presence of suction results in stiffness of the sample. In other words, the yield stress of soil increases with suction.

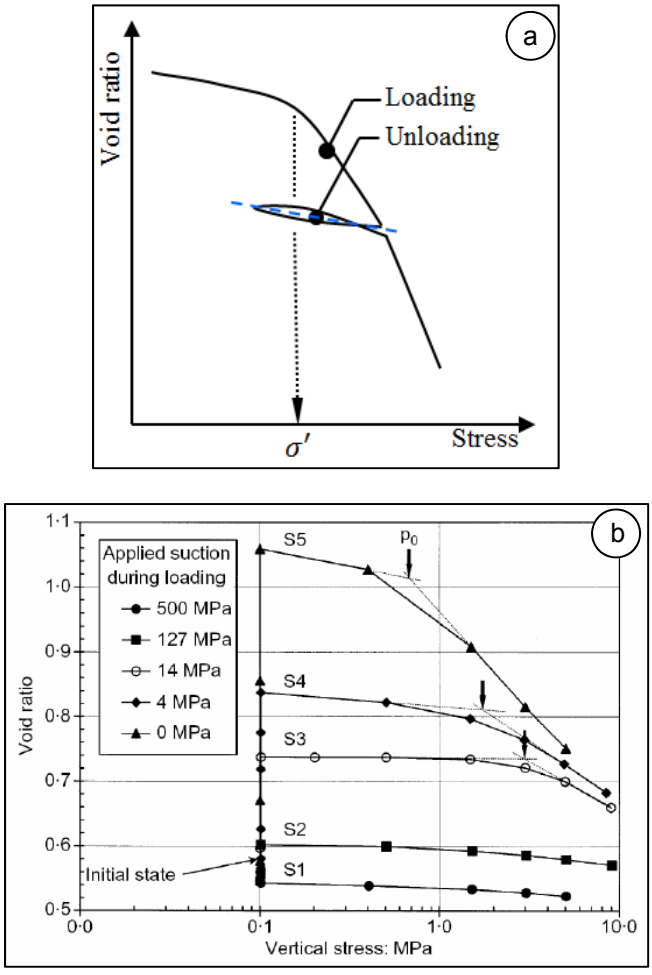

Figure 2. 10: a. compression under zero suction; b. compression with suction (Lloret et al, 2003)

2.2.2.3. Volume Change-Suction Relation under Zero or Constant Stress

Matric suction variations affect the volume change behavior in unsaturated soils. Suction-deformation relation under zero pressure is also known as soil's shrinkage curve and can be constitutively expressed as:

$$d(\varepsilon_x)_{(u_a-u_w)} = d(\varepsilon_y)_{(u_a-u_w)} = d(\varepsilon_z)_{(u_a-u_w)} = \alpha d(u_a - u_w) \quad \text{Eq. 2. 9}$$

$$d(\varepsilon_v)_{(u_a-u_w)} = \sum(\varepsilon_i)_{(u_a-u_w)}\, d = 3\alpha d(u_a - u_w) \quad \text{Eq. 2. 10}$$

There is a similarity between the compression curve due to suction variation and that of net normal stress, as shown in Figure 2. 11-a. Several researchers have observed hysteresis between suction-void ratio curves in wetting and drying processes (Fleureau et al, 1993). Alonso et al (1990) showed that the curve can be represented with two straight lines which intersect at the soil's yielding point. Fredlund et al (2000) suggested that void ratio-suction relation of a soil can be predicted from SWCC of the sample. Fredlund M.D. (2002) proposed the following equation to estimate soil's shrinkage curve.

$$e(w) = a_{sh}\left[\frac{w^{c_{sh}}}{b_{sh}^{c_{sh}}} + 1\right]^{\frac{1}{c_{sh}}} \quad \text{(Eq. 2. 11)}$$

Where:

e(w) = void ratio at any water content

a_{sh} = minimum void ratio

w = water content

c_{sh} = curvature of the shrinkage curve

b_{sh} = slope of the line of tangency

2.2.2.4. Volume Change-Suction under Variable Stress

Suction-deformation curve under normal stress is similar to that under no stress (Alonso et al, 1994; Lloret et al, 2003). The study suggests that the reduction in void will

continue with the same slope of the original deformation-suction curve; however, the start point ($e_{0-\sigma\neq0}$) will be less than $e^{i}_{0,\sigma=0}$, as shown in Figure 2. 11-b.

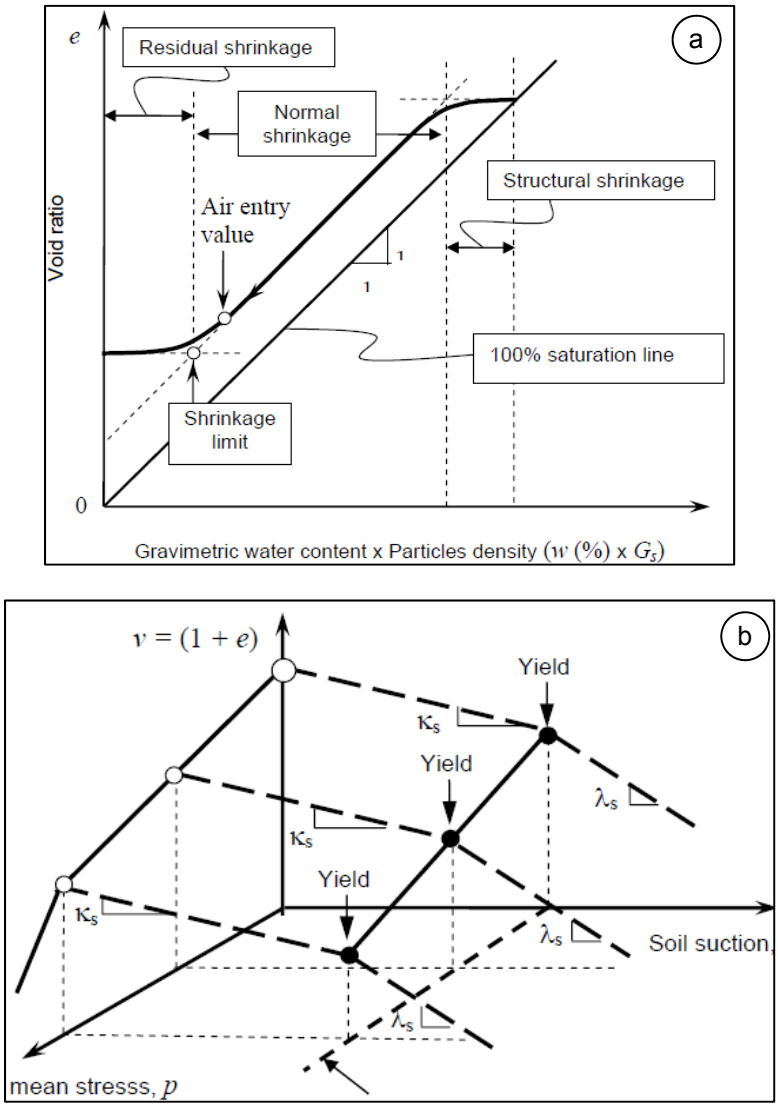

Figure 2. 11: a. *e-w (or ψ), σ* = 0; b. *e-w (or ψ), σ* ≠ 0

Zhang (2004) suggests that volumetric strain as a function of variable stress and suction can be constitutively written as:

$$d\varepsilon_v = \sum \varepsilon_i = 3 \times [\tfrac{(1-2\mu)}{E} d(\sigma_m - u_a) + \alpha d(u_a - u_w)] \qquad \text{Eq. 2. 12}$$

Where:

σ_m = Mean stress $= \frac{(\sigma_1+\sigma_2+\sigma_3)}{3}$

u_w = Pore water pressure

α = Factor relating volumetric strain to suction

2.2.2.5. Water Content-Suction under Zero or Constant Normal Stress

Under zero or constant mechanical stress, adding water to soil reduces matric suction which is defined by soil water characteristics (SWCC) (Figure 2. 12). SWCC is measured using pressure plate/Tempe cells and filter papers in low and high suction ranges, respectively.

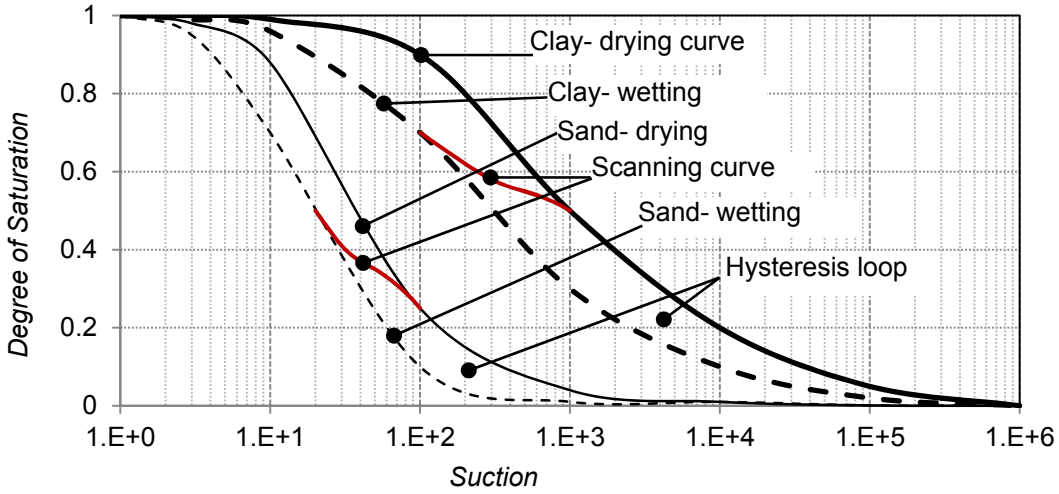

Figure 2. 12: Typical SWCC

Constitutive law for water content variation due to matric suction variations can be expressed using the semi-empirical method suggested by Fredlund et al. (2012), as:

$$d\theta_{(u_w-u_a)} = m_2^w d(u_w - u_a) \qquad \text{Eq. 2. 13}$$

Where

m_2^w = material parameter which illustrates the ability of matric suction to change soil water content

SWCC has been widely studied in the literature. Several methods to mathematically represent the SWCC mathematically are shown in Table 2. 4.

Table 2. 4: Existing models on predicting and data fitting the SWCC

Reference	Equation	Parameters
Gardner (1958)	$\theta_w = \theta_r + \frac{\theta_s - \theta_r}{1 + (\frac{h}{a})^b}$	θ_r = residual volumetric water content. a, b = curve fitting parameters
Brooks and Corey (1964)	$\theta_w = \theta_r + (\theta_s - \theta_r)(\frac{a_b}{h})^{b_b}$	θ_r = residual volumetric water content. a_b ,b_b = curve fitting parameters
van Genuchten (1980)	$\theta_\psi = \frac{\theta_s}{(1 + (a\psi)^n)^m}$	θ_s = Saturated volumetric water a, n, m= curve fitting parameters
Fredlund and Xing (1996)	$\theta_w = \left[1 - \frac{\ln\left(1 + \frac{\psi}{h_r}\right)}{\ln\left(1 + \frac{10^6}{h_r}\right)}\right]\left[\frac{\theta_s}{\left\{\ln\left[\exp(1) + \left(\frac{\psi}{a_f}\right)^{n_f}\right]\right\}^{m_f}}\right]$	a_f, n_f, m_f = curve fitting parameters

2.2.2.6. Water Content-Suction under Variable Normal Stress

This condition represents SWCC when measured under normal pressure. Mechanical stress can press water out of both saturated and unsaturated soils. The constitutive relation between water content variation and mechanical stress can be expressed similar to Eq. 2.7, as:

$$d\theta_\sigma = m_1^w d(\sigma_m - u_a) \qquad \text{Eq. 2. 14}$$

Where

m_1^w = material parameter illustrating the ability of mechanical stress to change water content

Huang et al (1998) showed that over consolidation and presence of net normal stress increases the air entry value and residual soil suction in SWCC. Zhang (2004) also noticed a similar behavior (Figure 2. 13); however, a major variation in SWCC was observed in greater normal stresses. In other words, under low normal stresses SWCC does not show extreme variations.

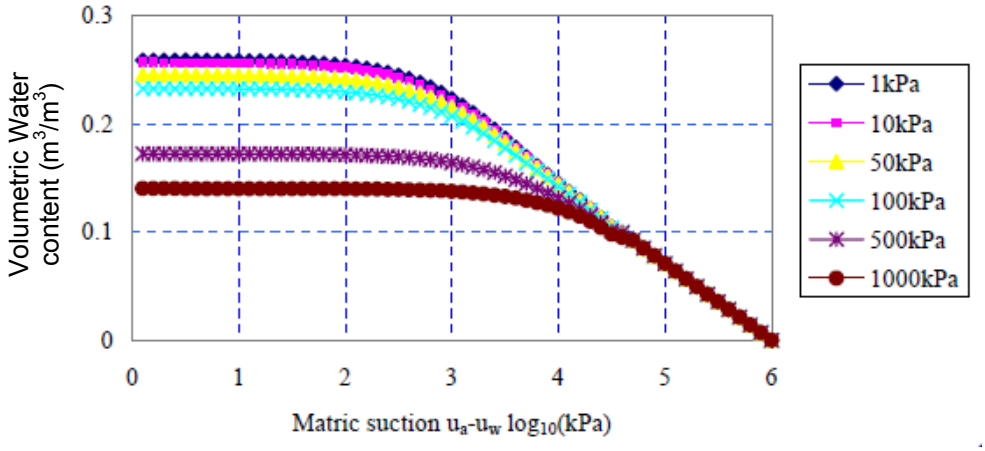

Figure 2. 13: SWCC under different pressure applications (Zhang, 2004)

2.2.2.7. Overall Construction of the Deformation/Stress/Water Pressure Surface

Based on the evaluated conditions, the combined/coupled analysis of the soil can be represented to depict the soil constitutive volumetric deformation surface. The comprehensive equations for volume change of unsaturated expansive soils are partial differential equations, as shown below. Each function relating a state parameter to a soil parameter is defined previously. The 3D surface of a sample clayey silt soil is shown in Figure 2. 14. Currently, there is no comprehensive method to mathematically represent the 3D surface completely.

$$de = \frac{\partial e}{\partial(\sigma_m - \sigma_a)} d(\sigma_m - u_a) + \frac{\partial e}{\partial(u_m - u_a)} d(u_m - u_a) \quad \text{(Eq. 2. 15)}$$

$$dw = \frac{\partial w}{\partial(\sigma_m - \sigma_a)} d(\sigma_m - u_a) + \frac{\partial w}{\partial(u_m - u_a)} d(u_m - u_a) \quad \text{(Eq. 2. 16)}$$

Where

$\sigma_m = \frac{(\sigma_1+\sigma_2+\sigma_3)}{3}$ = mean stress; and $\sigma_m - u_a$= mean net stress

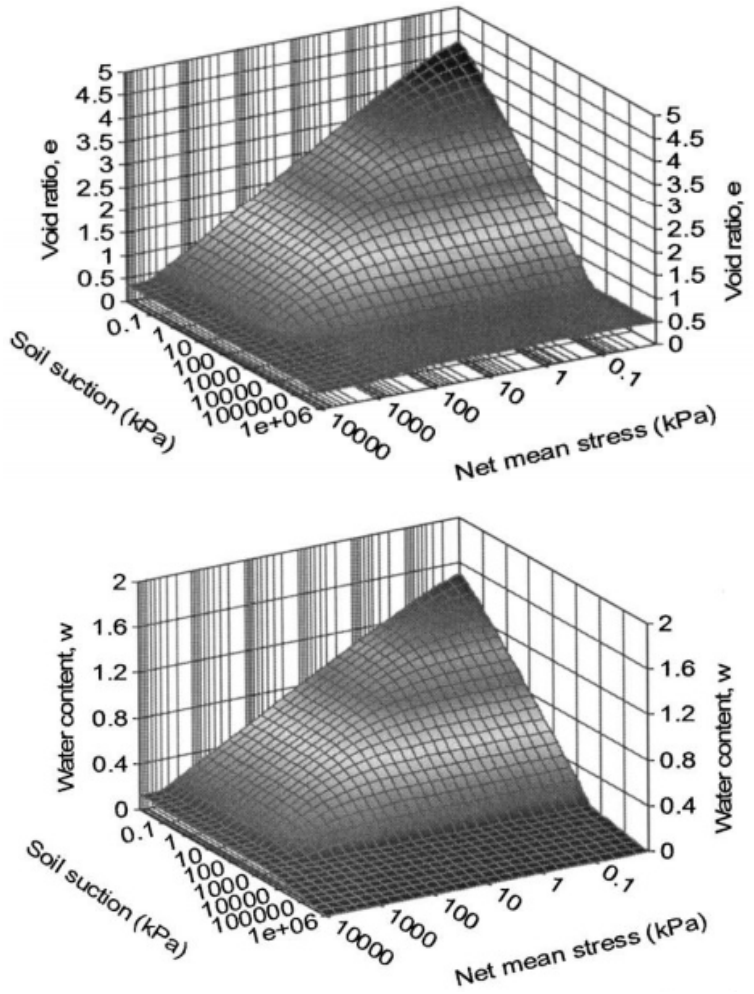

Figure 2. 14: Void ratio (top) and gravimetric water content (bot.) constitutive surface of Regina clay (Pham, 2005)

2.3. In-situ Instrumentation and Monitoring

To determine the real time deformation of expansive soil and its effect on long term pavement performance, it is absolutely necessary to have an accurate

understanding of moisture variation and infiltration behavior under pavement surface. In case of pavement systems, the unbound layer (i.e. subgrade) is most affected by moisture variations, while bound layers (i.e. surface and base) are significantly affected by temperature (Zapata et al, 2008). Results of such variations can be observed as deformation, cracking and increase pavement's roughness index. Instrumentation and long term on-site monitoring can provide valuable information for researchers. Usual field monitoring instruments include moisture and temperature sensors, suction probes, rain gauges, surveying, inclinometer profiling, resistivity imaging and ground penetrating radar. This section reviews currently utilized instruments and available literature on this subject.

2.3.1. Sensors for In-situ Monitoring

2.3.1.1. Moisture Sensors

Subgrade moisture content depends on a variety of climatic and physical factors including soil type, temperature, precipitation, vegetation, and others. The most reliable method for determining subgrade moisture variations is direct measurements over time. This is generally the most acceptable method used by the majority of the highway agencies (Bayomy and Salem, 2004). Sensors usually used for moisture data collection are Time Domain Reflectometry (TDR), dielectric sensors, and in some cases, neutron probes. Moisture sensors are extremely sensitive to installation process; Up to 45% error can occur as a result of wrong instrumentation (Decagon user manual, 2010).

Ease of installation, continuous in-situ monitoring and durable performance have improved utilization of dielectric sensors in novel research. The sensors determine the soil moisture by measuring the soil's dielectric constant, an electrical property that is highly dependent on moisture content. Changes in the moisture content cause a substantial change in the dielectric constant of the soil. Calibration equations are used to

relate the dielectric constant to the soil's volumetric moisture content which can be turned into gravimetric water content as:

$$w = \frac{\theta}{G_s.(1-n)} = \theta.\frac{\gamma_w}{\gamma_d} \quad \text{(Eq. 2. 17)}$$

Where:

w = Gravimetric water content

θ = Volumetric water content

G_s = Specific gravity of soil solids

n = Porosity of soil

γ_w = Unit weight of water

γ_d = Dry unit weight of soil

Several studies have been performed to measure the in-situ variation of moisture content. Presence of a seasonal variation trend in subgrade has been reported by researchers (Chen, 2012; Puppala et al., 2012; Jones and Jefferson, 2012; Wang et al., 2013; Kodikara et al., 2014). Marks and Haliburton (1969) observed that although subgrades continue to exhibit seasonal fluctuations in water content, they also trend toward an "equilibrium" value equal to 1.1 to1.3 times the soil's plastic limit. However, field observations indicate significant effect of temporary environmental conditions on soil moisture content that may cause variations in excess to seasonal changes. A formulation for accurate subgrade moisture variation does not currently exist.

2.3.1.2. Temperature Sensors

Information on ground temperatures is necessary for many construction projects, especially building industry, and can be utilized to determine heat losses of buildings, design of thermal energy storage equipment and possible use of the ground as a source for heat pump (Florides and Kalogirou, 2004). In unsaturated soil mechanics, temperature can provide substantial information on moisture evaporation,

elasticity modulus of surrounding media and suction variation (Nguyen et al., 2010). Usual instrumentation includes installation of a temperature sensor inside the media; no special consideration of soil disturbance is required

Perfect seasonal temperature variation inside pavement system is agreed among researchers which can be mathematically expressed as a first degree Fourier series, as below:

$$T = T_{ave} + a.\sin(t_{T,ave} + t) \quad \text{(Eq. 2. 18)}$$

Where:

T = Temperature of any layer of the soil

T_{ave} = Average temperature of soil layer

a = Domain of variation, function of soil temperature diffusion coefficient and moisture content

$t_{T,ave}$ = Time of the year corresponding to T_{ave}

t = Time

Ramadhan and Al-Abdul Wahhab (1997) suggest that the pattern follows the ambient temperature. The seasonal pattern is repeated through the depth of the soil; however, less variation from the mean temperature is observed with depth.

2.3.2. Pavement Deformation Monitoring

Topographic surveying is usually used for pavement movement monitoring. A survey plot normally includes points along the edge and across the pavement to obtain grids of the vertical coordinate of pavement surface. In addition to the survey, horizontal inclinometers can be installed inside or at interfaces of the base–sub base and subgrade materials to monitor the vertical deformations underneath the pavements and locate local deformations inside the pavement structure (Machan and Bennett, 2008). Inclinometer casings and cable return pipes are installed within a narrow trench and can

detect small movements earlier than normal pavement surface data-collection equipment (Figure 2. 15). After installation, the inclinometer measures the tilting angles and obtains the vertical profile of the casing using sinus law.

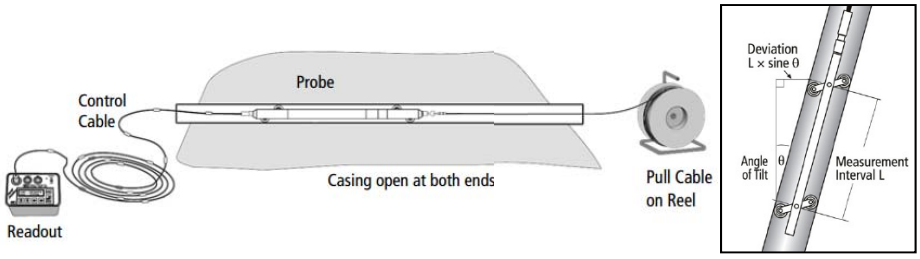

Figure 2. 15: Installation of horizontal inclinometer

2.4. Structural Characteristics of Asphalt Concrete

In a survey research, Wanyan et al (2010) reported that low volume pavements often fail prematurely before they can complete their design load repetitions. Kim and Buttlar (2009a) suggest causes include daily thermal variations, traffic loading, frost heave, moisture movement and destruction due to bearing subgrade soil. Volumetric changes of expansive clays are often overlooked in the design or addressed in an ineffective manner, which results in increase of pavement roughness and longitudinal shrinkage cracking (Intharasombat et al. 2007; Luo and Prozzi 2010). The current TxDOT design procedure suggests a predetermined protocol to mitigate longitudinal cracking caused by expansive subgrade soils. Therefore, reevaluation of the pavement design process and pavement-subgrade interaction is required to prevent loss of functional serviceability of the roads.

Pavement response to external loading is mechanistically determined by its structural strength. Stresses/strain analysis of the pavement's bound layers can determine whether the pavement is subjected to failure. Such analysis can be performed

through three stages, including material models, load models and analysis procedure (Sou, 2012).

2.4.1. Asphalt Concrete Material Model

Asphalt concrete is a heterogeneous complex of aggregates, bitumen and possible additives; therefore, a unique material definition may not be possible. For structural analysis purposes, roadway design manuals suggest general simplifications, including homogenous material definition and isotopic behavior (Kim and Buttlar, 2009a). Research suggests that a nonlinear viscoelastoplastic material definition best describes bitumen behavior, especially under rapid repetitive loading, such as passing tire loads (Park et al., 1996; Yi et al., 2014). However, since deformation due to expansive subgrade swelling happens at a slow pace, the nonlinear material definition provides an acceptable result while reducing the complexity of the problem significantly (Suo, 2012). Schwartz and Carvalho (2008) studied a pavement section using an elasto-plastic finite element model (EPFE) and concluded that using pure elastic material definition may under predict the horizontal strain. Maharaj and Gill (2014) suggest that nonlinear elastoplastic behavior yields closer results to the measurements.

Material behaves linearly elastic before failure strain, ε_y. For strains greater than ε_y (Figure 2. 16), the material will have permanent plastic deformation in addition to recoverable elastic strain. In this case, the overall deformation will be:

$$\varepsilon_t = \varepsilon_e + \varepsilon_p \qquad \text{(Eq. 2. 19)}$$

Where:

ε_t = Total strain

ε_e = Elastic strain

ε_p = Plastic strain

Excessive deformation in the plastic zone will eventually cause loss of strength and stiffness accompanied by cracks and fractures, resulting in pavement failure.

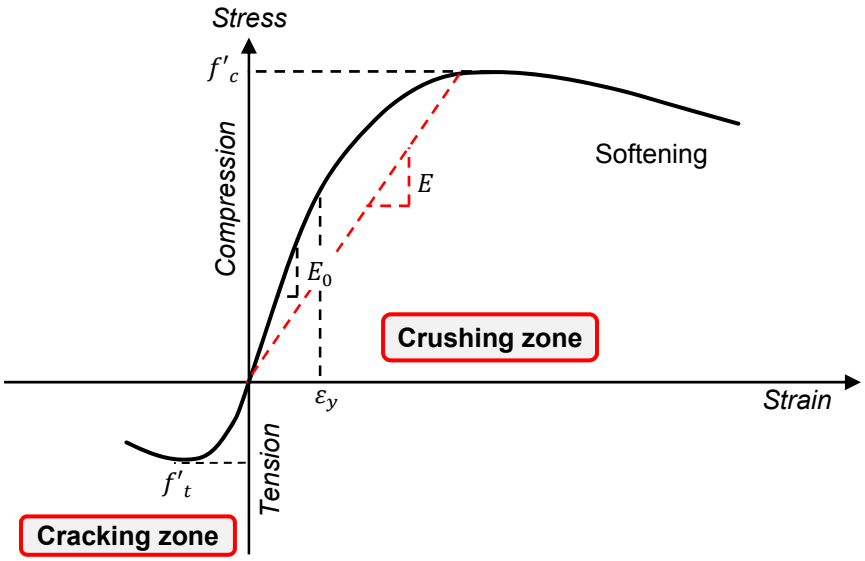

Figure 2. 16: Nonlinear elastic-plastic stress strain curve in tension and compression

Asphalt concrete possesses higher compressive strength than tensile strength. In addition, failure under crushing happens at strains larger than cracking. Therefore, the asphalt concrete section fails primarily because of excessive tensile stress.

2.4.2. Effect of Temperature

Behavior of asphalt concrete (i.e. the modulus of elasticity) changes from brittle in cold temperature to ductile in higher temperatures in a semi-log fashion. Aouad et al (1993) reported decrease of modulus from 3200 to 900 ksi as the temperature increased from 30 to 130°F. Meanwhile, Possion's ration increased from 0.3 to 0.9 for the same temperature period.

Different methods for describing temperature dependency of asphalt can be found in literature (Gibson, et al., 2003). Using Long Term Pavement Performance

(LTPP) lab data, Rada et al. (1991) proposed the SHRP equation to predict the modulus of asphalt concrete as formulated below. The most sensitive variable is temperature

$$\log(E_{AC}) = 0.553833 + 0.28829 \times \mathrm{P}_{200} \times f^{-0.17033} - 0.03476 \times V_a + 0.070377 \times \eta^{70,10*} + 0.000005 \times \left[\mathrm{t}_p{}^{(1.3+0.498251*\log(f))} \times \mathrm{P}_{AC}^{0.05}\right] - 0.00189 \times \left[\mathrm{t}_p{}^{(1.3+0.498251*\log(f))} \times \mathrm{P}_{AC}^{0.05} \times f - 1.1\right] + 0.93175 \times f - 0.02774$$

Where, (Eq. 2. 20)

E_{AC} = AC modulus, ×10^5

V_a = Percent air voids in mix

f = Test frequency

t_p = Mid depth AC layer temperature (F)

P_{200} = Percent aggregate weight passing # 200 sieve

$\eta^{70,10*}$ = Asphalt viscosity at 70 F

P_{ac} = Percent asphalt content by volume of mix

In another research based on LTTP site recorded data, Ali and Lopez (1996) proposed the following equation to relate AC elastic modulus layer temperature.

$$E = e^{9.372-0.0361\times \mathrm{T}} \quad \text{(Eq. 2. 21)}$$

Where:

E = AC modulus in MPa

T = Pavement temperature, 25mm below the surface (°C)

Due to considerable variation of characteristics due to temperature, structural response under variable temperatures is variable and should be studied.

2.4.3. Load Models

Roadway design manuals, including AASHTO, FHWA and USDOTs suggest considering two types of loading in pavement design process: structural and environmental.

Unlike structural loading, which is due to live service of the pavement, environmental loads are exerted by climatic conditions and can have significant impacts on performance of low-volume roads. A number of studies have been performed on pavement interaction with different environmental conditions. Rauhut et al. (1999) used LTPP data sets and analysis to evaluate design and construction procedures of flexible pavements and developed criteria for performance in roughness (IRI), rutting, transverse cracking, and fatigue cracking of pavements. However, direct conclusions and relations may not be obtained due to interdependency of the parameters. The authors summarized the main findings of the effect of different variables on pavement distress, as shown in Table 2. 5.

2.4.4. Structural Analysis Procedure

According to the elastic plastic plane theory, the maximum normal tensile strain occurs at the opposite face of the loading (Figure 2. 17). Most pavement design models are therefore based on straining of the pavement layer to predict performance due to loading (Mulungye et al., 2007). Although the vertical stress is effective within all the pavement layers, horizontal stress is only effective on wearing and base course (Akbulut and Aslantas, 2005). Therefore, a tensile crack within the pavement structure is usually initiated in bound layers and propagates towards outer surfaces.

Table 2. 5: Effects of variables on pavement performance (Rauhut et al., 1999)

Characteristics	Distress Type			
	Rutting	Fatigue Cracking	Transverse Cracking	Roughness
AC thickness	D	D	D	D
Base thickness	D	?	?	?
Air voids in AC	*	*	*	V
Asphalt viscosity	I	I	D	I
Base compaction	?	?	?	I
Structural number	D	D	?	D
Expected ESALs	I	I	I	I
Annual No of days with > 32°C	I	D	D	?
Freeze index	?	?	I	I
Annual no of freeze-thaw cycles	?	?	I	I
Annual precipitation	I	I	I	?
Subgrade < No. 200 (75μm)	?	?	?	I
Annual days with freezing temp	D	?	I	?
Age	?	?	I	?

* Only initial air voids are controllable but the data available are for air voids after consolidation by traffic

D = decrease in distress with an increase in the variable
I = increase in distress with an decrease in the variable
? = the effects are uncertain or variable

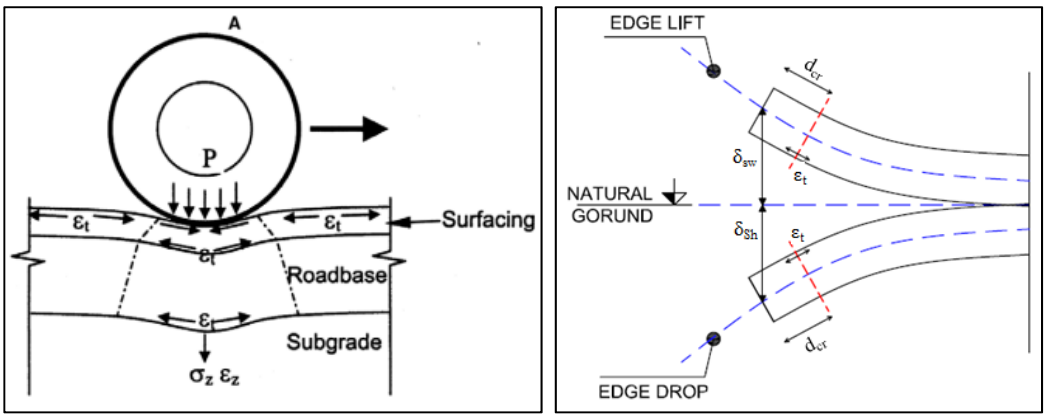

Figure 2. 17: Hot mix asphalt layer and stress/strain distribution due to a: loading, b: subgrade volume change

To address the environmental condition and excessive deformation of the pavement, Wanyan et al (2010) assumed that pavement shrinkage cracks start from the subgrade soil. However, it is also possible that asphalt cracking initiates due to stress concentration within the pavement structure itself (Luo and Prozzi, 2010). Both possibilities need to be considered in order to achieve a comprehensive design.

Ambassa et al. 2012 suggest that a shrinkage crack starting within the subgrade may propagate through the wearing course if the tensile strength of the asphalt is inadequate. This phenomenon is called bottom up or classical cracking and is a common observation for problematic subgrade soils. If the subgrade has a horizontal shrinkage strain of ε_{ss} due to loss of moisture, the induced tensile stress (σ_{ss}) will be:

$$\sigma_{SS} = \varepsilon_{SS} \times E \qquad \text{(Eq. 2. 22)}$$

Where E is the modulus of elasticity of soil. If σ_{SS} exceeds the tensile strength (σ_t) of the subgrade material, a fracture will develop. Luo (2007) suggested that due to structural continuity of the subgrade and asphalt overlay, same strain is developed inside the pavement section, which may cause further cracks (Figure 2. 18).

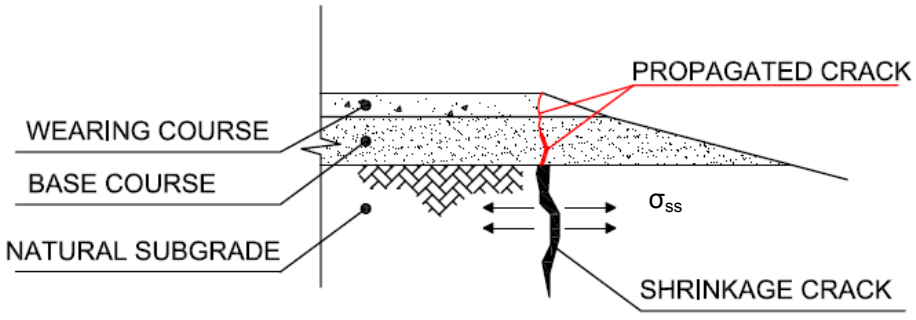

Figure 2. 18: Crack propagation

The author suggested considering the followings to numerically model this phenomenon:

(1) Estimation of ε_{ss} and E as a function of moisture content which can be performed through constitutive soil modeling. Currently, no general guideline for this analysis is available.

(2) Presentation of the analysis results in a fashion suitable for practicing engineers.

2.5. Previous Studies on Volumetric Deformation of Expansive Soils

Application of volumetric deformation monitoring, modeling and subsequent pavement distress analysis requires understanding the current state of research. Therefore it is important to study field instrumentations, stress modeling, infiltration analysis and volumetric deformation modeling.

Inclusion of swelling subgrade into pavement design was initiated by Lytton (1977). The researcher used initial and final estimated suction profile values, mean principal stress and compression coefficients to estimate subgrade volumetric deformation. Gay (1994) and Jayatilaka (1999) used Lytton's approach to estimate pavement roughness development over time with and without moisture barriers. Although the method provides good estimations of pavement performance over time, several assumptions made during the research (e.g. annual suction variation and constant soil profile along the road) are questionable. Other studies based on seasonal suction variation have also been proposed. Snethen (1979) proposed the following model to estimate the vertical swell movement of an expansive soil.

$$\frac{\Delta H}{H} = \frac{C_\tau}{1+e_0}[(A - Bw_0) - \log(\tau_{mf} + \alpha\sigma_f)] \qquad \text{(Eq. 2. 23)}$$

Where

ΔH = Vertical movement (ft)

H = Thickness of the layer (ft)

C_τ = Suction index

e_0 = Initial void ratio

A, B = Constants from SWCC

w_0 = Initial moisture content (%)

τ_{mf} = Final matric suction (kPa)

α = Compressibility factor

σ_f = Final applied pressure (kPa)

Holland and Cameron (1981) suggested performing conventional swell tests and considering a moisture correction factor for data interpretation, as below.

$$Log\left(\frac{P_a}{P_a}\right) = A_1 + A_2(LL) + A_3\left(\frac{\gamma_d}{\gamma_w}\right) + A_4(w_0) \quad \text{(Eq. 2. 24)}$$

$$Log(S_0) = B_1 + B_2(LL) + B_3\left(\frac{\gamma_d}{\gamma_w}\right) + B_4(w_0) \quad \text{(Eq. 2. 25)}$$

Where

P_0 = swelling pressure for zero movement

P_a = atmospheric pressure

S_0 = percent swell for zero load (%)

LL = liquid limit (%)

γ_d = dry density of soil

γ_w = unit weight of water

w_0 = in situ moisture content (%)

A_1, A_2, A_3, A_4, B_1, B_2, B_3 and B_4 are coefficients.

Hussein (2001) modeled the visco-plastic behavior of an expansive soil upon wetting and drying based on constitutive relations. Initial inputs were in-situ stress, water content and clay content, as well as environmental factors. The author concluded that the time-dependent deformation and stress changes are associated with pore-water migration, as well as the viscous nature of the material. Such hypothesis was used by

Briaud et al. (2003) who proposed a coupled water content-based method to replace suction in the current literature. In this method, movement of the soil is determined by tracing the changes of void ratio as a function of gravimetric water content. Heave and shrinkage were analyzed based on the extent of the water content variation. The method is user friendly; however, continuous boring of the site is required to measure water content and trace the volume change.

To provide measurements of water content in the field, Bayomy and Salem (2004) installed moisture sensors in a pavement subgrade site in Idaho and concluded that incorporation of the seasonal moisture variation in the pavement design process leads to significantly shorter pavement service life. The authors gathered monthly basis data and observed presence of a seasonal variation. However, due to the large time snap between the readings, some extra variations may not be captured. The authors also measured the temperature variations in the site, which followed a perfect seasonal pattern (Figure 2. 19).

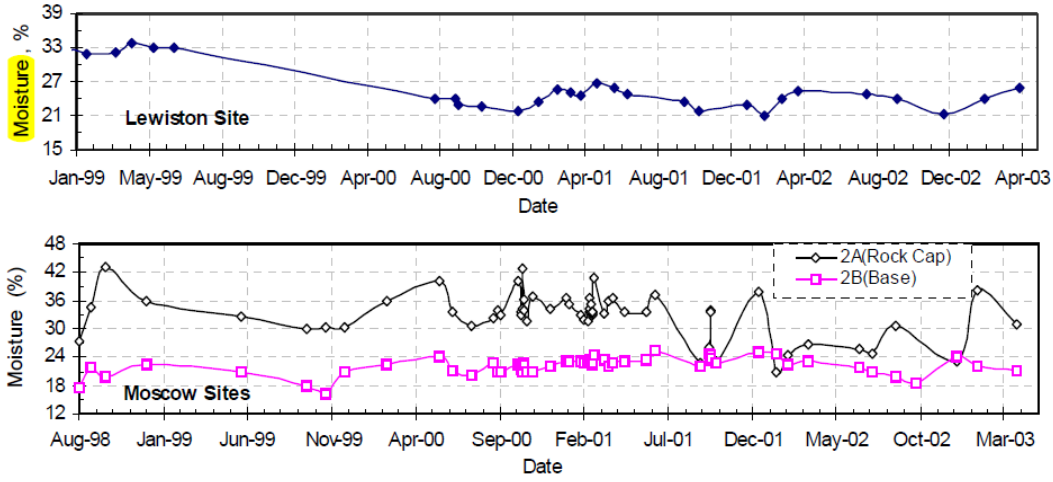

Figure 2. 19: Long term subgrade moisture content (Bayomy and Salem, 2004)

Fredlund et al (2006) studied the effect of suction variation on performance of foundation slabs constructed on expansive soils. The authors numerically modeled the

variation in suction due to moisture flow in the active zone and the resulting volumetric deformation. The researchers concluded that the stiffness of the slab does not contribute to control of the deformation of the foundation. In other words, structural strengthening of the footing may not mitigate expansive subgrade problems. The amount and duration of precipitation along with unsaturated soil properties, determine the zone of moisture variation in soil profiles. Suction varied between 0 to -1000 kpa, resulting in vertical deformation up to 70 mm (3%) at the edge of the slab. The authors did not look into the induced stress due to deformation. Real time deformation due to climatic conditions was not studied.

In an attempt to understand the infiltration behavior through high PI clay, Zornberg et al. (2007) determined the unsaturated hydraulic characteristic of high PI clay with laboratory testing. The author conducted a series of evaporation and infiltration experiments and observed considerably lower volumetric water content for the second drying phase. The authors suggested that due to increasing surcharge, the SWCC may vary with depth and appropriate hydraulic conductivity should be adopted to accurately predict the rainfall infiltration.

Manosuthkij (2008) instrumented the side slope an asphalt concrete road with TDR sensors. The sensors were installed 30-45cm below the surface and provided readings of moisture content over time. The author defined the monthly mean moisture content as the difference between maximum and minimum moisture contents. Based on the results, Wanyan et al (2010) concluded that cracking on the edge of the pavement is most likely to occur when the moisture content difference drops below 15%. No analyses of the extra saturation time and effect of additional moisture on the system were provided, as shown in Figure 2. 20.

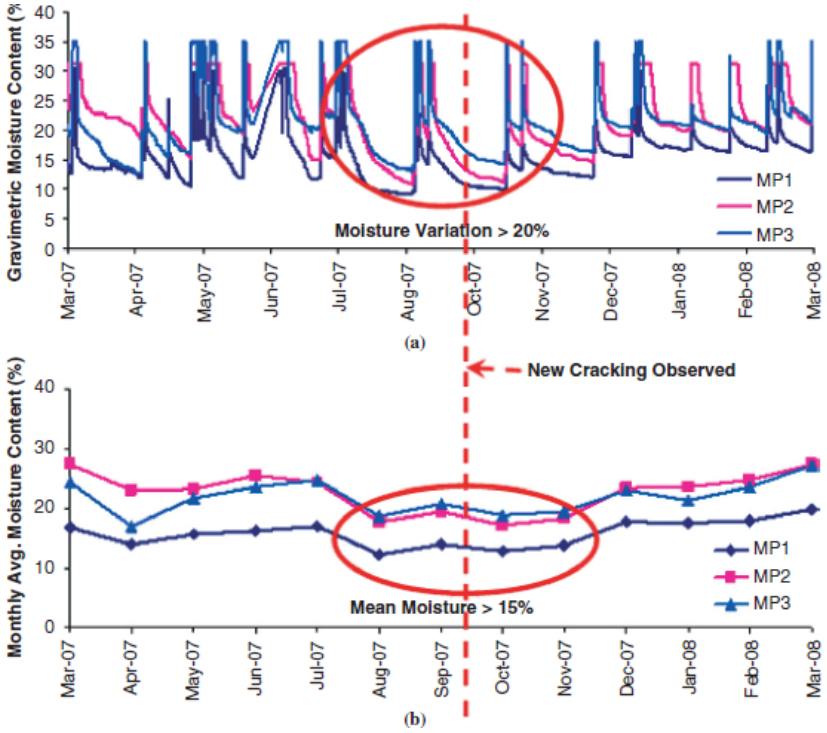

Figure 2. 20: Reported in-situ instrumentation results (Manosuthikij, 2008)

A similar pattern of moisture instability was also observed by Nguyen et al (2010). In this research, thermal conductivity sensors were used to report suction variations under the driving lane of 2-lane highways in Saskatchewan, Canada. The author studied the suction variations for extended periods of time and concluded that suction variation is mostly determined by climatic conditions (such as rainfall and freezing temperature) rather than soil conditions. Strong sensitivity was noticed at shallow depths and under the side slope with variations between 0.1-100 Mpa. Suction variation was limited to 25-100 kPa under the driving lane due to decreased infiltration. Based on the reports, the researchers defined the zone of suction variation as shown in Figure 2. 21. Differential suction profiles across the pavement can cause differential movement and distress the pavement. The authors did not report results of surveying to determine the vertical deformation.

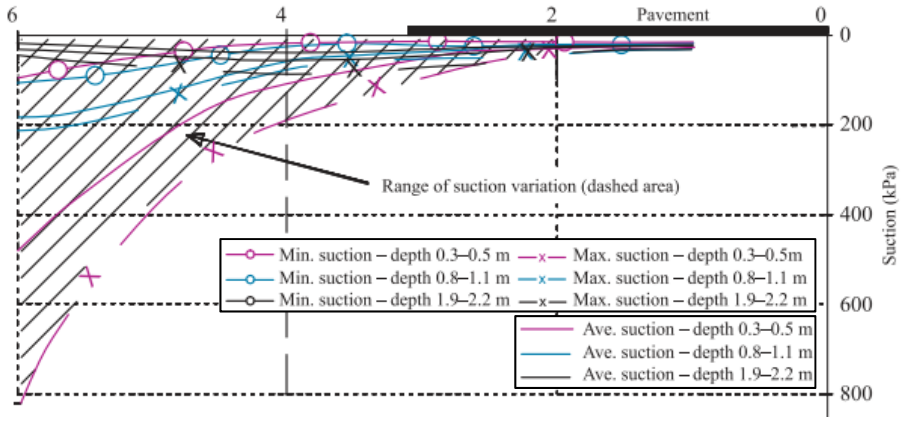

Figure 2. 21: Definition of active zone based on suction measurements (Nguyen et al, 2010)

External variations in addition to the main seasonal patterns, were more pronounced in the side slope and shallow depths. The author reported that the suction is mainly affected by microclimate “infiltration, freezing and evaporation”. When the ground water table was deep and stable, the suction was more affected by rainfall patterns and variations in seasonal temperature. The author concluded that more distress was observed in the pavement shoulder than in the pavement centerline.

Nelson et al (2010) proposed a method to predict the rate of heave progression as a function of moisture infiltration for residential homes. The authors stated that if the depth of heave of active zone is large, considering the maximum predicted heave may be impractical and result in overestimation of construction assumptions, especially in cases where the design life of the structure may be less than the time required for the entire amount of predicted heave to occur

Suggested suction based methods for volumetric deformation were compared by Talluri et al (2011). The authors concluded that a good match can be observed if the depth of the active zone is confined to 2 to 3 ft, which was justified based on considerable suction variations and less overburden pressure in shallow depths. The

results of study showed that the models become over predictive as the depth of analysis increases.

Houston et al. (2011) used surveys and interviews to provide updated heave forensic maps in urban areas of Phoenix, Arizona. The authors performed 1-D and 2-D unsaturated flow modeling and concluded that drainage conditions strongly determine foundation problems, including heave and settlement. Poor drainage, roof run off and surface ponding near structures reduce the suction throughout the active zone and cause differential swell and foundation movement. The forensic map provided expected volume change in the long term period of up to 11 years. Therefore, effects of daily evaporation, irrigation and precipitation were not considered.

Hossain (2013) used dielectric moisture and water potential sensors to investigate the infiltration into the highway embankment slope to determine the effect of moisture variations on unsaturated shear strength. The author observed suction variation between 0 to 800 kPa as a result of rainfall, which softened the soil and reduced the safety factor of the slope considerably. Results obtained from field instrumentation indicate that the moisture content and matric suction varied at different depths. The maximum variation often occurred near the ground surface (i.e. at 1.2 m depth) and the magnitude of variation decreased with increase in depth. The author also modeled the rainfall pattern and concluded that low intensity, long duration rainfall resulted in delayed penetration of rainwater as compared to the high intensity rainfall. Based on the swell tests results and in-situ measurements, the author concluded the depth of active zone to be 3.2m in Texas.

Puppala et al (2014) studied volume change behaviors of five different types of expansive clayey soils. The authors considered soil plasticity and compaction properties to estimate swell and shrinkage induced to civil infrastructure and concluded that

moisture content-based correlations show acceptable predictions of expansive soil behavior. Overall, the results showed that it is essential to characterize expansive soil behavior more realistically, which can lead to better and resilient civil infrastructure on expansive soils. No numerical analysis of transient volumetric deformation was provided.

As far as the pavement stress analysis, Burmister (1943) has performed the first closed-form solution for a two-layered linearly elastic half-space problem which was later extended to a three-layer. The stresses and strains calculated in these programs were checked against the defined failure criteria. In all these programs, pavement layers are considered as homogeneous, linear elastic.

Later, Huang (1993) listed assumptions in layered elastic theory as: 1) layers are homogenous and isotropic; 2) no inertia effect is considered; 3) all layers are infinite laterally; 4) all layers have a finite thickness except for the subgrade, which is assumed to be infinite; 5) pavement systems are loaded statically; and 6) the compatibility of strains and stresses is assumed to be satisfied at all layer interfaces.

Puppala et al (2014) related crack initiation in the pavement with in-situ suction measurements and observed that dry season's matric suctions exceeding 1500 kPa induce shrinkage cracking. The authors only considered the cracking due to shrinkage of the subgrade, and crack generation due to excessive tensile strain in the pavement section was not considered. The authors concluded that the shrinkage of the clay is linearly related to gravimetric moisture content of the soil, as below. The moisture content change is defined as the difference between the specimen moisture content after the completion of shrinkage tests and the original compaction moisture content.

$$\varepsilon_{sh,vert} = 0.23\Delta w \qquad \text{Eq. 2. 26}$$

$$\varepsilon_{sh,vol} = 0.66\Delta w \qquad \text{Eq. 2. 27}$$

Where

$\varepsilon_{sh,vert}$ = vertical shrinkage strain

$\varepsilon_{sh,vol}$ = volumetric shrinkage crack

Δw = variation of gravimetric moisture content

Based on the results, elastic vertical strain was determined almost 1/3rd of volumetric strain.

2.6. Limitations of the Current Studies

Previous studies have proved the importance of an accurate evaluation of expansive soil volume change; however, no comprehensive study has been performed to describe the pattern of moisture variation based on actual field-obtained data. In addition, infiltration behavior under the geological and weather conditions of North Texas has not been widely studied. Real time damage development due to transient volume change in pavement would be a valuable asset for low volume pavement design. Results of such a study could be interpreted as a comprehensive pavement design guide for use of practicing engineers. Therefore, it is imperative to verify the climatic structural interaction of subgrade/pavement, as well as to establish a design protocol for better design process.

Chapter 3

Methodology

3.1. Introduction

The adopted methodology for this research is presented in this chapter. Site investigation, sample collection and soil characterization are discussed, and details of field instrumentation, monitoring and data collection are described. Data analyzing and trending procedures are explained, followed by numerical modeling of volumetric deformation and pavement stress analysis. Real time moisture variations in pavement subgrades and subsequent volumetric deformation are modeled using coupled stress/fluid flow analysis. The resulting stress concentration in the overlaying hot mix asphalt is studied and the process of failure of pavement section is obtained.

3.2. Field Studies

Field-based data collection and investigation is an important part of this dissertation. Field data are controlled by many factors and are complicated to interpret. However, good understanding of data variations along with strong data analysis are critical as they reflect conditions encountered by practicing engineers. Therefore, comprehensive instrumentation, monitoring, data collection and analysis are required and are described in following sections.

3.2.1. Site Selection

Several criteria were considered in selecting an in-service site, including availability of design records, indications of expansive subgrade such as cracks and pavement distresses, uniform subgrade soil strata and absence of tree roots. A pavement site located in Farm to Market (FM) road 2757, Kaufman County Texas (Figure 3. 1) was selected. Existing soil surveys reported presence of deposits of Eagle Ford clay formation

in the area. Surficial indications of such expansive subgrades were observed during initial field visits (Figure 3. 2)

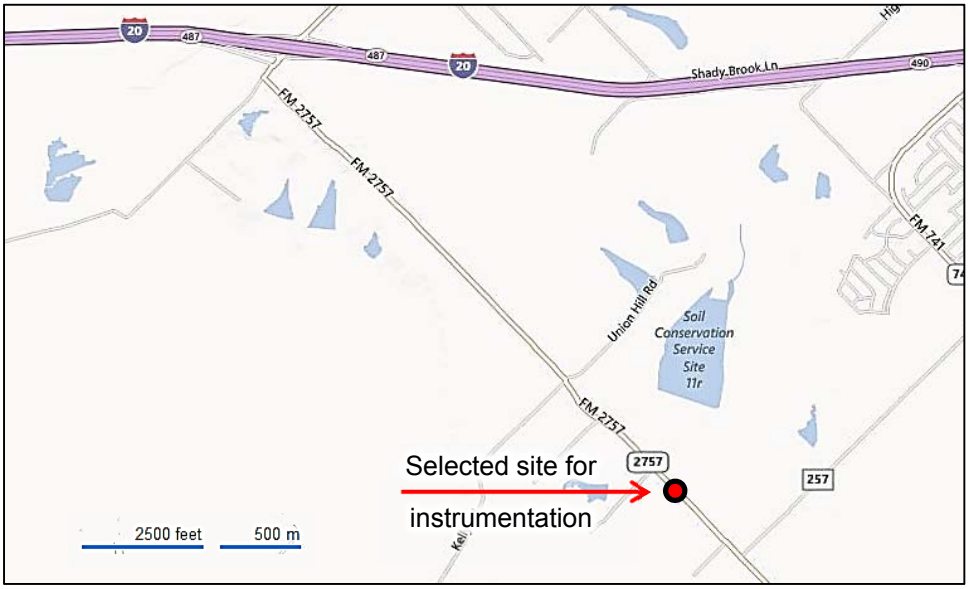

Figure 3. 1: Location of the proposed test site

Figure 3. 2: Surficial pavement damages due to expansive subgrade soil

The selected site is a 2-lane, hot mix asphalt pavement and is constructed based on TxDOT standards for farm to market roads, as shown in Figure 3. 3. A typical cross section of the road consists of a 6 inch (150mm) hot mix asphalt overlay paved over the natural compacted subgrade. Based on set of plans, no base course was provided. The

side slopes are grass covered, with 1:4 and 1:8 slopes on either side. Ditches were provided to collect excess run-off; however, no lining was observed for moisture control.

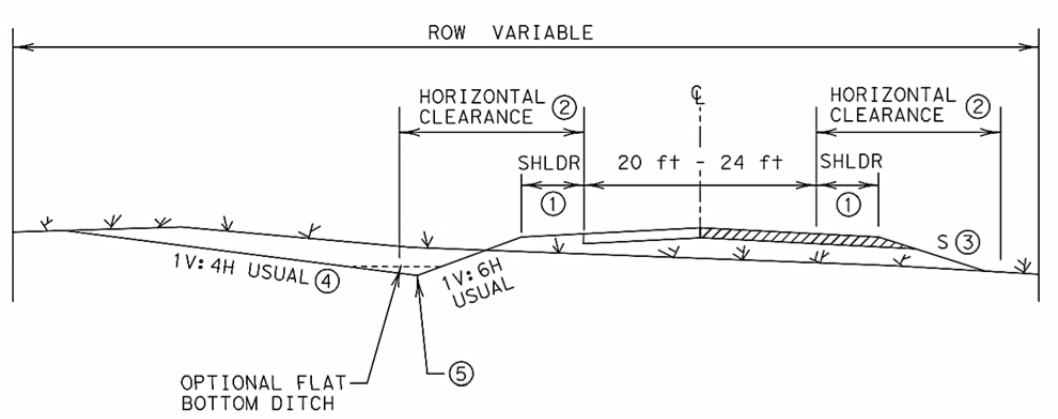

Figure 3. 3: Cross section for arterial and collector two-lane rural highways (TxDOT)

3.2.2. Site Investigation

The site was investigated using Resistivity Imaging (RI), Dynamic Cone Penetrometer (DCP), soil test boring and sample collection.

3.2.2.1. Resistivity Imaging

To obtain a continuous profile of subsurface soil condition and moisture content, two 2D RI were performed across (line A-A) and along (line B-B) the pavement, as shown in Figure 3. 4. The system consisted of 56 electrodes with 0.6 m spacing. Zones of high resistivity typically reflect low moisture content, while low resistivity zones indicate high moisture content or in some cases, saturation.

In section A-A, resistivity varied between 1 and 100 Ω.m as shown in Figure 3. 5-a. The high resistivity zone close to the surface represents the pavement section with low moisture content. Resistivity significantly decreased below the pavement, which signifies high moisture content of the subgrade soil. Since the pavement is considered impermeable, high moisture content of the subgrade may be due to capillary action from the groundwater table.

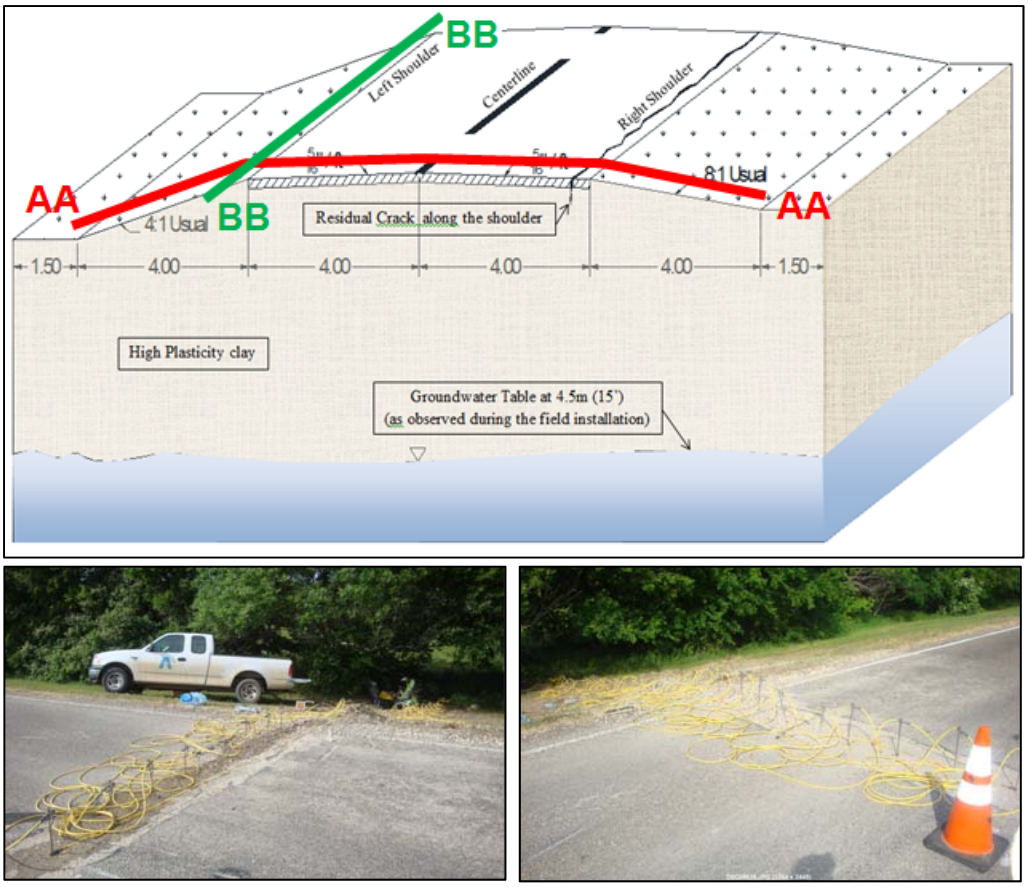

Figure 3. 4: Resistivity imaging

Zones of lower resistivity exist below the edges of the pavement as well, which indicates infiltration of moisture from side slopes toward the pavement. The zone of moisture intake was measured approximately 1.4m from the edge toward the centerline of the pavement. Therefore, most of the pavement distresses caused by moisture variations were expected to be within this area. The hypothesis was confirmed by a pavement condition evaluation, as longitudinal cracks and an uneven surface profile were primarily limited to the outer half of the main driving lanes.

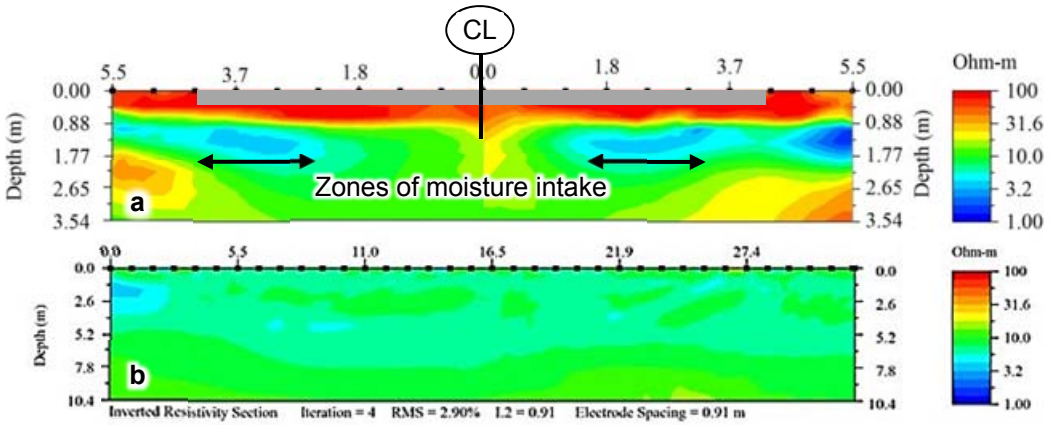

Figure 3. 5: RI results in lines AA and BB

RI results of line B-B were limited between 5-15 Ω.m (Figure 3. 5-b), and no significant variation was noticed. The smooth resistivity profile reflects the presence of almost constant moisture content at the time of survey. Low resistivity captured in line B-B suggests that the subgrade is close to saturation. As the soil under line BB is located under the side slopes with no covered portion, high moisture content is expected and justified.

3.2.2.2. Determination of Soil resilient Modulus

Dynamic cone penetrometer was used to measure the resilient modulus of the soil. Two points on either sides of the road were selected and resilient moduli of different layers were determined, as shown in Figure 3. 6.

Based on the obtained data (Figure 3. 7), the soil possessed higher resilient modulus within the top 15cm of the soil, which was to be expected as this layer is subjected to live load of passing vehicles as well as cyclic swelling and shrinkage. However, the modulus significantly reduced and maintained a constant value of approximately 35MPa as the depth increased. As the modulus showed no sensitivity to depth, this value was later used for numerical modeling.

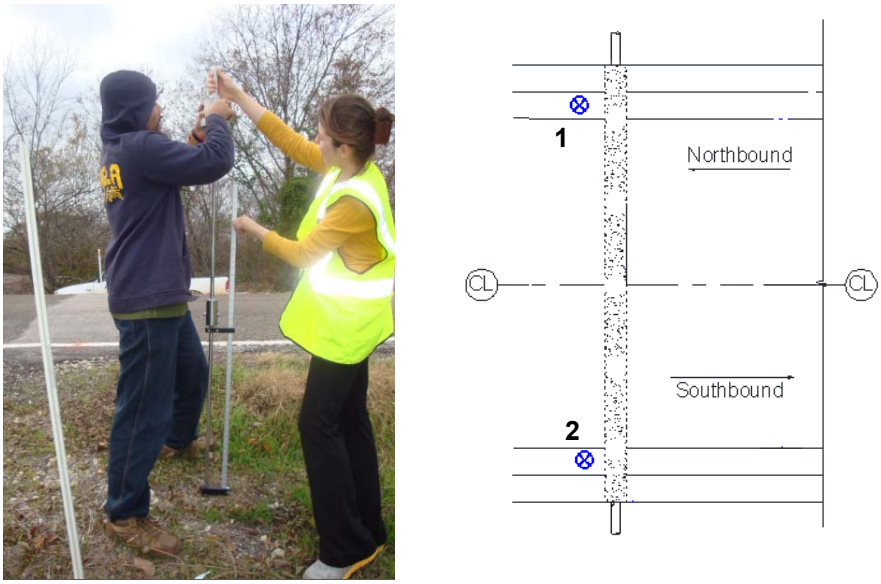

Figure 3. 6: Measurement of resilient modulus

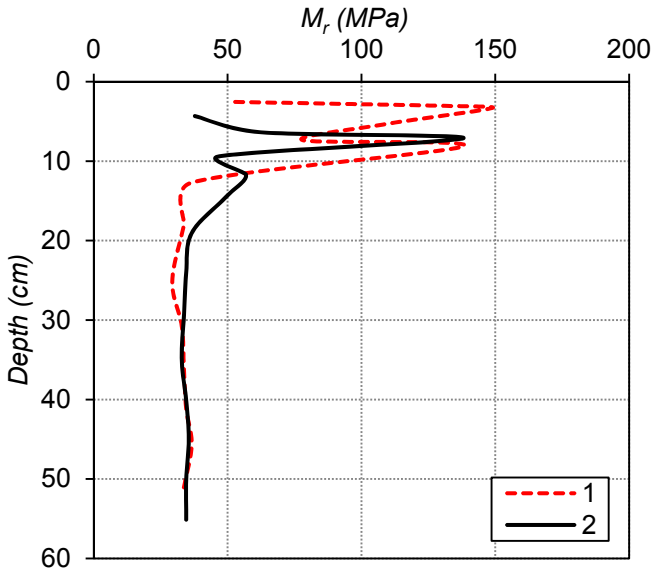

Figure 3. 7: Resilient modulus of the pavement subgrade

3.2.3. Sample Collection and Laboratory Investigation

Four soil test borings were conducted under one lane of the pavement as shown in Figure 3. 8.

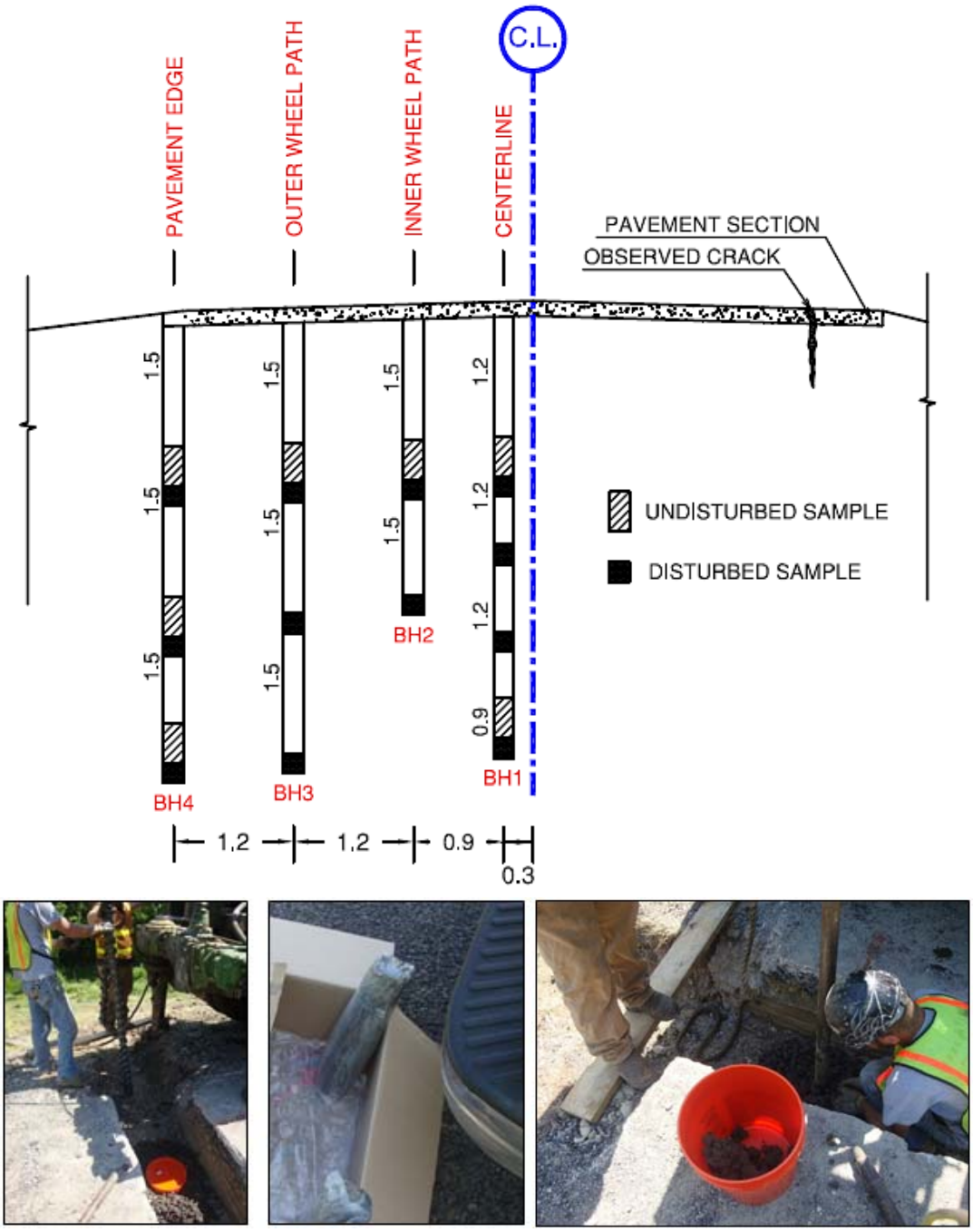

Figure 3. 8: Boreholes and sample collection layout

The boreholes were placed under the centerline, inner wheel path, outer wheel path and edge of the pavement. Disturbed and undisturbed sampling and Texas Cone Penetration (TCP) tests were performed at borehole locations. Based on in-situ observations, predominant soil strata were dark brown high plasticity clay interlayered with light tan clay. Ground water table was observed at 4.5m depth. Bore logs of the samples are shown in Appendix I.

The collected samples were transported to the laboratory and stored in a humidity-controlled room. Physical characteristics of the collected soil samples were determined through the following tests.

3.2.3.1. In-situ Gravimetric Moisture Content

Moisture profile of the subgrade soil was measured according to ASTM D2216 Standard Test Methods for Laboratory Determination of Water (Moisture) Content of Soil and Rock by Mass, and the results are presented in Figure 3. 9-a. The subgrade's moisture content varied between 17 to 27% and gradually increased with depth. The lowest initial moisture content was observed in BH1 (located under the centerline of the pavement), which was expected due to the presence of pavement cover. The moisture profile in BH4 showed a concentrated increase between 2 and 3 m depth, which was a trend similar to the resistivity imaging results (Figure 3. 9-b). This was attributed to moisture infiltration through side slope and surficial cracks, as observed during the initial field investigation. The samples had constant moisture content of 24% at 4.5m due to the groundwater table and saturation of the samples.

3.2.3.2. Grain Size Distribution

Samples' particle size distribution curves were determined according to ASTM D 422-63 Standard Test Method for Particle-Size Analysis of Soils. Combination of sieve series analysis and hydrometer soil tests was used to obtain full range of soil particle

sizes. The soil was dried at 120°F, crushed and washed through sieve #200. The remaining soils were oven-dried and sieved using #4, #10, #30, #40, #60, #100 and #200 US. Soil passed through sieve #200 was then used for the hydrometer test. Figure 3. 10 shows the envelope of maximum and minimum particle size distribution curves for the collected samples. It is observed that in all samples, clay percent is above 80%, indicating presence of very fine subgrade soil.

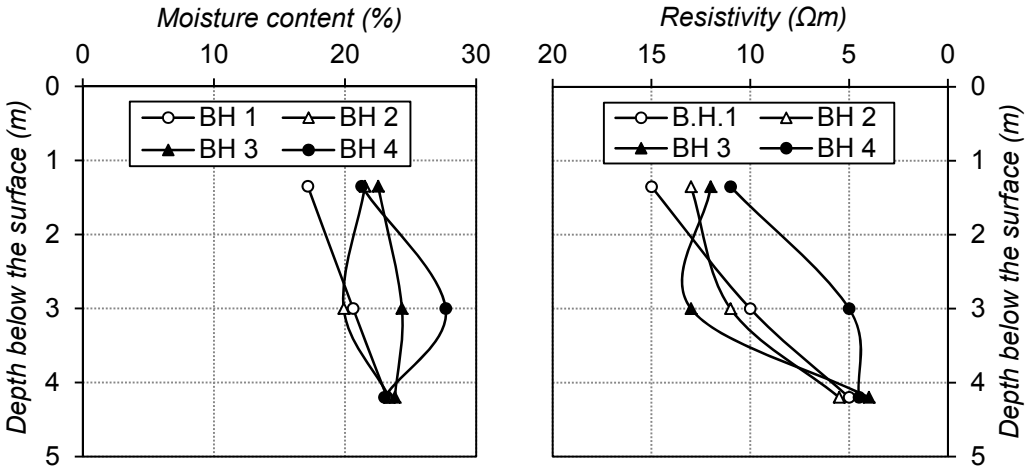

Figure 3. 9: Moisture and resistivity profile of the borehole

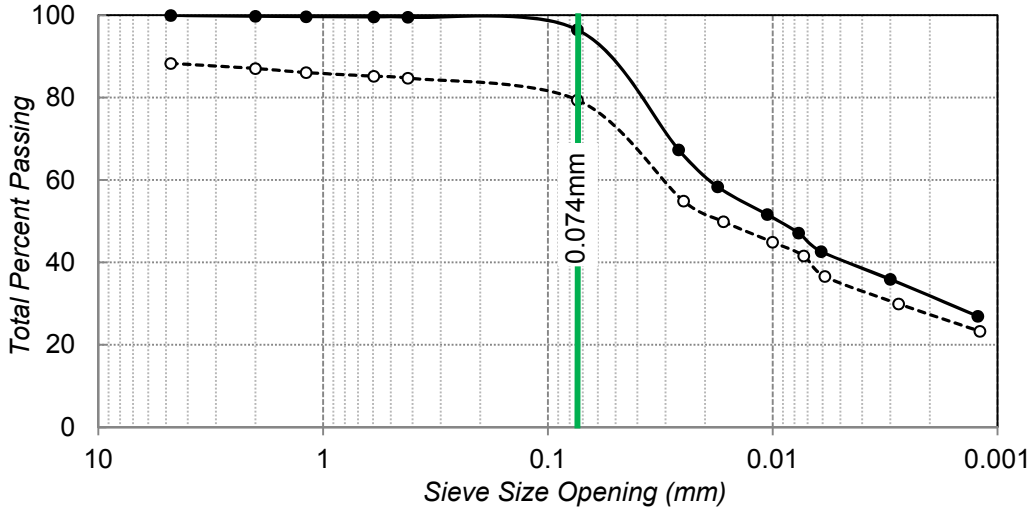

Figure 3. 10: Envelope of soil particle distribution

3.2.3.3. Atterberg Limits

Atterberg limits of soil samples were measured according to ASTM D 4318 Standard Test Methods for Liquid Limit, Plastic Limit, and Plasticity Index of Soils and presented in Table 3. 1. Liquid limit varied between 51 and 65%, while plasticity was between 30 and 46%. The plasticity chart of the soil samples is presented in Figure 3. 11. Given the sieve series and Atterberg limits results and according to the Unified Soil Classification System (USCS), the soil was classified as highly plastic clay (CH).

Table 3. 1: Atterberg limits of collected samples

B.H.	Depth (m)	LL (%)	PL (%)	PI (%)
B.H.1	2.1	57	19	38
B.H.1	3.6	59	21	38
B.H.1	4.2	51	21	30
B.H.2	1.2	51	19	32
B.H.2	3	64	22	42
B.H.3	1.2	65	19	46
B.H.3	3	57	23	34
B.H.3	4.5	57	22	35
B.H.4	1.5	60	22	38
B.H.4	3	62	21	41
B.H.4	4.5	51	20	31

3.2.3.4. Specific Gravity

Based on ASTM D845 Standard Test Methods for Specific Gravity of Soil Solids by Water Pycnometer, specific gravity of the samples was measured which ranged between 2.72 and 2.74. The averaged specific gravity was 2.73.

3.2.3.5. Organic Content

Organic content of the soil samples was measured according to ASTM D3960 Standard Practice for Determining Volatile Organic Compound (VOC) Content of Paints

and Related Coatings. Average organic content of the samples was 8.3%, which is not a high organic content percentage.

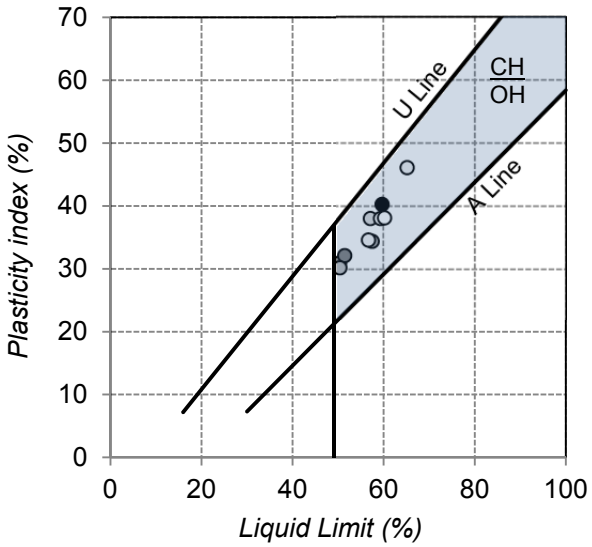

Figure 3. 11: Plasticity chart of the subgrade soil

3.2.3.6. Compaction Curve

Hossain (2013) performed Standard Proctor compaction tests based on ASTM D 698-00a Standard Test Methods for Laboratory Compaction Characteristics of Soil Using Standard Effort. The author measured OMC as 21.05% with dry unit weight of 15.3 kN/m^3.

3.2.3.7. Bulk and Saturated Unit Weight, Void Ratio and Degree of Saturation

Undisturbed soil samples were used to determine bulk and saturated densities. In addition, void ratio and degree of saturation of samples were measured using samples with known volume, weight and moisture content. The results are shown in Table 3. 2.

3.2.3.8. Permeability Test

Falling head permeameter was used to measure the soil's permeability. The results are shown in Table 3. 3.

Table 3. 2: Bulk and saturated unit weight, void ratio and degree of saturation

measured parameter	value
Bulk density	13.24 - 17.48 kN/m^3
Saturated density	15.1 - 19.17 kN/m^3
Void ratio	0.51 - 0.78
Degree of saturation	75 - 100%

Table 3. 3: Permeability results

Dry density	moisture content	permeability (m/s)
15.6	18%	1×10^{-5}
15.6	27%	3.54×10^{-7}

3.2.3.9. Swell Test

Results of one-dimensional swell tests were extracted from Hossain (2013) and are shown in Figure 3. 12. Based on the test results, soil starts to collapse under 70 kPa normal stress, which is approximately 4 m depth in the field with total density of 17.48 kN/m^3.

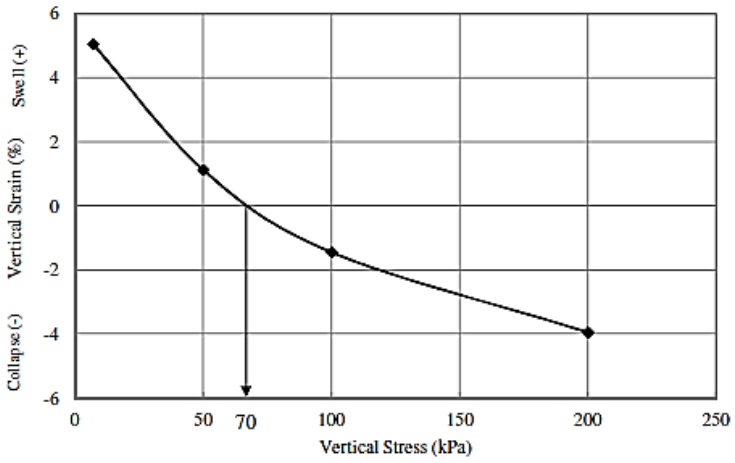

Figure 3. 12: One-dimensional swell tests (Hossain, 2013)

3.2.3.10. Soil Water Characteristics Curve (SWCC)

Hossain (2013) measured the SWCC of the samples for soil compacted wet and dry of optimum moisture content under normal stress, both with and without considering volumetric deformation of the soil. The authors used vanGenuchten (1980) equation to mathematically represent the data points, as

$$\Theta = \frac{\theta-\theta_r}{\theta_s-\theta_r} = \left(\frac{1}{(1+(\alpha\Psi)^n)}\right)^m \quad \text{Eq. 3. 1}$$

Where:

Θ = Relative water content

θ_r = Residual water content

θ_s = Saturated water content

Ψ = Suction

α = Fitting parameter related to air entry value of the soil

n,m = Fitting parameters

The fitting parameters were reported as presented in Table 3. 4. Details of the tests can be extracted from Hossain (2013).

Table 3. 4: Measurement of SWCC (Hossain, 2013)

Sample preparation condition	Normal Stress (kPa)	SWCC with considering sample volume change			SWCC without considering sample volume change		
		α (1/kPa)	n	m	α (1/kPa)	N	m
δ_d = 14.18 kN/m^3 ω = 29.5%	25	0.0064	1.2190	0.1717	0.0089	1.3116	0.2376
	50	0.0063	1.2184	0.1908	0.0096	1.3009	0.2313
	100	0.0064	1.2357	0. 1792	0.0072	1.3122	0.2379
δ_d = 14.18 kN/m^3 ω = 18%	25	0.0159	1.1454	0.1269	0.0123	1.2407	0.1940
	50	0.0123	1.1335	0.1178	0.0134	2.335	0.0833

3.2.4. Field Instrumentation

To date, few field scales studied have been performed on the real time effect of rainfall infiltration on unsaturated expansive subgrade soil. Therefore, a detailed instrumentation program was developed to study temperature/moisture variations, deformation of the pavement and the resulting stress increase in pavement structure. Data collection and monitoring processes were continued for an extended period of time. Collected data were later used for analysis, trending and calibration of numerical modeling.

3.2.4.1. Instruments

Model 5TM soil temperature/moisture sensors by Decagon were used to measure the temperature and volumetric water content of the soil (Figure 3. 13-a). The sensor uses measurements of the soil's dielectric constant to determine volumetric water content of the surrounding media. By pushing the sensor directly into the soil, it can measure volumetric water content from 0-100% with accuracy of ±2%. Prior to installation, the instruments were calibrated in the lab based on method suggested by Cobos and Chambers, 2010 and the calibration factor was later used in data interpretation.

A 100ECRN high resolution rain gauge by Decagon (Figure 3. 13-b) was installed to monitor the daily rainfall at the site. The rain gauge has a double spoon tipping bucket-type sensor and is capable of measuring rainfall with 0.2mm accuracy. The rain gauge is connected with data loggers placed at the field to record the amount of hourly rainfall. The total daily rainfall amount is the summation of all the recorded data in a day.

Recordings were continuously stored in an automatic data acquisition system. Three Em-50G data loggers by Decagon (Figure 3. 13-c) were set up in the field to

accommodate all the sensors. The Em-50 is a 5-port, self-contained data logger which can measure the data in a continuous interval and can store up to 36800 scans.

Figure 3. 13: 5TM Temp/moist. sensor, 100ECRN rain gauge and Em-50G data logger

To measure the local deflections of the pavement, a Horizontal Digitilt Inclinometer Probe by Slope Indicator was used (Figure 3. 14). The inclinometer uses two sensors 600mm apart, which measure the tilting angle of the device from a horizontal line. A vertical profile within ±0.01% accuracy can be obtained using the sinus law for measured angle.

Figure 3. 14: Horizontal inclinometer

3.2.4.2. Instrumentation Layout

A comprehensive instrumentation layout was designed to study moisture variation in the entire active zone of subgrade soil and subsequent pavement deformation. Fourteen (14) moisture and temperature sensors were installed in four

boreholes representing centerline, inner wheel path, outer wheel path and edge of the pavement. Location and depths of sensors are presented in Table 3. 5 and Figure 3. 15. Gridded pattern of the sensor recorded the moisture contour of the subgrade soil at any time.

Table 3. 5: Location of sensors

Tag#	Distance from C.L. (m)	Depth beneath the surface (m)
TM1/1	0.3	1.2
TM1/2	0.3	2.4
TM1/3	0.3	3.6
TM1/4	0.3	4.5
TM2/1	1.4	1.5
TM2/2	1.4	3.0
TM3/1	2.5	1.5
TM3/2	2.5	3.0
TM3/3	2.5	4.5
TM4/1	3.6	0.9
TM4/2	3.6	1.8
TM4/3	3.6	2.7
TM4/4	3.6	3.6
TM4/5	3.6	4.5

3.2.4.3. Installation Process

Based on TxDOT's requirement to maintain the rout open for local access, the instrumentation was carried out in two stages, on April 18 and 19, 2012. Each lane of the road was instrumented in a separate stage while the other lane was kept open to traffic.

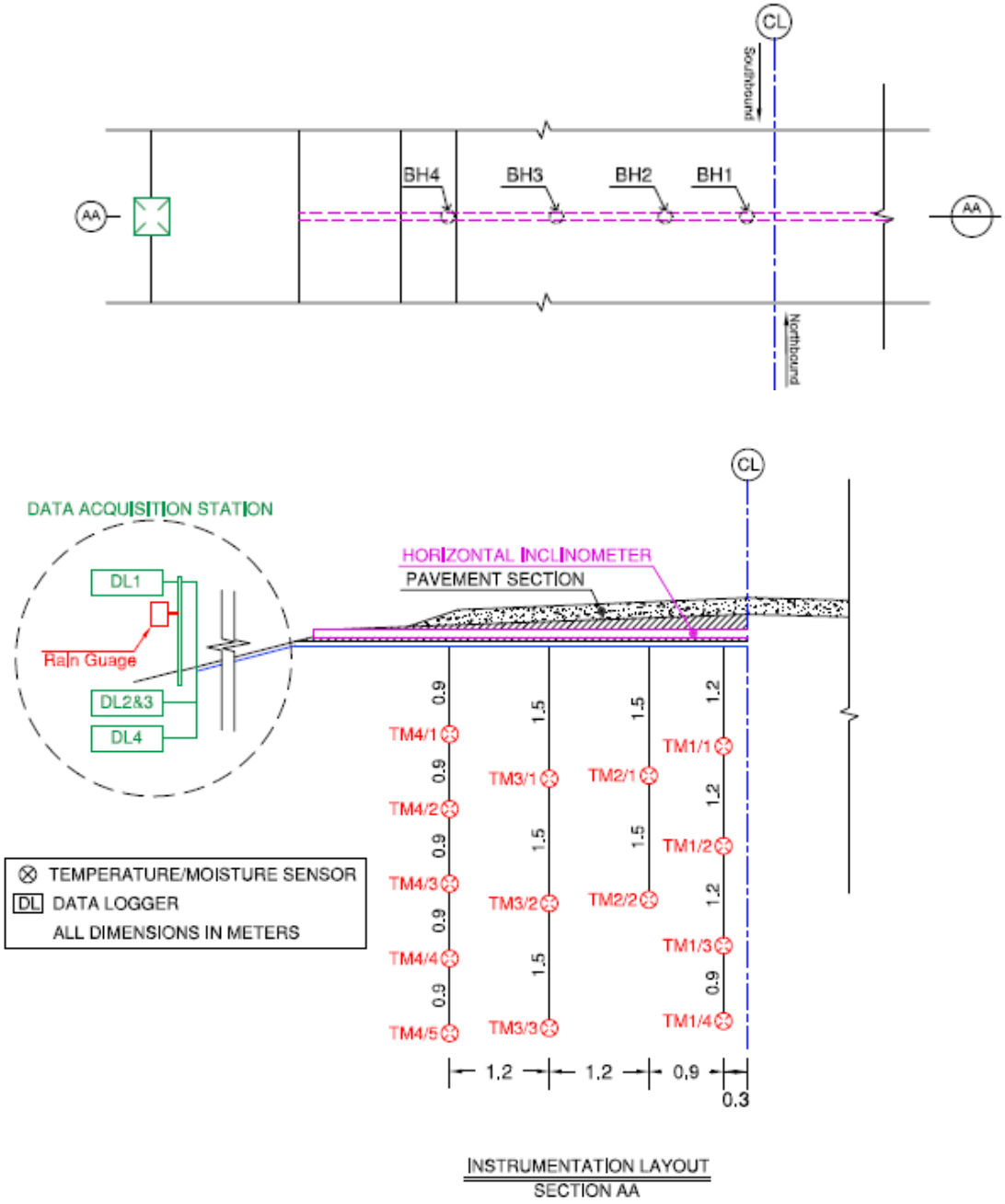

Figure 3. 15: Instrumentation plan (top) and layout (bot)

FIRST INSTRUMENTATION STAGE: NORTHBOUND LANE

The first installation stage included excavation of a trench to install the inclinometer casing beneath the northbound lane. A trench (45^{cm} W × 45^{cm} D × 600^{cm} L) was excavated and leveled using a backhoe loader (Figure 3. 16-a). 15^{cm} of sand was placed to eliminate sharp edges and stress points that might endanger the casing (Figure 3. 16-b). The inclinometer casing was placed and aligned so that the grooves inside the casing were perfectly vertical (Figure 3. 16-c, d). The trench was backfilled with the in-situ material (Figure 3. 16-e) and compacted (Figure 3. 16-f). The surface was repaved approximately 7 days after compaction to allow initial settlement.

Figure 3. 16: Instrumentation of northbound lane (first stage)

SECOND INSTRUMENTATION STAGE: SOUTHBOUND LANE

The second instrumentation stage included completion of the casing installation, instrumentation of the sensors and rain gauge, connection of the data loggers and compaction of the trench. A trench (45^{cm} W × 45^{cm} D × 600^{cm} L) was excavated under the southbound lane (Figure 3. 17-a), in line with the trench excavated during the previous stage and four soil test borings were drilled (Figure 3. 17-b). According to the instrumentation plan and using an instrumentation device (Figure 3. 17-c), sensors were lowered to the predetermined depth and pushed into the in-situ soil (Figure 3. 17-d). The boreholes were backfilled using the in-situ material and compacted to the in-situ density. This sequence was followed until all the sensors were installed. The signal wires were tied, covered with sand to prevent damages and conveyed outside the roadway.

The instrumented trench was leveled and covered with 15^{cm} of sand bed (Figure 3. 17-e); which acted as a cover for the signal wires and a bed for the inclinometer casing. The sand bed was compacted and the inclinometer casings were placed, aligned and connected to the casings of northbound lane. The trench was backfilled with fill material and compacted.

At a safe distance outside the pavement, a rain gauge was mounted and leveled vertically. The signal wires were connected to the data loggers and tested for proper functioning. The sensors and the rain gauge were set to record temperature, volumetric moisture content and precipitation data every 60 minutes (Figure 3. 17-f).

Figure 3. 17: Instrumentation of southbound lane (second stage)

3.2.4.4. Topographic Survey

Vertical deformation of the pavement site was monitored through monthly surveying. The surveys were performed according to the survey layout shown in Figure 3. 18. Three permanent points were selected on a nearby bridge which was constructed on deep concrete foundation. The initial survey was conducted in May 2012 and considered as base line. Other points were surveyed monthly and aligned, so that the vertical deformation of the surface could be measured. A tolerance between ± 1 inch was allowed to account for possible errors.

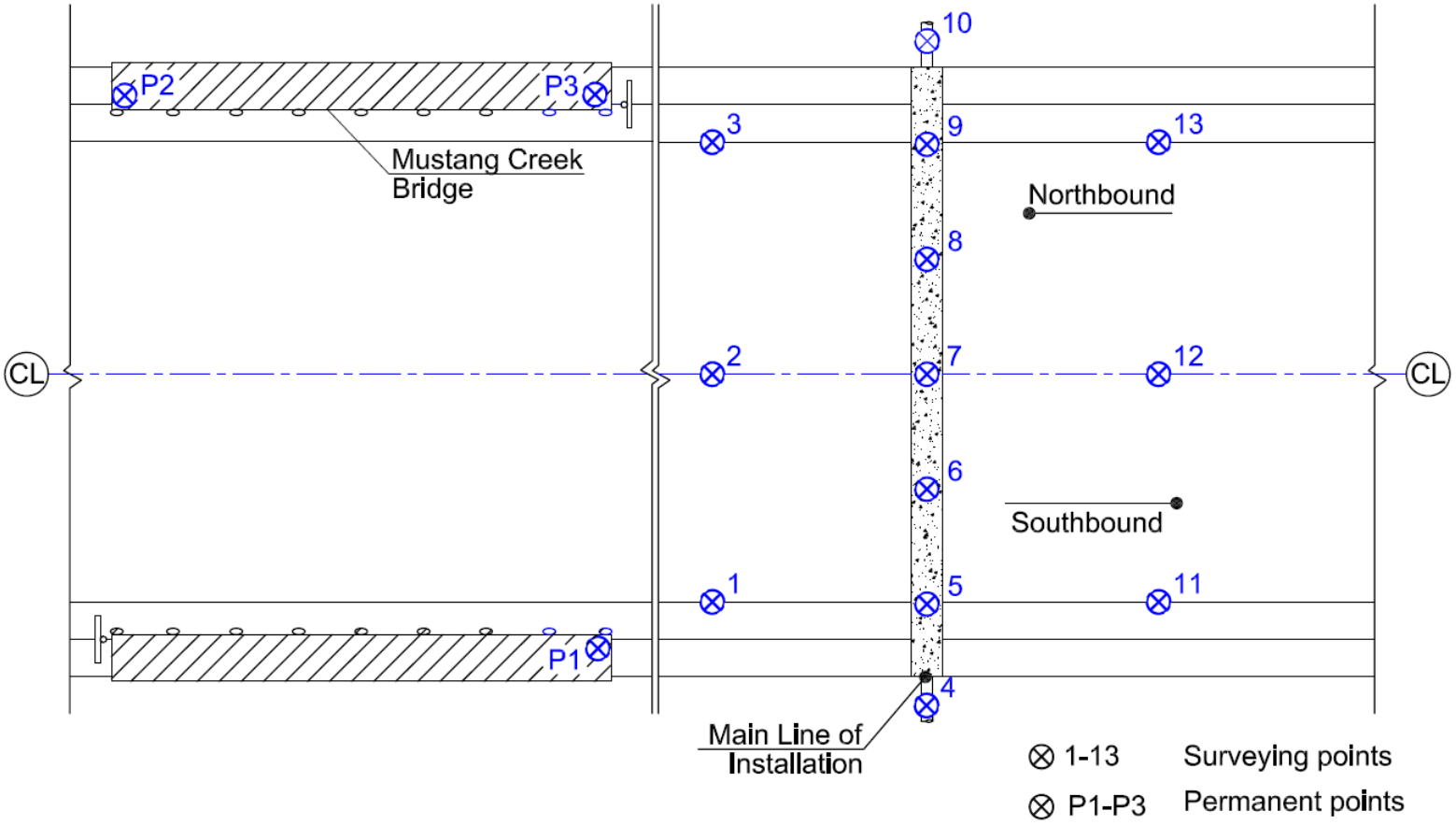

Figure 3. 18: Survey layout

3.2.4.5. Performance Monitoring

The instrumented site was monitored for an extended period of time. Monitoring included downloading the data from data loggers (Figure 3. 19-a), profiling the pavement with the inclinometer (Figure 3. 19-b), measuring the crack depth and width (Figure 3. 19-c, d) and topographic survey. The monitoring was performed according to Table 3. 6.

Figure 3. 19: Monitoring Performance

Table 3. 6: monitoring schedule

	4/26/12	5/14/12	6/5/12	6/16/12	7/5/12	7/14/12	8/3/12	9/8/12	9/25/12	10/6/12	10/22/12	11/10/12	12/13/12	1/10/13	1/23/13	2/9/13
Rain Gauge	✓	✓	✓	--	✓	✓	✓	✓	✓	✓	✓	✓	✓	✓	✓	✓
Moisture sensor	✓	✓	✓	--	✓	✓	✓	✓	✓	✓	✓	✓	✓	✓	✓	✓
Temperature sensors	✓	✓	✓	--	✓	✓	✓	✓	✓	✓	✓	✓	✓	✓	✓	✓
Inclinometer	類	✓	✓	--	✓	✓	✓	✓	✓	✓	✓	✓	✓	✓	✓	✓
survey	--	✓	--	✓		✓	✓	✓	--	✓	--	✓	✓	✓	--	✓

	2/14/13	2/23/13	3/2/13	4/5/13	4/25/13	5/20/13	6/11/13	7/1/13	8/7/13	9/22/13	10/21/13	12/1/13	1/4/14	2/9/14	3/23/14	5/21/14
Rain Gauge	✓	✓	✓	✓	✓	✓	✓	✓	✓	✓	✓	✓	✓	✓	✓	✓
Moisture sensor	✓	✓	✓	✓	✓	✓	✓	✓	✓	✓	✓	✓	✓	✓	✓	✓
Temperature sensors	✓	✓	✓	✓	✓	✓	✓	✓	✓	✓	✓	✓	✓	✓	✓	✓
Inclinometer	✓	✓	✓	✓	✓	✓	✓	✓	✓	✓	✓	✓	✓	✓	✓	✓
survey	--	--	✓	--	✓	✓	✓	✓	✓	✓	✓	✓	✓	✓	✓	--

3.3. Trending and Data Analysis

After obtaining the time series of moisture, temperature and deformation, the data sets were investigated in Matlab, using non-parametric data analysis. Non-parametric methods are best for studying data sets with a random or unpredictable order in time which fall in any of the following categories:

1. No clear numerical interpretation exists
2. Distribution pattern of field obtained data is unknown
3. The data do not belong to any particular statistical distribution
4. Only available information is the set of data points over time

In non-parametric data interpretation, the output model does not include typical statistical parameters including mean, variance, standard deviation, etc. Typically, the procedure trends the data without assuming any kind of parametric relation between the variables, and the model grows in size to accommodate the complexity of the data. This technique involves fitting a large number of curves to local data subsets (including main signal and noisy data) and then combining them into a single larger curve. Smoothing techniques, such and localized regression, are examples of this procedure. Accuracy of the technique depends on choosing the appropriate smoothing parameter. A large smoothing parameter will under fit the data (Figure 3. 20-black curve), while selecting a small value results in over fitting the data and making it un-interpretable (Figure 3. 20-red curve). In the latter case, the model tries to capture both the trend and the noise.

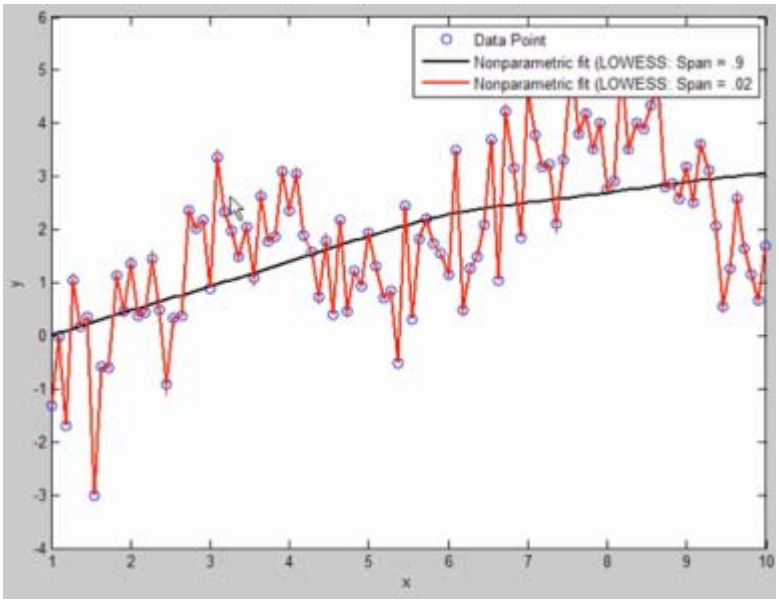

Figure 3. 20: Nonparametric analysis and data fitting (Matlab Manual)

The optimal value for the smoothing parameter can be obtained through cross validation. Since in field-obtained data the true equation is unknown, a trial and error method can be conducted to best fit the data. This technic, allows the user to generate

confidence bands to account for outlier data that is too close to the curve to be considered noise.

3.3.1. Analysis of Field Moisture Content

Moisture content at field conditions strongly depends on climatic loading and can be difficult to interpret. To analyze the field data, several simplifying assumptions are essential. It is assumed that moisture variations at the field can be mathematically explained through the combination of two behaviors: an annual seasonal variation and excessive temporary increase in moisture content. Such behavior is observed in many in-situ field studies (Nguyen et al., 2010; Hossain, 2013; Manosuthikij, 2008; Hedayati et al., 2014). Due to the depth of water table, it is also assumed that the soil is located within the capillary fringe; therefore, equilibrium moisture at the soil's field capacity is close to saturation. In addition, Darcy's law is assumed valid for moisture distribution in the media.

The data processing method was selected after an initial evaluation of the recorded data. Two trends were diagnosed within the time series: a main seasonal trend and additional peak values due to environmental loading. To statistically evaluate the data, non-parametric analysis was used. The main seasonal trend was assumed as the main signal, while the peaks were treated as hypothetical "noise" in addition to the main signal. Such assumptions made data interpretation possible.

To analyze the main signal, an initial Fourier series was captured and based on the determined series, 95% confidence band of the data were generated. The Fourier series was reevaluated one more time with the data points that were inside the confidence band. After confirmation of the series equation, it was considered final.

To analyze the peak values, the *additional* water content was determined by subtracting the peak value from the main seasonal value. The *additional* water content was later analyzed against rainfall data to find any particular trend. The overall model

containing both seasonal variations and peak values was generated by adding of the two determined series as a function of time. Finally, the determined model was validated against recordings of two sensors that were not used for model development.

To provide an analytical solution for the moisture variation pattern, the following procedure was undertaken. Based on Darcy's law, the average seasonal moisture variation within a uniform soil layer at different depths was explained, using the partial differential one-dimensional diffusion equation:

$$\frac{\partial \theta}{\partial t} = \frac{\partial}{\partial z}\left(D(\theta)\frac{\partial \theta}{\partial z}\right) \qquad \text{Eq. 3. 2}$$

Where:

θ = Volumetric water content at depth z at time t

D(θ) = Soil moisture diffusivity (material coefficient controlling moisture flow following Fick's law in nonlinear from)

The partial differential nonlinear equation was solved by establishing known boundary conditions, including:

1. Surficial soil (z=0) is subjected to harmonic sinusoidal variation ignoring rainfall induced transient moisture increase. The same assumption was considered and confirmed in non-parametric analysis in Matlab.

2. At infinite depth (or at ground water table depth) the soil moisture is constant (it is not affected by surficial climatic events). This assumption was also justified by measuring the water content of samples collected from 4.5 depth (Figure 3. 9) and from the recordings of deep installed sensors.

3. Moisture diffusivity parameter is independent of time and depth of soil profile and can be determined based on soil type and moisture content. Several studies suggest that variation of moisture diffusivity parameter is limited for regular moisture content variations observed in the field. Therefore, it is assumed constant which is a good

practical assumption especially for clayey soils (Kutilek, 1984). Mabirizi and Bulut (2009) reported moisture diffusivity of clayey soil equal to 1 on average. Based on the assumptions above, the problem was solved as a first degree Fourier series:

$$\theta(z,t) = \theta_0 + \theta_a \sin(\omega t - \frac{z}{d} + \theta_p) \quad \text{Eq. 3. 3}$$

Where

$\theta(z,t)$ = Soil moisture at depth z and time t

θ_0 = Average soil moisture at depth z over time

θ_p = Phase correction factor

θ_a = Domain of moisture variation. Kodikara et al (2014) suggest

$$\theta_a = \theta_s e^{-\frac{z}{d}}$$

Where θ_s = saturated volumetric water content, z= depth and d= damping depth. Parameter *d* reflects reduction in soil moisture variation with increase of depth and can be estimated as

$$d = \sqrt{\frac{2D}{\omega}}$$

D = Diffusivity

ω = Angular frequency (=2π/T, T= time period)

Final solution and the determined values are discussed in chapter 4: Results and discussion.

3.3.2. Analysis of the Temperature Variation

Based on the initial sensors recording, the method of data analysis was selected as a first degree Fourier series. The data from nine sensors was used for trending, while the remaining data was used for calibration and validation.

To acquire the analytical solution, the same process as in moisture content was undertaken. The reason is that both functions follow the same general solution, as they are both seasonal variations. The main trend was expected to be as:

$$T(z,t) = T_0 + T_a \ \sin(\omega t + T_p) \quad \text{Eq. 3. 4}$$

Where

$T(z,t)$ = Soil temperature at depth z and time t

T_0 = Average soil temperature at depth z over time

T_p = Phase correction factor

T_a = Domain of temperature variation, which is a function of depth and soil temperature diffusivity. Average value for wet clay soil can be assumed as 0.015 cm^2/s.

Possible trends and solutions are discussed in Chapter 4: Results and Discussion.

3.3.3. Recorded Vertical Deformation

Recorded surveys over time were mathematically analyzed using a non-parametrical regression approach. Several variable interactions were considered, such as deformation- time, deformation- rainfall, excessive movement-excessive moisture content and excessive movement-total saturation time.

To statistically analyze the recorded data, non-parametric data fitting was initially performed in Matlab environment. Since it is suggested that deformation follows the climatic conditions, a mixed behavior of seasonal variation with excessive movement due to scattered rainfall data was expected. The function representing deformation can also be expressed using a first degree Fourier series, as below:

$$\Delta H = A.sin(\omega t + B) + f(t,R) \quad \text{Eq. 3. 5}$$

Where:

ΔH = Vertical movement of the pavement

A = Amplitude of variation

ω = Angular frequency

B = Phase correction

$f(t,R)$ = A function of time and rainfall which may cause excessive movement

The data was processed following the same procedure as in moisture content data analysis, and the determined function is explained and discussed in Chapter 4.

3.4. Numerical Modeling

Finite Element Method (FEM) has been successfully utilized to account for effects of many practical conditions more realistically than theoretical solutions based on infinite slab and other idealized assumptions (Kuo and Huang, 2006). Among many FE softwares, Abaqus® is becoming more promising due to its ability to perform multiple nonlinear equations simultaneously. In addition, it is the only software capable of modeling volume change of expansive soils and structural stress analysis together.

In the numerical modeling part of this study, unsaturated moisture diffusion and volume change in subgrade soils were modeled. Subsequent stress distribution and process of damage development was evaluated. Analysis was performed in two parts, soil moisture diffusion/swelling analysis and stress generation in pavement section.

3.4.1. Model Geometry

The pavement was modeled in three-dimensional space. The geometry of the model was as field measurements (Figure 3. 21). Since the road geometry is symmetric, one driving lane and the adjacent side slopes were used for modeling. The depth of the model was 4.5m, representing depth of the groundwater table measured in the field.

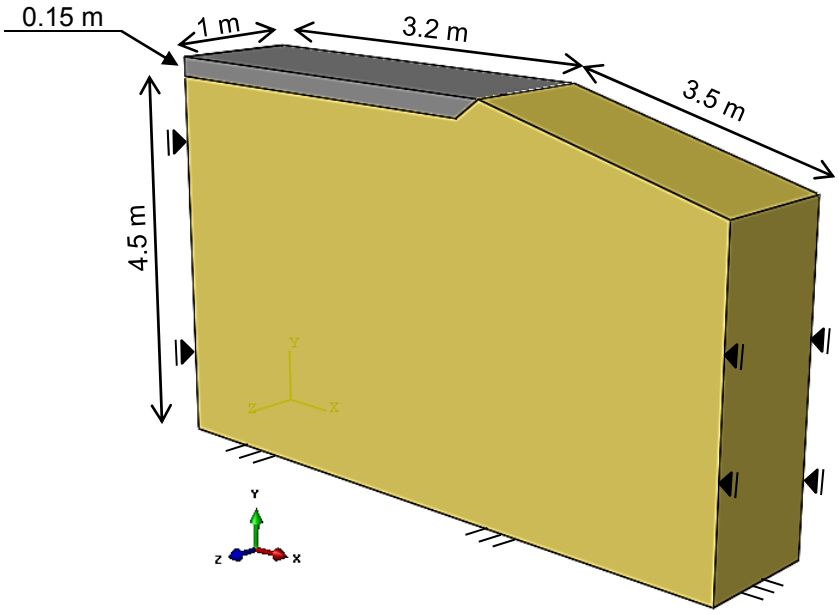

Figure 3. 21: 3D model geometry

3.4.2. Boundary Conditions

3.4.2.1. Structural Boundary

The bottom of the model was fixed in all directions and considered motionless. To allow vertical movement, the sides of the model were only fixed in horizontal directions. Lateral fixtures also represented confining pressure at depth. Top of the model was not fixed in any direction.

3.4.2.2. Pore Fluid Flow Boundary Conditions

Suction boundary conditions represented pore water pressure and initial moisture content. As ground water table was observed at 4.5m below surface, the boundary condition at this depth was defined by assigning zero suction at the bottom of the model. After initial assignment, suction was let to increase linearly up to the surface. Based on linear suction distribution and SWCC material definition, Abaqus evaluated the moisture content corresponding to the suction value at each depth. In other words, moisture content and suction in any element, reflects the SWCC that is assigned in material

definition. Several interactions were performed to reach an equilibrium between soil suction, moisture content and capillary action.

3.4.3. Subgrade Moisture Diffusion/Deformation Modeling

A coupled stress fluid flow approach was used to model the unsaturated flow in soil porous medium. This means that in material definition, the effects of both surcharge and suction on soil parameters were considered. Interactions between deformation-stress-suction were defined through the constitutive surface described earlier. Results of tests performed by Hossain (2013) were used to define the surface, as explained below.

3.4.3.1. Element Type

Three dimensional C3D8P elements were used to perform coupled stress/displacement -pore fluid flow analysis. This element is a continuum stress/displacement, three-dimensional, linear hexahedron element type, which allows pore pressure to vary. Therefore, it is most suitable for flow analysis.

An initial mesh size of 10 cm was selected. Several models were run with decreasing element sizes and it was noted that deformation results tend to converge to a single value as the element size decreases. However, model output did not improve with elements smaller than 45mm. Therefore, this value was selected as the mesh size.

3.4.3.2. Material Definition

Linear elastic behavior was selected to model clay. This is a reasonable assumption since deformation due to swelling and shrinkage usually does not enter the soil plastic behavior zone. In addition, repeated cycles of swelling and shrinkage results in over consolidation of the soil, which increases the elastic portion of the matrix's stress strain curve. Other soil parameters were obtained from laboratory analysis, as summarized in Table 3. 7. Research has shown that in volume change modeling, resilient modulus has the lowest impact on accuracy of the model.

Table 3. 7: Soil properties

Soil properties	value
Void ratio	0.75
Bulk density	15.6 kN/m^3
Poison ratio	0.3
Modulus of elasticity	35MPa
Specific gravity	2.73

3.4.3.3. Unsaturated Flow Modeling

To model the flow and moisture distribution, relations between moisture content and suction (SWCC) should be defined. Permeability function can be predicted based on the determined SWCC.

In Abaqus, this behavior is defined using “sorption” material property which explains absorption and exsorption of a partially saturated porous medium in coupled flow and stress analysis. The curves represent the soil’s water characteristics curve while measured under wetting and drying. Based on Abaqus internal definition, any assigned moisture content should have a suction value that is between boundary wetting and drying curves of the SWCC; i.e. the hysteresis loop. Examples are shown as points A and B in Figure 3. 22.

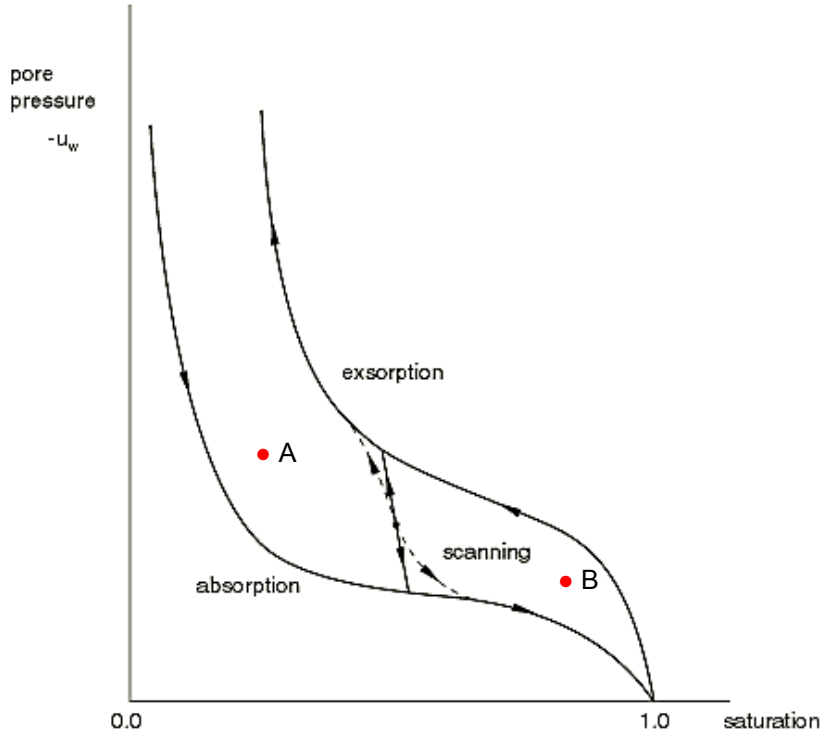

Figure 3. 22: Limiting curves of the SWCC (Abaqus manual, 2013)

Results of Hossain (2013) were used for sorption definition. As stated previously, the author proposed parameters of van-Genuchten formula to mathematically explain suction versus volumetric water content of the soil. Degree of saturation was defined as:

$$S = \frac{\theta - \theta_r}{\theta_s - \theta_r} \qquad \text{Eq. 3. 6}$$

Where:

S = Degree of saturation

θ = Volumetric water content at any suction

θ_r = Residual water content

θ_s = Saturated water content (suction=0)

After calculations of SWCC for two different surcharge values, the curves of sorption material properties were defined as Table 3. 8.

Table 3. 8: Sorption material properties

Suction (kPa)	σ=25 kPa VC ω = 29.5%	σ=50 kPa NVC ω = 29.5%
-1	0.99	1
-10	0.98	0.99
-100	0.92	0.94
-1000	0.65	0.70
-10000	0.40	0.45
-100000	0.24	0.31
-1000000	0.15	0.19

Transition between two curves happens along almost straight lines known as scanning curves, with usual slopes of 1.25 (Abaqus Manual, 2013). Sorption and exorption curves were defined separately, resulting in more accurate estimations of subgrade water balance.

3.4.3.4. Definition of Permeability Function

Abaqus is capable of solving nonlinear equations to consider unsaturated permeability and flow within a coupled stress flow analysis. Initially the saturated permeability (k_s) and in-situ void ratio (e_0) were defined, as measured in the laboratory. Afterwards, relative permeability was calculated using Maulem (1976) equation as below.

$$\mathrm{k_r} = \Theta^{1/2}[1 - \left(1 - \Theta^{1/\mathrm{m}}\right)]^{\mathrm{m}} \qquad \text{Eq. 3. 7}$$

Where:

$\mathrm{k_r}$ = Relative permeability = $\frac{k}{k_s}$

Θ = Degree of saturation

m = vanGenuchten parameter for SWCC data fitting parameter

Unsaturated permeability of the soil was defined as “saturation dependence” sub option while defining the permeability function. Input values are shown in Table 3. 9.

Table 3. 9: Relative permeability sub option (k_s=3.54×10^{-7} m/s, e_0=0.75)

saturation	σ=25 kPa, VC ω = 29.5% m=0.17	σ=50 kPa, NVC ω = 29.5% m= 0.19
0.1	0.32	0.31
0.2	0.445	0.44
0.4	0.63	0.62
0.6	0.77	0.76
0.8	0.85	0.82
1	1	1

3.4.3.5. Moisture Swelling

The moisture swelling model defines the saturation-driven volumetric swelling of a porous medium in partially saturated flow conditions. It can be used in the analysis of coupled wetting liquid flow and porous medium stress. The moisture swelling model assumes that the volumetric swelling of a porous medium's solid skeleton is a function of the saturation of the wetting liquid in partially saturated flow conditions, i.e. when pore water pressure (u_w) is below zero. The swelling behavior is assumed to be reversible and happening within the elastic zone of the soil. Based on Abaqus internal definition, logarithmic measure of swelling strain is calculated with reference to the initial saturation so that

$$\varepsilon_{ii}^{ms} = r_{ii} \times \frac{1}{3}\left(\varepsilon^{ms}(s) - \varepsilon^{ms}(S^I)\right) \qquad \text{Eq. 3. 8}$$

Where:

ε_{ii}^{ms} = Strain in ii direction

$\varepsilon^{ms}(s)$ = Volumetric swelling at the current saturation

$\varepsilon^{ms}(S^I)$ = Volumetric swelling at the initial saturation

r_{ii} = Ratio of anisotropic swelling (=1 for isotropic conditions)

To model volumetric deformation of the soil due to moisture variation, volumetric swelling strain, ε^{ms}, should be defined as a tabular function of the wetting liquid saturation, *S*. Hossain (2013) reported results of SWCC considering volume change of the sample and measured soil's shrinkage as it lost moisture. The volumetric strains corresponding to suction/saturation at each SWCC data point were calculated as below and shown in Table 3. 10:

$$\varepsilon^{ms} = \frac{\Delta V}{V_0} \qquad \text{Eq. 3. 9}$$

Where

ΔV = Volume change due to decrease in suction

V_0 = Initial volume at zero saturation

Table 3. 10: Moisture swelling behavior

ε^{ms}	S
0.013	0.22
0.074	0.31
0.127	0.46
0.181	0.54
0.199	0.64
0.235	0.66
0.251	0.70
0.273	0.72
0.302	0.78
0.359	0.81
0.402	0.87
0.422	0.95
0.432	0.97
0.438	1

3.4.3.6. Step Definition

The model was run in several modes and steps. The initial step was used to define the overall condition and predefined values of the model which represent the model in time zero. During this step, the initial void ratio and pore pressure throughout the model were assigned. In addition, the weight of the soil material was defined using a geostatic stress field distribution, where vertical stresses corresponding to the vertical component of the model were assigned. Abaqus is able to extract vertical stresses in the points lying within. This type of procedure is usually the first step of a geotechnical analysis, followed by a coupled pore fluid diffusion/stress or static analysis procedure. Application of a geostatic stress field procedure allows the user to verify that the initial geostatic stress field is in equilibrium, with applied loads and boundary conditions. Otherwise, the displacements corresponding to the equilibrium state might be large.

After the initial step, a geostatic stress step was defined, during which, the source of the previous vertical stress was established. In other words, by defining this step, it is ensured that the model has weight, but no displacement. This is particularly important if the model is going to have stress analysis. The weight of the soil material was assigned by defining the gravitational acceleration equal to -10m/s^2.

The following steps were defined in “soil, consolidation” mode. In this mode, the model was loaded by applying surface pore pressure on the model side slope to represent rainfall infiltration. Two types of modeling were performed:

1. Loading real time rainfall as recorded at the field: In this case, real time volume change of the soil was modeled and compared to the field recordings. Results are shown in Chapter 4.

2. Loading of individual rainfall amounts selected based on rainfall return period of the area: This trend is part of the parametric study, which is explained in section 3.5.

Results of the volume change modeling were used to measure stress development inside the pavement structure.

3.4.4. Model Calibration

Before initiation of simulation, the model was calibrated for both unsaturated flow and volume change, using laboratory results and field observations.

Rainfall and field moisture content values of December 25, 2012 were used for calibration. A number of simulations were performed until the observed moisture contents in the model were in good agreement with the sensor recordings.

For volumetric deformation modeling, the material properties of the model were used to replicate the swelling test that was earlier performed in the lab. The samples size and confinement were used and the seating load was applied. The model was let to absorb moisture from the bottom and the corresponding swell was simulated. The material properties were slightly adjusted so that the model output would reflect the laboratory-measured values. The results are discussed in Chapter 4.

3.4.5. Pavement Structural Modeling

The ultimate goal of subgrade deformation modeling is to determine the subsequent effects on pavement section. Excessive subgrade movement may result in initiation of tensile micro cracks, which will propagate into macro cracks as the environmental loading is repeated. To obtain a clear idea of the cracking due to environmental factors, stress increase caused by subgrade swelling was modeled and analyzed. The process of pavement structural analysis due to environmental loading is explained below.

3.4.5.1. General Descriptions of Model

A three-dimensional model was used to model hot mix asphalt structure in Abaqus environment. Element type C3D8R for stress analysis was used which allows three dimensional stress without considering pore pressure. That is a valid assumption since the pavement is impermeable. The model was built based on actual field measurements with unit length of the pavement profile. General coordinates of the model were as shown in Figure 3. 21. The asphalt layer was considered a homogenous, isotropic, nonlinear, elastic plastic material placed on natural ground, as instructed by TxDOT manual for farm to market roads. The thickness of the asphalt layer was 0.15^{m}. The width of the model was 3.2^{m}, as measured in the field. The general dimensions of the elements were 4.5^{cm}, to be compatible with size of the elements of the subgrade.

The asphalt section was loaded to simulate the load of passing vehicles. Based on surveys, most vehicles passing on FM roads are sedans, pickups and delivery trucks. AASTO suggests considering the ESAL of the vehicles, as shown in Figure 3. 23.

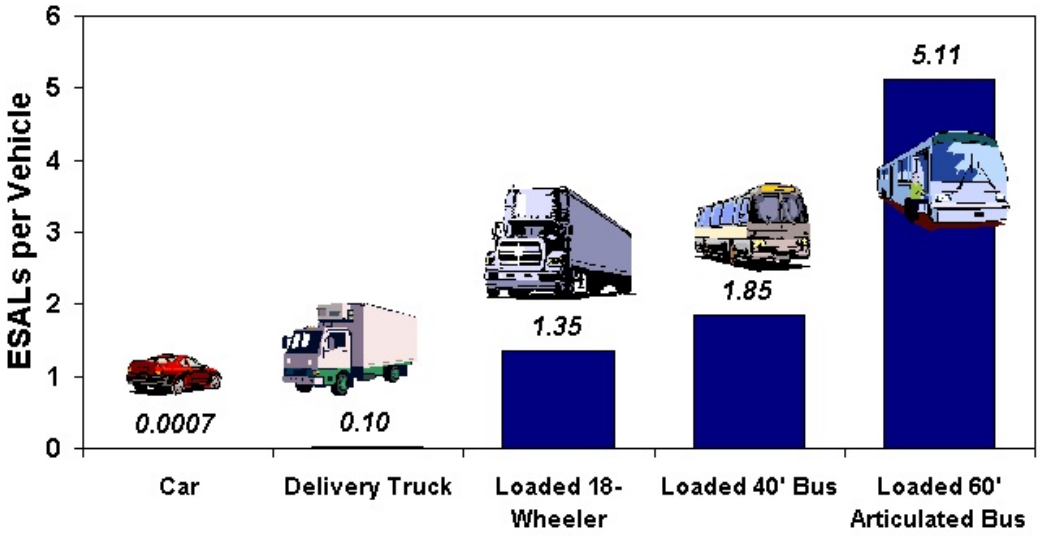

Figure 3. 23: ESAL of different vehicles

To determine the average ESAL, the assumptions in Table 3. 11 were made. The weighted average load was determined as 0.035ESAL or 2.8KN. Therefore, the load on each tire would be 2.8/4=0.7 KN, which was statically applied on the model at locations corresponding to the wheel path (Figure 3. 24).

Table 3. 11: Assumptions to determine the ESAL (=18 kips or 80 KN)

Item	Assumption
Passing vehicles	400/day
% Sedan	50%, ESAL=0.0007
% Pick up 2-Axle Single Unit Truck	30%, ESAL=0.05
% Delivery, 2 Axle single unit truck	20%, ESAL=0.1

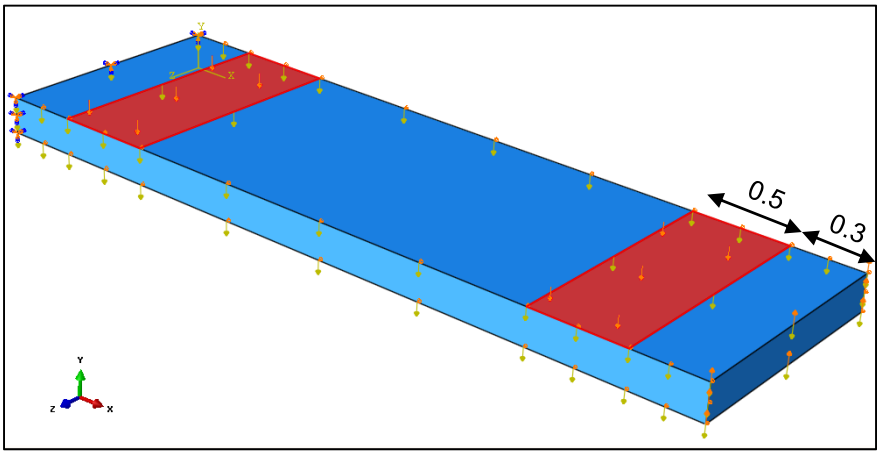

Figure 3. 24: Loaded model (dimensions in m)

3.4.5.2. Material Definition

As stated previously, the asphalt section was assumed to be isotropic, homogenous and elastoplastic. Properties of the mix ingredients, including bitumen, aggregates and additives are the major parameter determining the asphalt stress strain behavior. However, for the same mix, the material properties are significantly affected by

temperature. Behavior of asphalt concrete changes from brittle in colder climates to more ductile as the temperature increases. As wide range of temperatures in the upper range of annual variation is experienced in Texas, this factor was considered in modeling and parametric study. Stress strain curves reported by FHWA were used to define the behavior. The properties of asphalt concrete pavement under different temperatures are reported in Table 3. 12 and shown in Figure 3. 25.

Table 3. 12: Material definition of asphalt concrete

	Compression		Tension	
	σ_f (kPa)	ε_{crush}	σ_f(kPa)	ε_{crack}
T= 5°C	8400	0.036	2780	0.004
T= 25°C	4000	0.04	1600	0.007
T= 40°C	2000	0.045	750	0.008

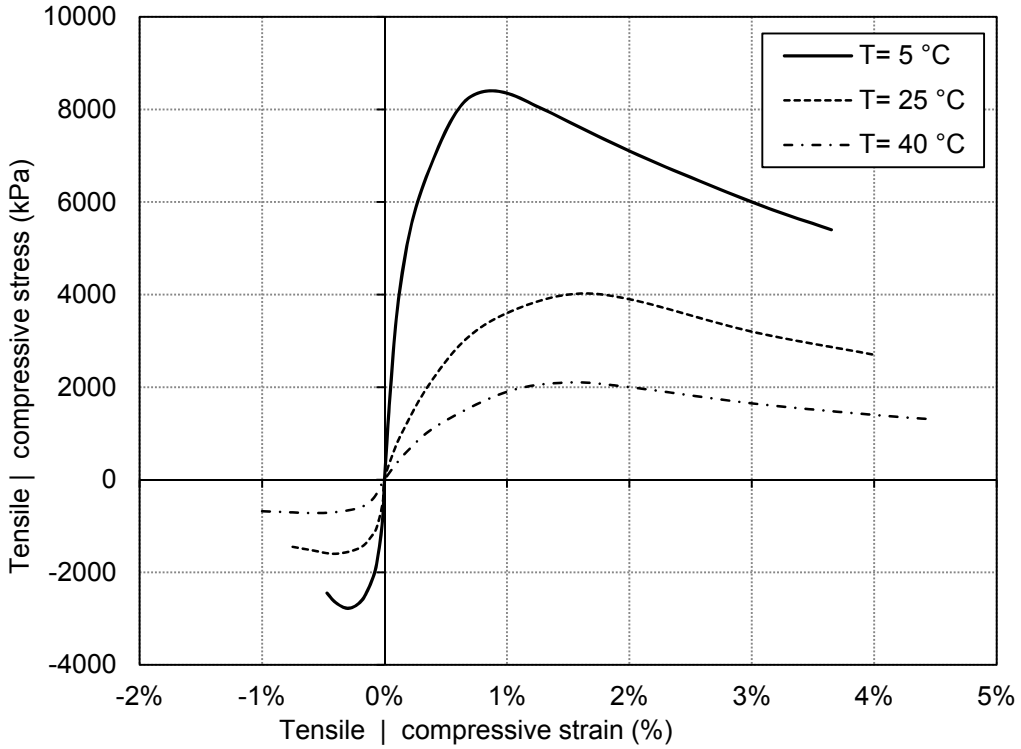

Figure 3. 25: Stress strain curve of asphalt concrete in different temperature

It is obvious that the failure stress of the asphalt mix significantly reduces with increase of temperature, while the maximum strain increases. During the tension test performed at T=40°C, no clear yield stress is observed and the material strains until failure occurs. This case simulates behavior in summer, when the mix has more tolerance towards applied strains. Three different models with variable stress strain curves were constructed and loaded under similar deformation conditions to analyze the effect on temperature on performance of asphalt concrete mix.

3.4.5.3. Failure Criteria in Numerical Modeling of Asphalt Concrete

In mechanics, three modes of fracture are usually assumed; i.e., mode I; opening, mode II; sliding and mode III; tearing (Figure 3. 26). In case of pavements constructed on expansive soils, most of the failure happens on mode I, due to excessive tensile stresses.

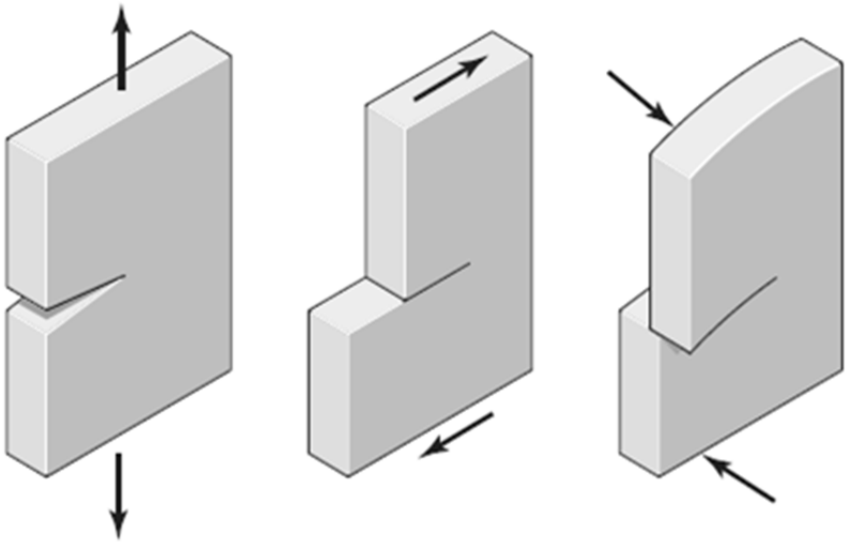

Figure 3. 26: Modes of fracture in a part, from left to right: I, II and III

Usual failure criteria in asphalt pavement were considered, including:

1. Excessive deformation due to static uniaxial loading:

In this criterion, tensile strain through the model was measured and compared with maximum tensile strain of the material. Section fails if

$$\varepsilon > \varepsilon_t \qquad \text{Eq. 3. 10}$$

Where:

ε = Maximum strain

ε_t = Maximum tensile strain prior to fracture initiation

This case is particularly valid when maximum tensile strain is more limiting than compression strain.

2. Damage theory: D=50%

Damage theory due to repetitive loading is one of the widely used criteria. It is assumed that the section loses some of its stiffness as the load repeats. Modulus of elasticity is measured after each load application and the section is considered failed when the elasticity modulus reaches below 50% of its original value. Damage is defined as:

$$D = 1 - \frac{E\prime}{E} \qquad \text{Eq. 3. 11}$$

Where:

D = Damage

E' = Reduced modulus of elasticity due to damage

E = Initial modulus of elasticity

Conversely, damage above 50% is not acceptable.

Both of the stated criteria were initially considered; however, since the load was static and repetition was not modeled, damage could not be measured. Therefore, the failure criterion was confirmed as excessive tensile strain.

3.5. Parametric Study and Model Development

To study the response of the pavement to variable climatic events, it was further evaluated through a parametric study. Various parameters considered in this study were:

1. Overall rainfall return period: The rainfall was selected based on the rainfall return period provided by the National Oceanic and Atmospheric Administration (NOAA), as shown in Table 3. 13.
2. Rainfall intensity: Based on the records of data loggers in the field, the range of rainfall intensities for North Texas area was obtained and used for the parametric study. The highest value for the rainfall was measured as 80mm, which happened over 3 hours, equal to 0.04cm/min. However, to include unpredicted intense rainfall in modeling, the range included from 0.01cm/min to 0.1cm/min, by 0.01 intervals.

Table 3. 13: Rainfall overall volume and return period

return period (Yr.)	Rainfall (cm)
2	6.75
5	12.5
10	15
25	17.5
50	20
100	22.5

3. Duration of the rainfall: The duration of the rainfall varied between 10min to 1440min. For each rainfall, the duration continued until the overall rainfall (intensity times duration) exceeded the 100 years return period.

4. Temperature of the surface: This parameter was defined as variable stress strain curves, as described before. The target temperatures were 5, 25 and 40 degrees, as they were available in the FHWA database.

Different combination of environmental loading and structural properties of pavement were considered, as presented in Figure 3. 27.

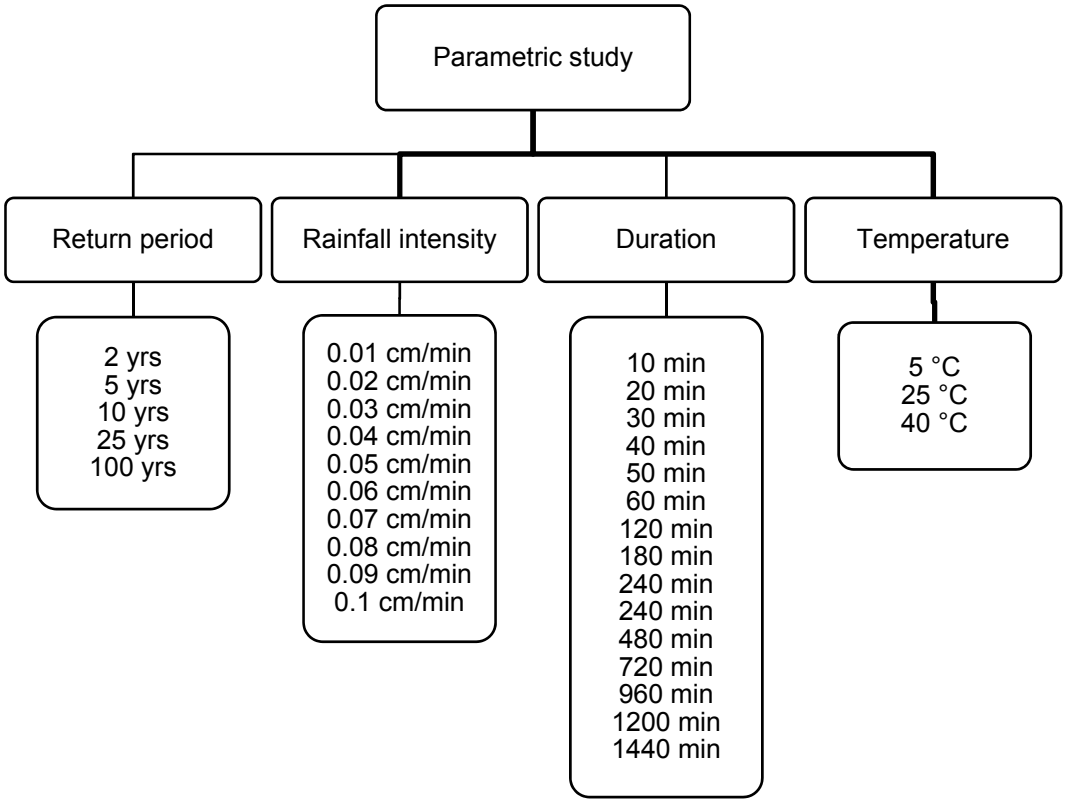

Figure 3. 27: Parametric study variables

Chapter 4

Results and Discussion

In this chapter, results of all of the research processes are presented, discussed and compared with existing literature. Field instrumentation outputs, including moisture and temperature variation and deformation monitoring are outlined. Results of interpretation in Matlab environment are stated and the proposed model for moisture/temperature variation is explained. Numerical modeling conclusions and finite element analyses are subsequently shown followed by pavement section stress analysis. Statistical evaluation and developed model are presented at the end.

4.1. Field Instrumentation and Results

4.1.1. Sensor Calibration

Moisture is the most sensitive parameter to measure in the field. To ensure acceptable performance, the sensors were tested and calibrated before installation. Moisture content of several samples was manually determined and compared with sensor measurements (Cobos and Chambers, 2010). Measured values along with probe outputs and 97% and 99% confidence bands are shown in Figure 4. 1.

It was observed that the recorded values showed good agreement with manually measured volumetric moisture contents. Sensors reported values within 97% accuracy. The calibration factor was defined as the slope of the scatter plot and applied to field measurements to adjust the sensors' readings.

$$f\ (calibration\ factor) = \frac{\theta_{sensor}}{\theta_{manual}} = 0.947 \qquad \text{Eq. 4. 1}$$

In addition, the initial recording of the sensors in the field were matched with the gravimetric water content that was determined earlier. A period of two weeks was allowed for moisture sensors to adjust to the environment. After this period, the results were downloaded and used for interpretation.

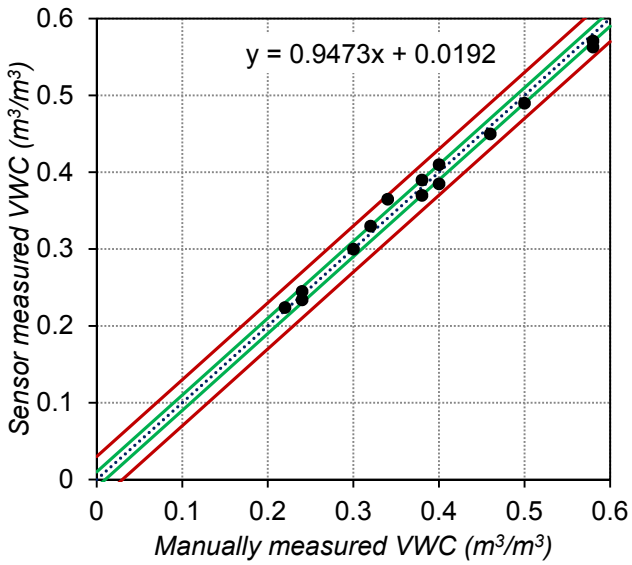

Figure 4. 1: Calibration of sensors

4.1.2. Moisture Content Variation

Results of moisture content variations in pavement subgrades are shown in Figure 4. 4 to Figure 4. 4. The results represent data collected over a two-year monitoring period from April 2012 until April 2014. Among 14 original sensors, 13 were installed successfully. However, during operation, four became unresponsive and reported either negative or above-saturation values. Survival rate of the moisture sensors after two years of operation was close to 70%.

4.1.2.1. Moisture Variation along Pavement Centerline (B.H.1)

Moisture measurements of three sensors, TM1/2, 1/3 and 1/4, located at 2.4, 3.6 and 4.5m respectively, are shown in Figure 4. 4. A general decrease in the average moisture content (0.416, 0.377 and 0.298, respectively) was observed with increase in depth. Variations recorded by TM1/2 and 1/3 were similar, while TM1/4 showed a slightly different pattern.

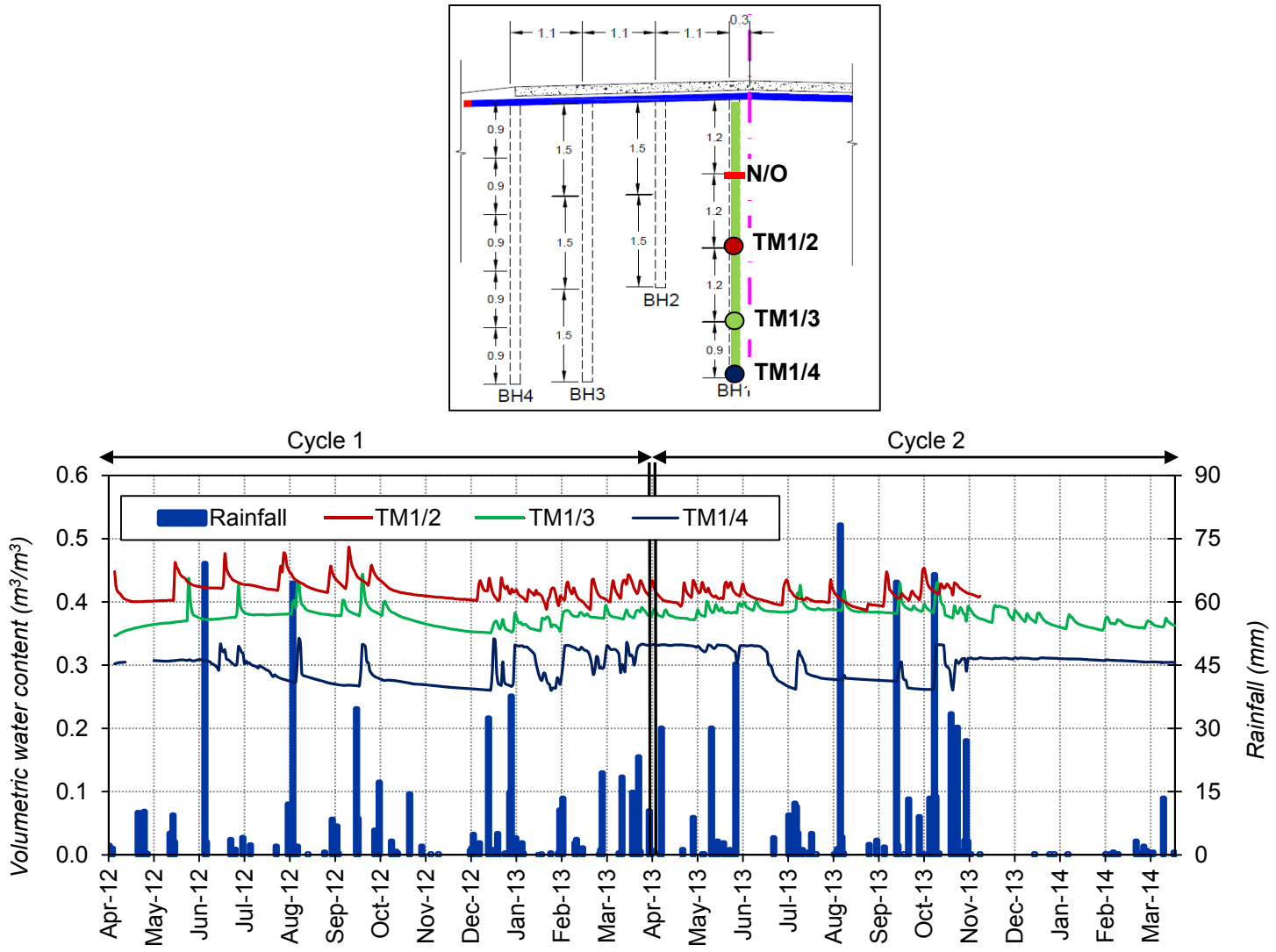

Figure 4. 2: Moisture variation time series: centerline

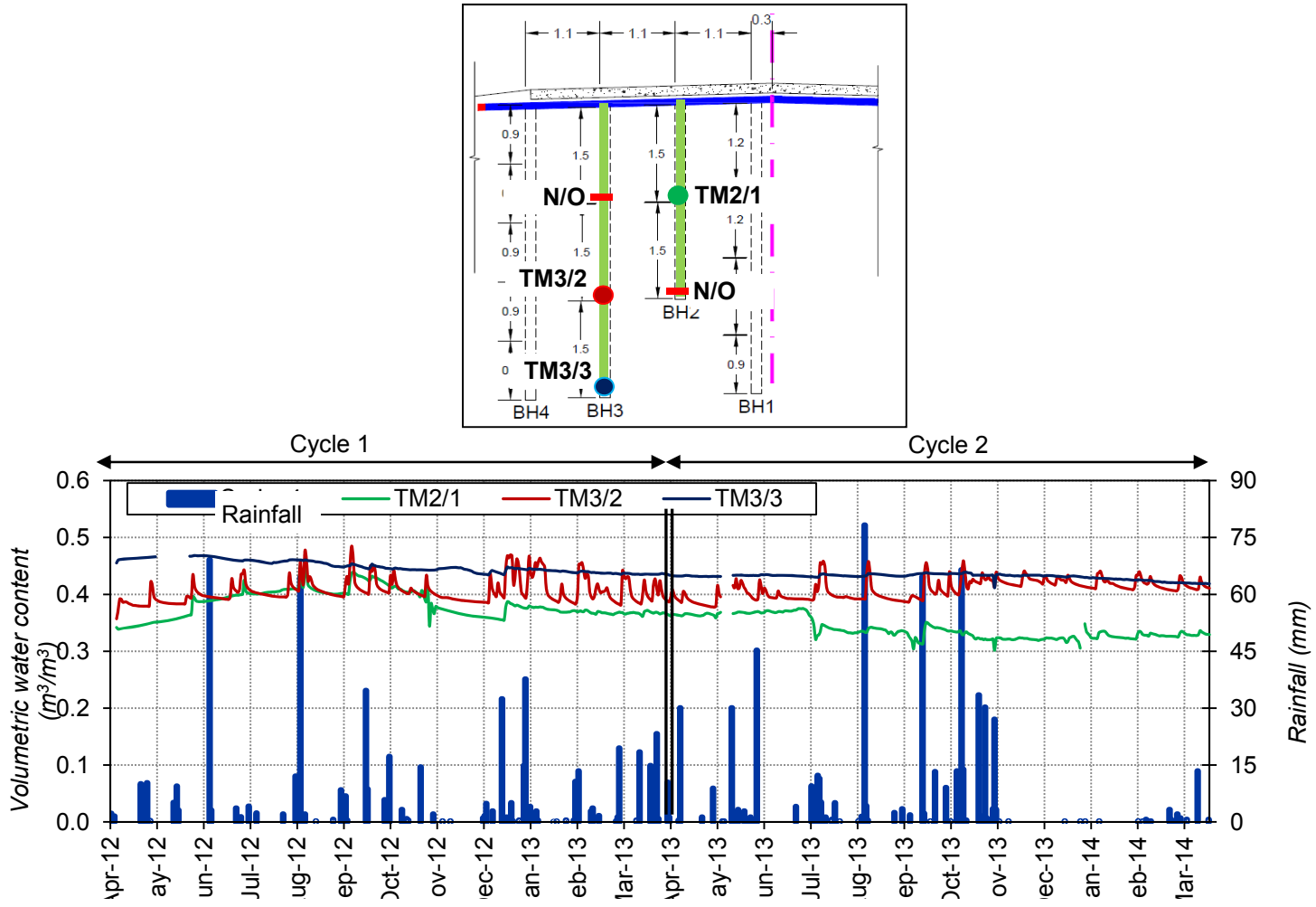

Figure 4. 3: Moisture variation time series: inner and outer wheel paths

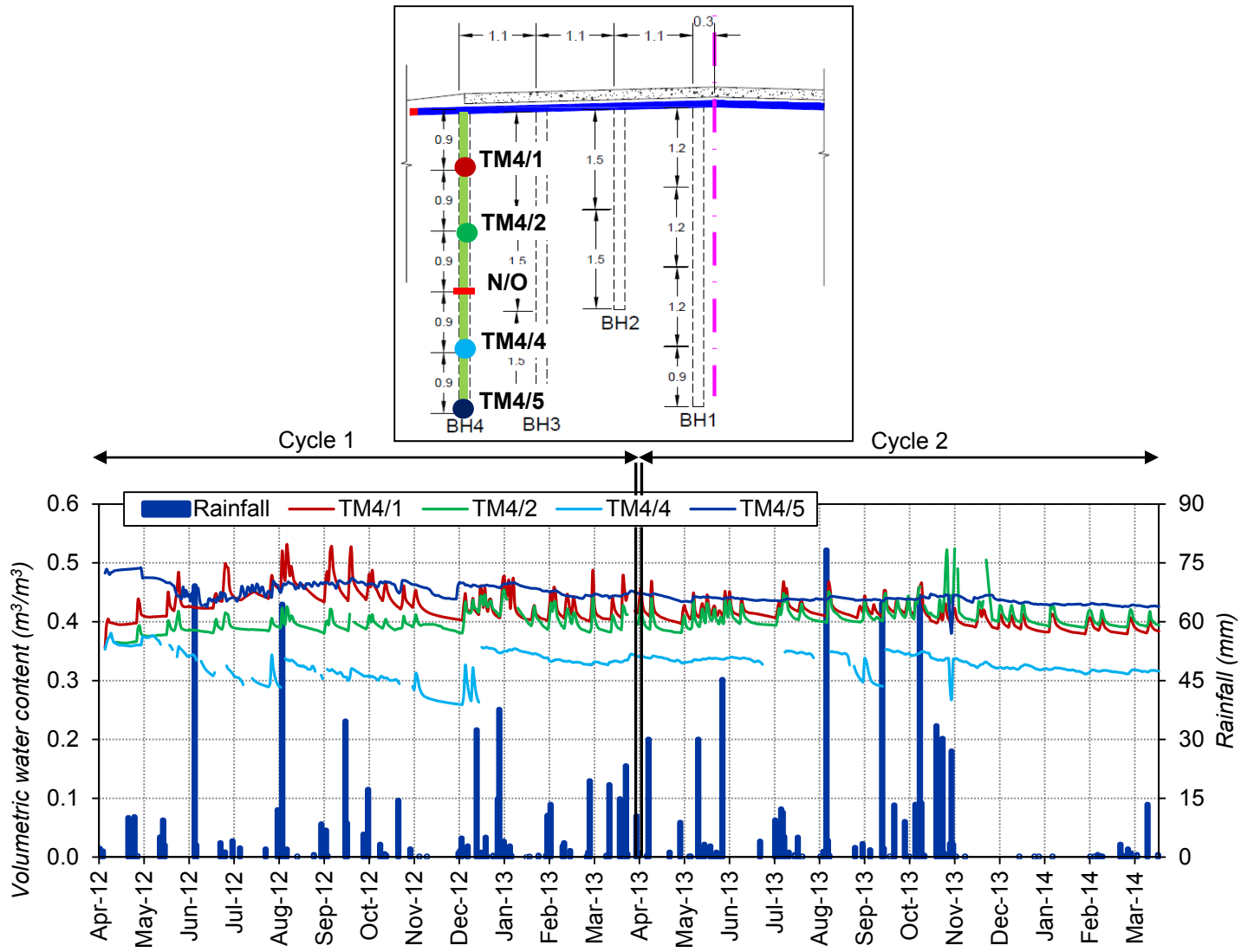

Figure 4. 4: Moisture variation time series: pavement edge

The overall trend of TM1/2 and TM1/3 can be explained as a combination of seasonal pattern and temporary saturation due to climatic loading. The general seasonal trend peaked during summer (wet season) with an average rainfall over 150mm while lowest average water content was recorded in winter toward the end of the dry season. The domain of seasonal variation was between 0.419 and 0.393 for TM1/2 and 0.385 and 0.360 for TM1/3. The usual increase in water content as a result of climatic loading was between 15 to 20% of moisture content at the time of rainfall. The temporary increase in water content happened as the wetting front passed downward, which temporarily saturated the soil. This anomaly dissipated as the soil returned to its field capacity and reached a new equilibrium with surrounding environment.

Sensor TM1/4 reported that the soil remained fairly saturated during the wet period of January to June 2013, during which accumulated rainfall was approximately 222 mm. The high volumetric water content reported during this period was 0.331 m^3/m^3, which can be due to the recharge and rise of the groundwater table that was initially recorded at 4.5m depth. Excessive water infiltration due to rainfall accompanied with low evaporation, resulted in soil maintaining its moisture content and preservation of excessive water. The moisture content decreased with the decrease of rainfall and increase of evaporation. Although the considerable variation of moisture could cause significant volume change, it is expected that high surcharge load at this depth prevented further swelling. This is in line with results of swelling tests previously performed in the laboratory. No significant moisture variation was noticed in winter 2014 as a result of low climatic loading.

4.1.2.2. Moisture Content under the Driving Lane (B.H. 2 and B.H.3)

Sensors installed in boreholes 2 and 3 reported moisture variations in inner and outer wheel paths, respectively (Figure 4. 3). Based on records of sensor TM2/1 installed

at 1.5 m depth, a slight seasonal trend was observed during the first cycle. The peak value was noticed in August 2012, similar to moisture variations at centerline. After this period, the sensor did not report any significant variation due to rainfall and had small fluctuations around an average moisture content equal to 0.361 m^3/m^3. The seasonal trend did not continue as well and the moisture content became unresponsive except on a few occasions. This may be due to stabilization of the soil structure around the sensor installation points and formation of a bypass plane for moisture passing around the sensor. The average moisture content reported by this sensor was measured as 0.346 m^3/m^3.

On the other hand, recordings of sensor TM3/2 installed under the outer wheel path at 3m depth, showed more sensitivity to the rainfall in a pattern similar to recordings of TM1/2 and TM1/3. A combination of seasonal and temporal moisture variations was observed. The initial cycle had a peak in August-September 2012, which can be attributed to total rainfall of 150mm during previous months. The outcome of cumulative rainfall between September to November 2013, was observed at a peak in December 2013. It seems that the seasonal trend is mostly dominated by intense consecutive rainfalls, which prevents moisture dissipation. The average measured moisture content was 0.407 m^3/m^3. Temporary increase in moisture content was between 15 and 20%, in line with recordings of previous sensors.

TM3/3, located at 4.5m depth, maintained a presumably constant value of approximately 0.435 m^3/m^3. No visible variations, high moisture content and deep installation depth indicated that variation pattern is mostly dictated by presence of ground water table. Full saturation of the soil prevents any variation while fluctuations happened between maximum and minimum values of 0.467 and 0.423 m^3/m^3. High normal stress along with lack of moisture variation prevents soil layer to experience volume change.

4.1.2.3. Moisture Variation along the Edge of the Pavement (B.H.4)

Among the five originally installed sensors, four are operating successfully. Sensors installed at the edge of the pavement showed the most sensitivity to rainfall events (Figure 4. 4).

The same combined pattern of seasonal variations and temporary responses to rainfall was observed in TM4/1 at 0.9m and TM4/2 at 1.8m. For TM4/1, the seasonal trend peaked in August 2012 and had it lowest value in February 2013, and the pattern was repeated in 2013-2014. Loss of moisture was specifically significant due to a dry period between November 2013 and March 2014. Average moisture content recorded by this sensor was 0.405 m^3/m^3. Rainfalls caused a temporary increase in moisture content equal to 18.6% on average. This increase usually dissipated 6-12 hours after rainfall.

Temporary and seasonal increases in moisture content were less significant in TM4/2. A slightly higher average water content was observed in August 2013. The trend also tended to increase in summer 2012. The lowest water content was observed during a severely dry period between November 2013 and March 2014. The average water content recorded by this sensor was 0.385 m^3/m^3. Rainfalls caused between 10-15% of temporary increase in water content.

Recordings of TM4/4 at 3.6m showed sensitivity to rainfall events and were hard to interpret. However, the trend of moisture dissipation did not happen instantly. Instead, a steady decrease in water content happened at 1×10^{-4} m^3/m^3/day, which was observed in gradual moisture loss during periods of May 2012 to November 2012, December 2012 to August 2013 and September 2013 to March 2014. This trend may indicate the presence of a saturate zone and capillary fringe above groundwater table, which prevents additional increase in water content. Average moisture content for this sensor was 0.332 m^3/m^3.

Recordings of TM4/5 at 4.5m were close to TM3/3. High and almost constant water content recorded by this sensor indicated that the moisture content is mostly dominated by groundwater, which is compatible with field observations during installation. Average water content recorded by this sensor was 0.435 m^3/m^3.

4.1.2.4. Evaluation and Discussion of the Recorded Pattern

Among the sensors with interpretable trends, 4 were selected for model development, while two were kept for validation. Based on the overall observation, moisture content variation of the soil layers can be summarized as Table 4. 1 and explained as below.

Table 4. 1: Summary of the recorded moisture contents

Operating sensor	Dist. from C.L. (m)	Depth (m)	Observed behavior				Average VWC (m^3/m^3)	Usage*
			Seasonal	Temporary	Constant	Uninterp.		
TM1/2	0.3	2.4	✓	✓			0.406	D
TM1/3	0.3	3.6	✓	✓			0.377	V
TM1/4	0.3	4.5				✓	0.331	---
TM2/1	1.4	3	✓	✓		✓	0.361	D
TM3/2	2.5	3	✓	✓			0.407	D
TM3/3	2.5	4.5			✓		0.435	D
TM4/1	3.6	0.9	✓	✓			0.405	V
TM4/2	3.6	1.8	✓	✓			0.385	D
TM4/4	3.6	3.6				✓	0.332	---
TM4/5	3.6	4.5			✓		0.435	D

* D: model development; V: model verification

1. Deep located sensors: Behavior of these sensors is mostly dominated by the presence of groundwater table. These sensors maintained approximately constant water content at high values. Examples include TM4/5 and TM3/3, both at 4.5 m.

2. Shallow located sensors: Such sensors show a seasonal trend combined with temporary increase due to climatic events. These sensors are located within the

active zone and affect the swelling behavior of the soil significantly. Examples include TM4/1, TM4/2, TM1/2 and TM1/3.

3. Sensors located at mid depth: Soil around these sensors tend to maintain an increase in moisture content for extended periods of time, while also being affected by the climatic factors. Examples include TM4/4 and TM1/4. It seems both proposed trends move towards equilibrium as the depth increases. The overall trends can be plotted as the contours shown in Figure 4. 5.

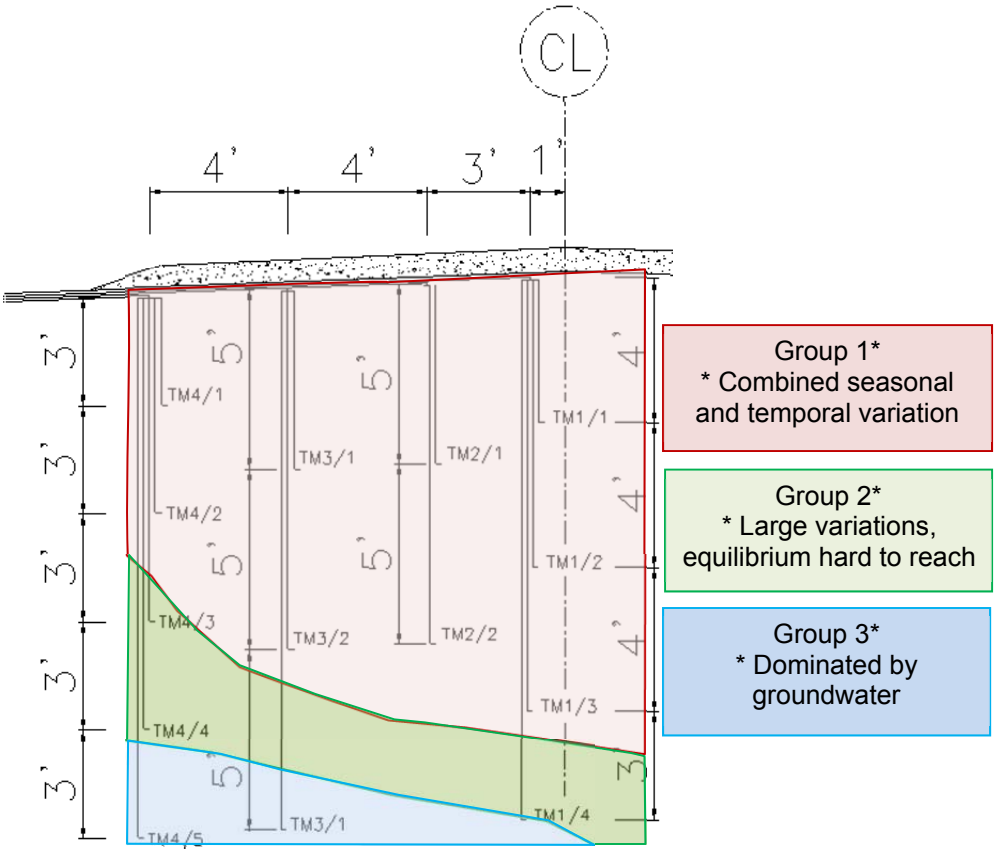

Figure 4. 5: Contour plot of moisture variation under pavement cover

The plotted contours can be used to determine the range of variations of many soil parameters including suction, permeability, deformation, shearing strength and resilient modules. Nguyen (2006) observed a similar pattern for suction variation in

subgrade of a 2-lane pavement site in Canada, as shown in Figure 4. 6. It is observed that the determined moisture pattern resembles suction contour and the zone of large variations is mainly refrained to side slope area with suction variation between 100-466 kPa. Lower suction values of 54 to 88 kPa were maintained at depth. The author suggested that the overall suction variation contour can be plotted as Figure 4. 6-b. It should be noted that suction varies logarithmically with moisture content. Therefore, larger variations of suction should be expected in response to smaller moisture variations.

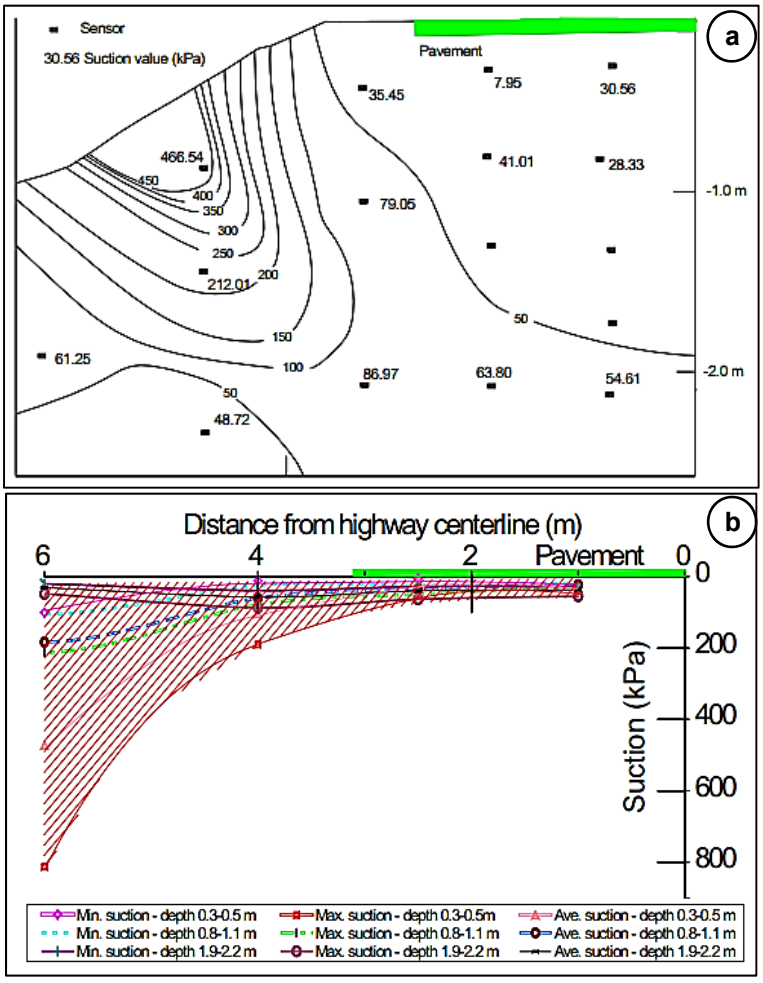

Figure 4. 6: Contour plot of suction variation (Nguyen, 2006)

Based on measured data and the magnitude of the moisture variation, Kodikara et al (2014) proposed dividing the soil profile into three layers of different moisture variations. On a smaller scale, the authors classified the soil layers beneath the surface as three layers: shallow, mid-depth and deep (Figure 4. 7). In shallow depths, the moisture content of the soil layer is highly sensitive to climatic conditions, and percentage variation of the moisture content can vary between -21 and +34% of the original measured value. On the other hand, deep layer moisture content can vary between -14 and +16%, showing a limited range of variation. These layers are considered less important in swelling and shrinkage calculations due to less moisture variation and presence of high overburden pressure. Although the seasonal classification is widely explained, the authors did not consider local variations in their model. Also the zone of variation in that study was limited to 800mm, which does not cover the depth of active zone.

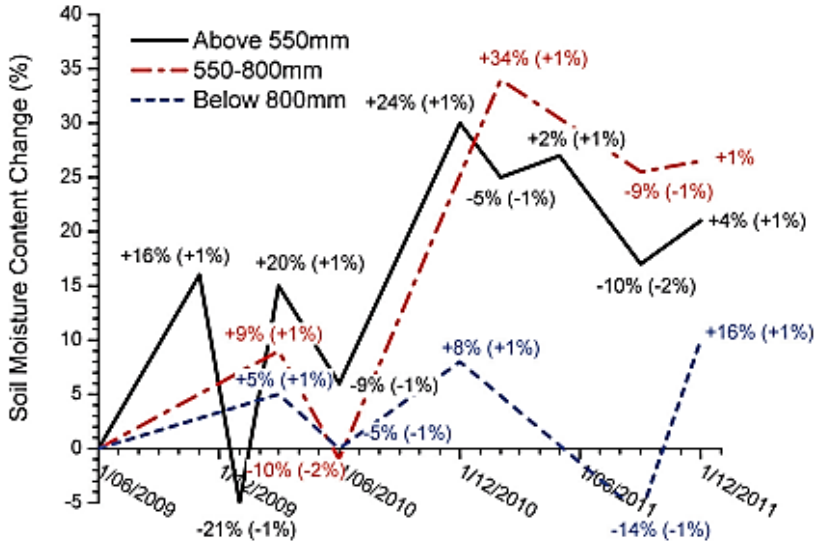

Figure 4. 7: Soil zoning, as performed by Kodikara et al (2014)

The overall observation of moisture content variation indicated that moisture is not constant under pavement surfaces, especially in case of narrow two-lane, low-volume pavements. Temporary saturation happens in a shorter timeframe, while increasing the water content between 10-20%.The seasonal trend happens in longer periods without changing the water content significantly. Therefore, the effect of temporary climatic loading is significant and cannot be neglected in estimating moisture variation/subgrade deformation patterns.

This observation challenges the Mechanistic Empirical Pavement Design Guide. For design purposes, AASHTO suggests using an equilibrium moisture content under covered areas to determine soil parameters such as resilient modulus and shear strength (AASHTO, 2004). Such hypothesis is supported by several researchers, indicating that moisture content beneath pavements reaches an equilibrium condition several years after construction (Aitchison and Richards, 1965; Basma and Al-Suleiman, 1991; Richards, 1965) while it still can alter seasonally (Zapata et al, 2009). This is mainly based on the assumption that the pavement is impermeable. Zapata et al (2009) argue that although the moisture may tend toward an equilibrium, fluctuations around the equilibrium moisture content may be observed that rise from two sources: freeze thaw cycles and fluctuation of groundwater table. However, in arid and semi-arid regions, where the two aforementioned cases are not common, the variations are considered insignificant and moisture is considered constant. This assumption can be greatly affected by considering the temporary effect of climatic loading.

Based on the recordings presented in this study, all sensors recorded sensitivity to rainfall events even if installed under the pavement. Sources of moisture sensitivity can be either moisture infiltration from surficial pavement cracks or lateral transport of water from pavement edge toward the pavement centerline Figure 4. 8. This indicates that

assuming constant equilibrium moisture content under pavements, especially narrow roadways, may result in inaccurate estimation of soil properties and behavior. Similar variation patterns were observed in researches conducted by Nguyen (2006), Manosuthikij (2008) and Kodikara (2014) and many other studies. However, no model containing both variations has been developed so far.

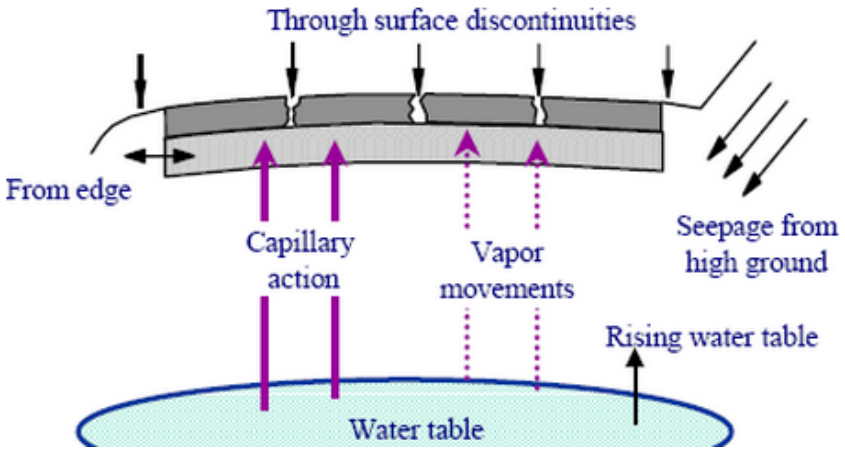

Figure 4. 8: Sources of moisture in pavement systems (FHWA, 2006)

4.1.2.5. Model Development

Records of the moisture sensors indicate that moisture content is not only variable, but has fluctuations in addition to seasonal variations, which can be as much as 20%. Therefore, assuming a rough seasonal pattern for moisture variation can lead to considerable errors in soil parameters and behavior and temporal fluctuations of the moisture need to be considered in the moisture evaluation balance.

To develop the final model, five sensors of interpretable recordings (i.e. TM1/2, 1/3, 3/2, 4/1 and 4/2) were selected. Four sensors were chosen for model development, while one was were used for validation. Non-parametric analysis in Matlab was selected as the data processing procedure. The overall processing was performed in two steps: determination of the seasonal trend and evaluation of the additional moisture variation

1. Determining of the main seasonal trend:

This step was performed by temporarily removing any data outside the main seasonal trend. The data was treated as hypothetical “noise” to the main signal (Figure 4. 9). Zero reference time was set as May 1, 2012.

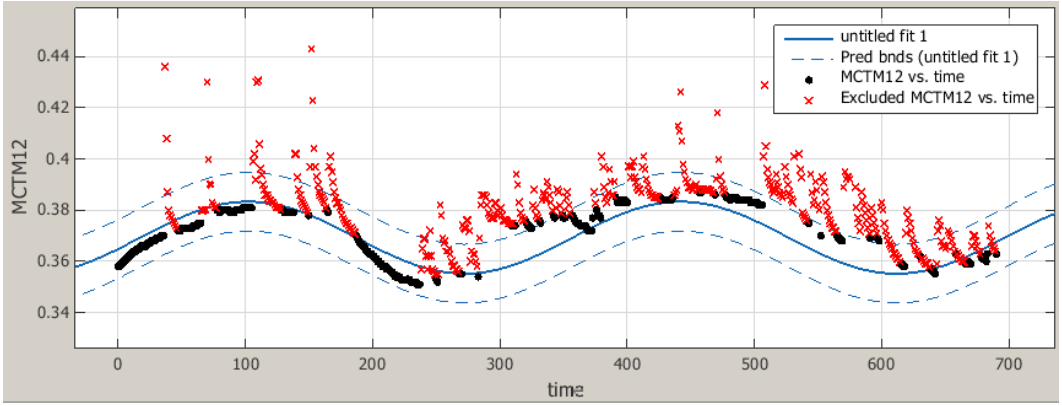

Figure 4. 9: Trending analysis of TM1/2

The seasonal trend can be described as a first degree Fourier series, which is a harmonic analysis and an extremely useful way to break up an arbitrary periodic function into a set of simple terms. In this case, since Fourier series could presented in closed form, analytic solutions were obtained.

The main seasonal trend can be explained as:

$$\theta = \theta_0 + \theta_a Sin(\omega t + C_0) \qquad \text{Eq. 4. 2}$$

Where:

θ = volumetric moisture content (m^3/m^3)

θ_0 = average moisture content (m^3/m^3)

θ_a = domain of variation (m^3/m^3)

ω = frequency (day^{-1})

C_0 = phase correction angle

The analysis was performed for all sensors, and the extracted parameters are shown in Table 4. 2. The output of the model, along with 95% confidence band presented as a dashed red line, is shown in Figure 4. 10.

Table 4. 2: Parameters of main seasonal trend of moisture content

Sensor name	a_0 (m^3/m^3)	a_1(m^3/m^3)	ω (day^{-1})	R^2
TM1/2	0.370	0.0127	0.0172	0.68
TM1/3	0.4112	0.008	0.0172	0.51
TM3/2	0.393	0.006	0.0172	0.59
TM4/2	0.413	0.0188	0.0172	0.53
Average	0.397	0.011	0.0172	----

The series parameters were studied against location of the sensors. Domain of variation, frequency and average moisture content of the sensors were analyzed, as presented in Figure 4. 11.

It was observed that among the three dependent variables, domain of average moisture variation showed the most variation with depth. Trending analysis showed that the function can be best explained through an exponential function with R^2=0.82, as below:

$$\theta_a = 0.053e^{-0.639z} \quad \text{Eq. 4. 3}$$

Where:

θ_a = Domain of variation (m^3/m^3)

z = Depth (m)

The trend indicates that most variation occurs in the shallow depths and it decreases rapidly as the depth increases.

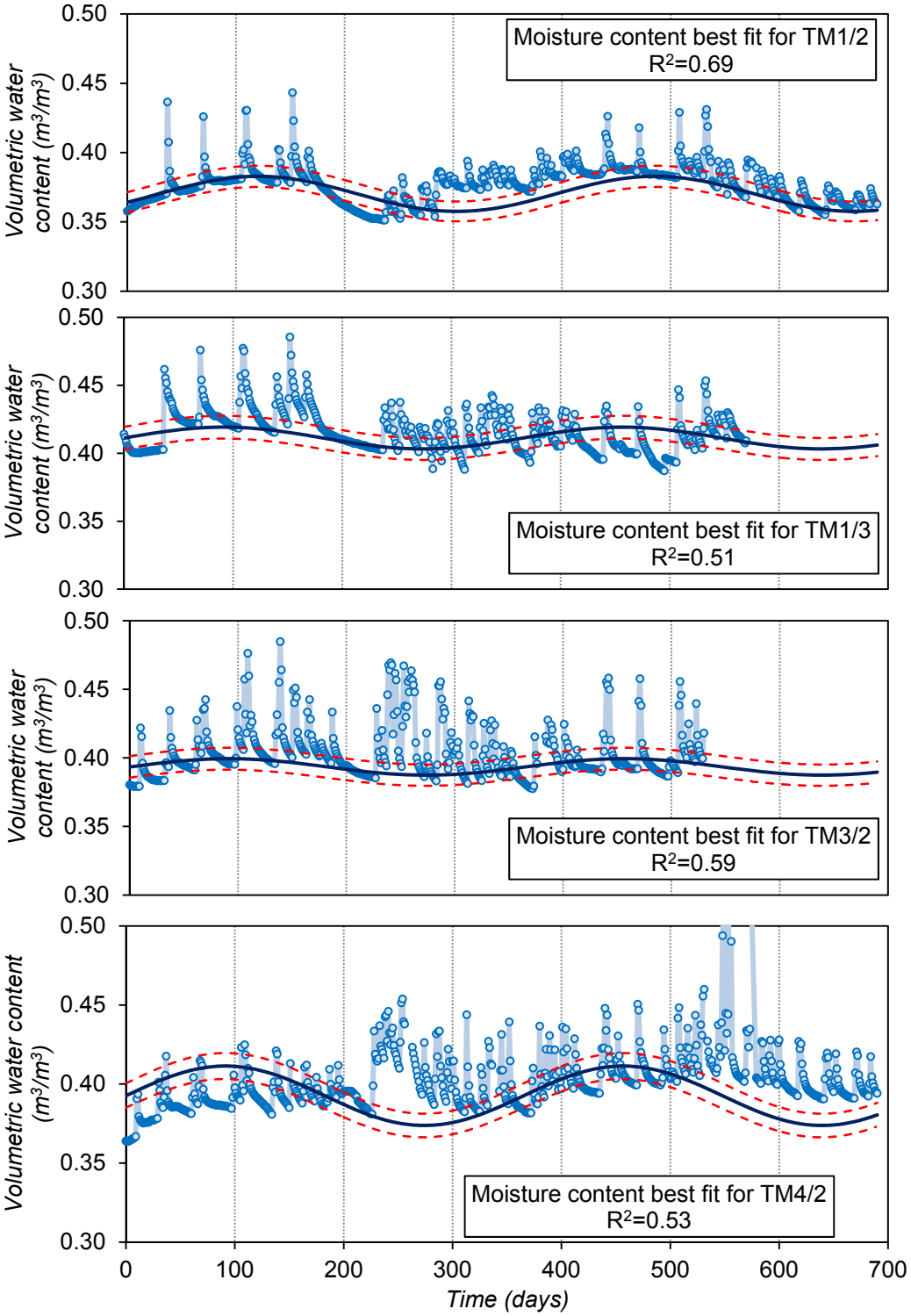

Figure 4. 10: Recorded/fitted data (start time: 21 May 2012)

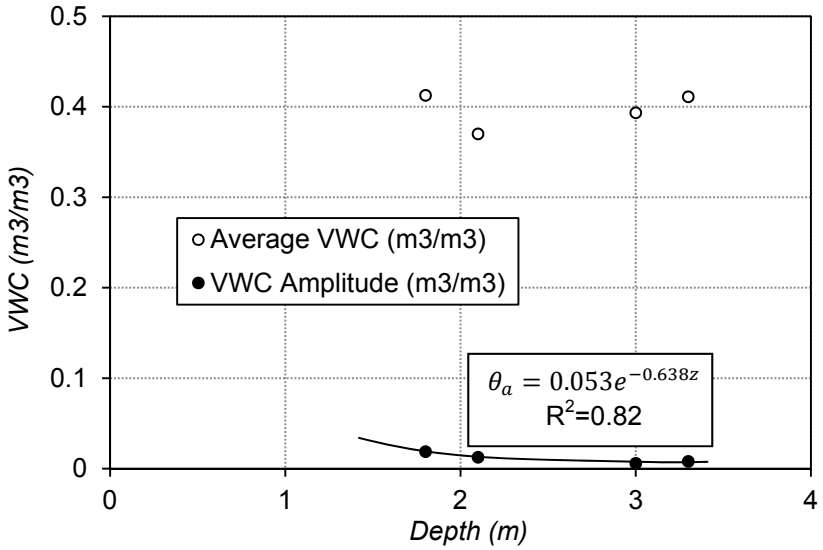

Figure 4. 11: Dependency of moisture variation parameters on sensor location

The average moisture content did not show any particular sensitivity to the depth of the sensor and stayed in the vicinity of the soil's field capacity. In high plasticity clays, this value is close to saturation (average = 0.39 m^3/m^3). In addition, frequency of the data points did not vary with the location of the sensors, which is acceptable as the frequency of moisture variation is a function of climate rather than soil specific properties.

Variations of the parameters were also studied against distance from the centerline of the pavement to find out whether presence of an impermeable cover has affected moisture variation in any way. No particular trend was observed between the horizontal location of the sensor and the trend of moisture variation, which may indicate that presence of a narrow impermeable surface is not affecting the moisture content.

2. Determining the temporary saturation and additional moisture fluctuations

Analysis of the excessive moisture content, also known as the noise data was also performed in Matlab environment. For this stage, the increase of moisture content in excess of main seasonal trend was determined and statistically analyzed for possible

trends. The independent variable was selected as rainfall, while the dependent parameter was studied as net increase and percentage increase. Results of the analysis are displayed in Figure 4. 12.

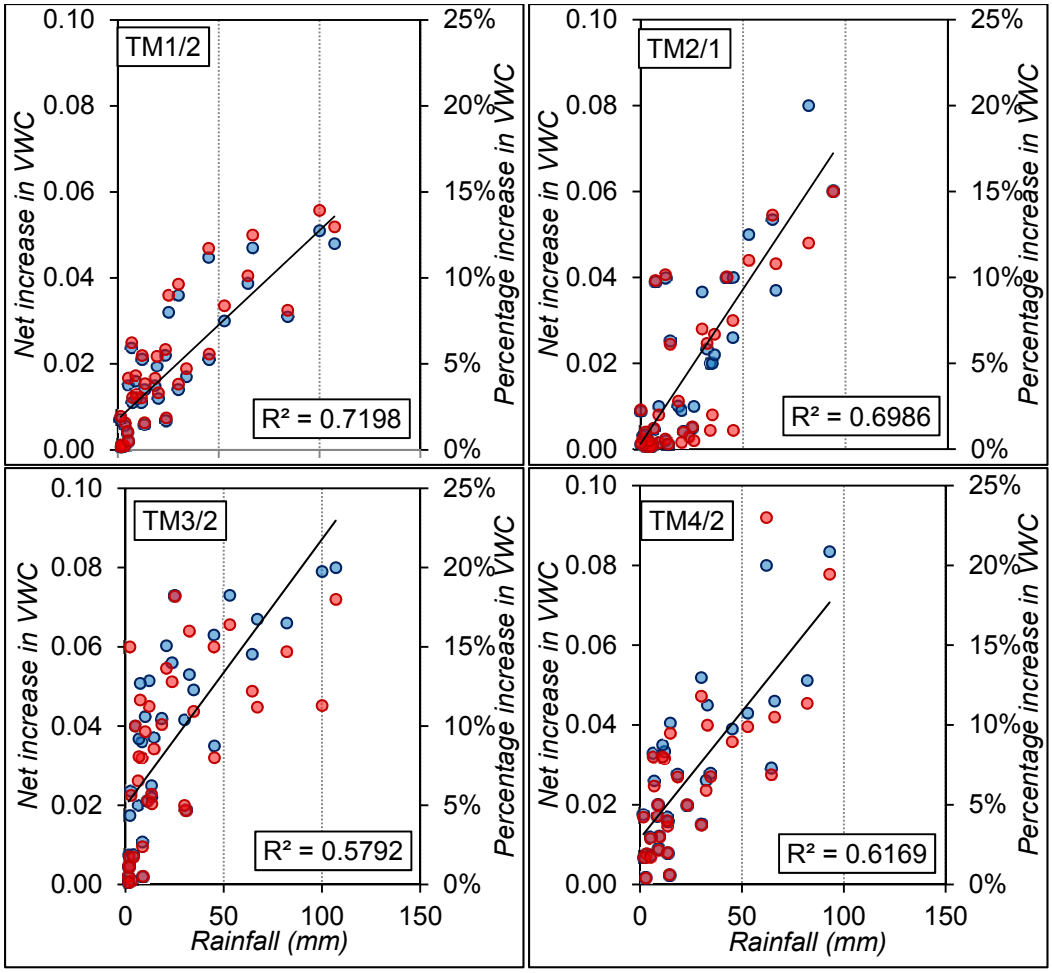

Figure 4. 12: Relation between net/percentile increase in VWC and rainfall, ● net increase in VWC, ● percentage increase in the water content of the soil

Several equations (including exponential, power and polynomial) were considered; however, accuracy of the model did not increase with increasing the complexity order of the equation. It was observed that the net increase in water content as a function of rainfall follows a scattered pattern which can be best described as a

linear function. Both net increase and percentile increase in water content showed the same dependency on the rainfall amounts. Parameters of data analysis for net increase of volumetric water content in response to rainfall are presented in Table 4. 3.

Table 4. 3: Relation between the net increase in water content

Sensor tag number	Slope	Intersection
TM1/2	0.004	0.0071
TM2/1	0.007	0.0013
TM3/2	0.007	0.0199
TM4/2	0.006	0.0116
Average	0.0058	0.0134

As shown in the table, the slope of the rainfall versus net increase in volumetric water content of the soil does not vary with the amount of rainfall. On average, any amount of rainfall may generate 0.006 or 0.6% increase in water content. Therefore, the soil may not experience saturation as a result of rainfall. In fact, the increased water content and the amount of excess moisture that the soil can absorb significantly depends on the current status of moisture content in the soil.

Based on the overall analysis results, moisture content of different soil layers can be explained as:

$$\theta = f(t,z) + f(t,rainfall)$$
$$= [0.397 + 0.053e^{-0.639z}\sin(0.0172t)] + [0.0134 + 0.0058Rain_t]$$
$$= 0.4104 + 0.053e^{-0.639z}\sin(0.0172t) + 0.0058Rain_t \quad \text{Eq. 4. 4}$$

Where

z = Depth (m)

t = Time from an arbitrary staring point (day)

$Rain_t$ =Rainfall defined in time series (mm)

4.1.2.6. Cross Validation

To ensure accuracy of the model, sensor TM4/1 was randomly selected for cross validation. Measured and predicted volumetric water contents of the soil versus time are presented in Figure 4. 13. In addition, accuracy of the model is shown in Figure 4. 14.

It was observed that the model provides acceptable estimations on the overall behavior and is able to capture both seasonal variation and temporary saturation in soil moisture variation. Prediction of TM4/ located outside the pavement cover had very good agreement with the observed trend. Increasing the accuracy of the model during desaturation process can increase the efficiency significantly.

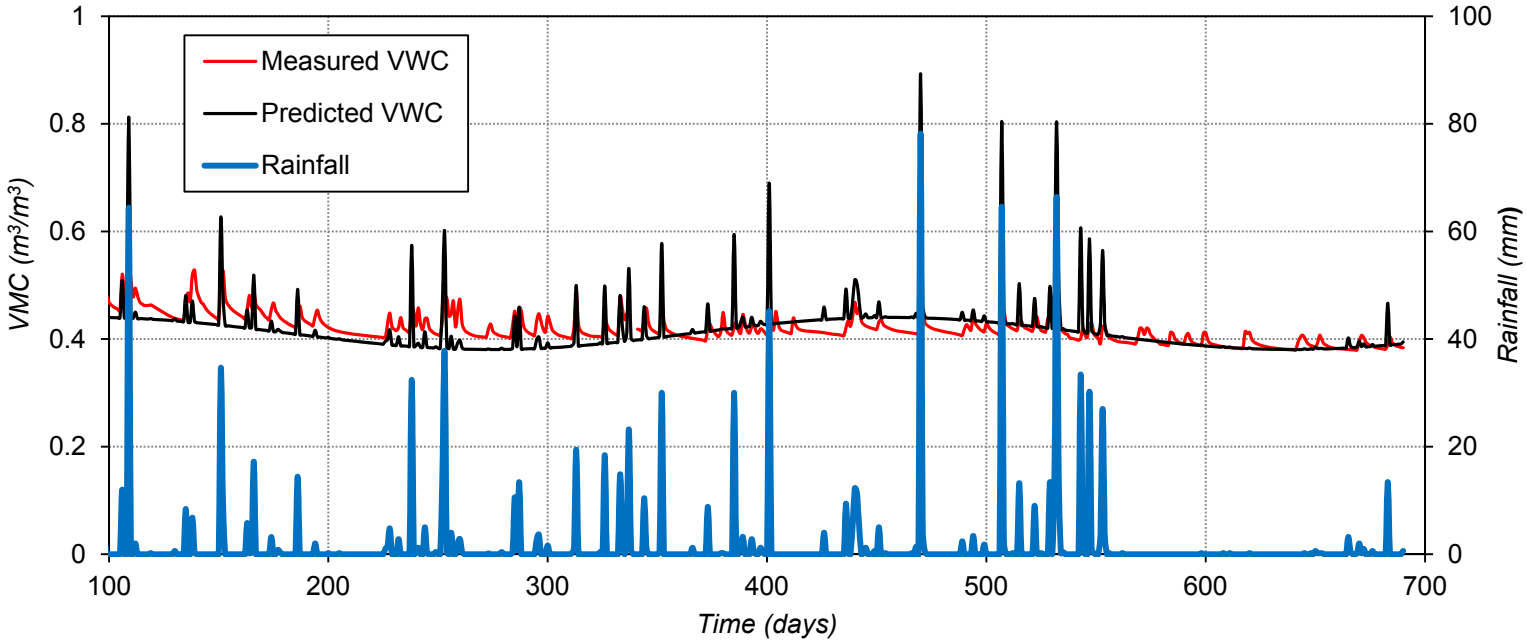

Figure 4. 13: Time series of moisture and rainfall of predicted and measured values and accuracy of the model

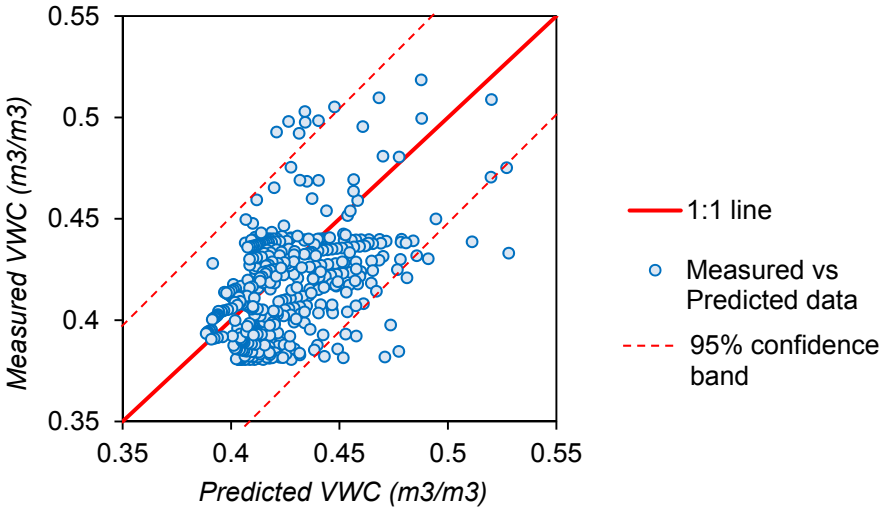

Figure 4. 14: Accuracy of the predicted model

By comparing the predicted and measured values, it was concluded that the model provided coherent results while slightly under-predicting the value. The reason was attributed to rate of desaturation of the soil which was not included in the modeling assumptions. However, comparison of the model outputs with current literature (e.g. Figure 4. 15) makes it evident that the model improved the predictions significantly. Not many moisture-predicting models exist in the literature for comparison purposes.

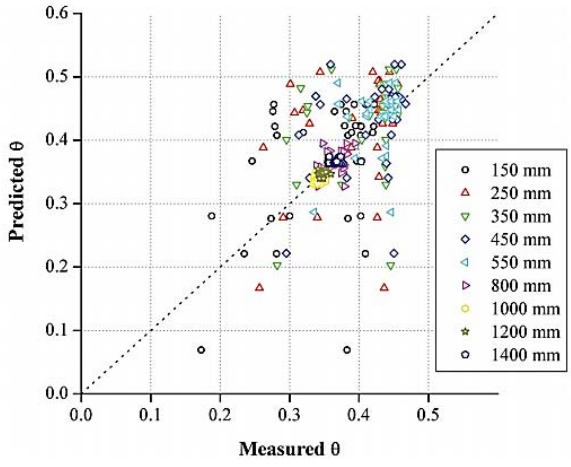

Figure 4. 15: Predicted versus measured moisture content (Kodikara et al, 2014)

4.1.2.7. Analytical Solution

Based on an assumption of seasonal behavior, an analytical solution can be provided for moisture variation in the soil. As stated in Chapter 3, by considering a one-dimensional equation for water balance in the soil, volumetric water content (VWC) as a function of depth can be written as:

$$\frac{\partial \theta}{\partial t} = \frac{\partial}{\partial z}\left(D(\theta)\frac{\partial \theta}{\partial z}\right) \qquad \text{Eq. 4. 5}$$

Where:

θ = Volumetric water content at depth z at time t

D(θ) = Soil moisture diffusivity (material coefficient controlling moisture flow following Fick's law in nonlinear from)

Solving partial differential nonlinear equations is possible by establishing known boundary conditions, including:

1. Surficial soil (z=0) is subjected to harmonic sinusoidal variations, ignoring rainfall induced transient moisture variation.
2. At infinite depth (or at ground water table depth), the soil moisture is constant (it is not affected by surficial climatic events).
3. Moisture diffusivity parameter is independent of time and depth of soil profile and can be determined based on soil type and moisture content. Several studies suggest that variation of moisture diffusivity parameter is limited for moisture content variations observed in the field (Kutilek, 1984). Mabirizi and Bulut (2009) reported moisture diffusivity of clayey soil equal to 1 on average. With constant D parameter, the problem can be solved as a first degree Fourier series:

$$\theta(z,t) = \theta_0 + \theta_a \sin(\omega t - \frac{z}{d} + C_0) \qquad \text{Eq. 4. 6}$$

Where

$\theta_{(z,t)}$ = Soil moisture at depth z and time t

θ_0 = Average soil moisture at depth z over time

θ_a = Domain of moisture variation. Kodikara et al (2014) suggest

$$\theta_a = \theta_s e^{-\frac{z}{d}} \quad \text{Eq. 4. 7}$$

Where θ_s = Saturated volumetric water content

z = Depth

d = Damping depth. Parameter *d* reflects reduction in soil moisture variation with increase of depth and can be estimated as

$$d = \sqrt{\frac{2D}{\omega}}$$

D = Diffusivity

ω = Angular frequency ($2\pi/365 = 0.0172$)

C_0 = Phase correction factor

Determination of the domain of variation ($\theta_a = \theta_s e^{-\frac{z}{d}}$) is compatible with statistical analysis ($\theta_a = 0.1251e^{-0.783z}$). However, a difference is observed between θ_s and the reflecting coefficient in the statistically determined parameter. This is due to the assumption that the soil at z=0, experiences full saturation. However, this can only be true if the surficial soil is under hydraulic loading or is adjacent to 100% humid air. Otherwise, relative humidity will desaturate the soil and reduce its saturation at surface. To consider this issue, it is suggested that the formulation be revised as:

$$\theta_a = k\,\theta_s e^{-\frac{z}{d}} \quad \text{Eq. 4. 8}$$

Where

k = Coefficient of surface saturation, which is a function of environmental conditions. As per current study, k is determined as 0.053/0.39 = 0.136.

Generalized solution for Fourier series can be expressed in form of a summation series as below:

$$\theta(z,t) = \theta_0 + \sum_{N=1}^{\infty} \underbrace{k.\theta_{SN} e^{\left(-\frac{z}{d}\sqrt{N}\right)}}_{\text{Variation amplitude } [A_N(z)]} . \sin\underbrace{\left(N\omega t - \frac{z}{d} \times \sqrt{N} + B_N\right)}_{\text{Phase correction angle } [\Phi_N(z)]} \quad \text{Eq. 4. 9}$$

Where

N = Number of dominant harmonics of Fourier series

θ_S = Volumetric moisture content at the surface ($m^{3/}m^3$)

4.1.3. Variation of Temperature in the Subgrade

Among the 14 original sensors, 13 were successfully installed, 12 of which are operating. The survival rate of temperature sensors was 92%, considerably more than that of the moisture sensors. Temperature variation of the subgrade soil was recorded over the period of two years. The results are presented in Figure 4. 19 to Figure 4. 19. Perfect seasonal temperature variation was observed in all the sensors that reflect the ambient temperature.

4.1.3.1. Temperature Variation in the Pavement Centerline (B.H.1)

Based on initial observations, behavior of all sensors can be explained through a first degree Fourier series. Sensor TM1/1 at 1.2m stopped working after approximately three months. However, final recorded points show that the temperature had reached approximately 35°C and surpassed the ambient value, which may be due to the heat absorption capacity of the soil and presence of dark asphalt pavement.

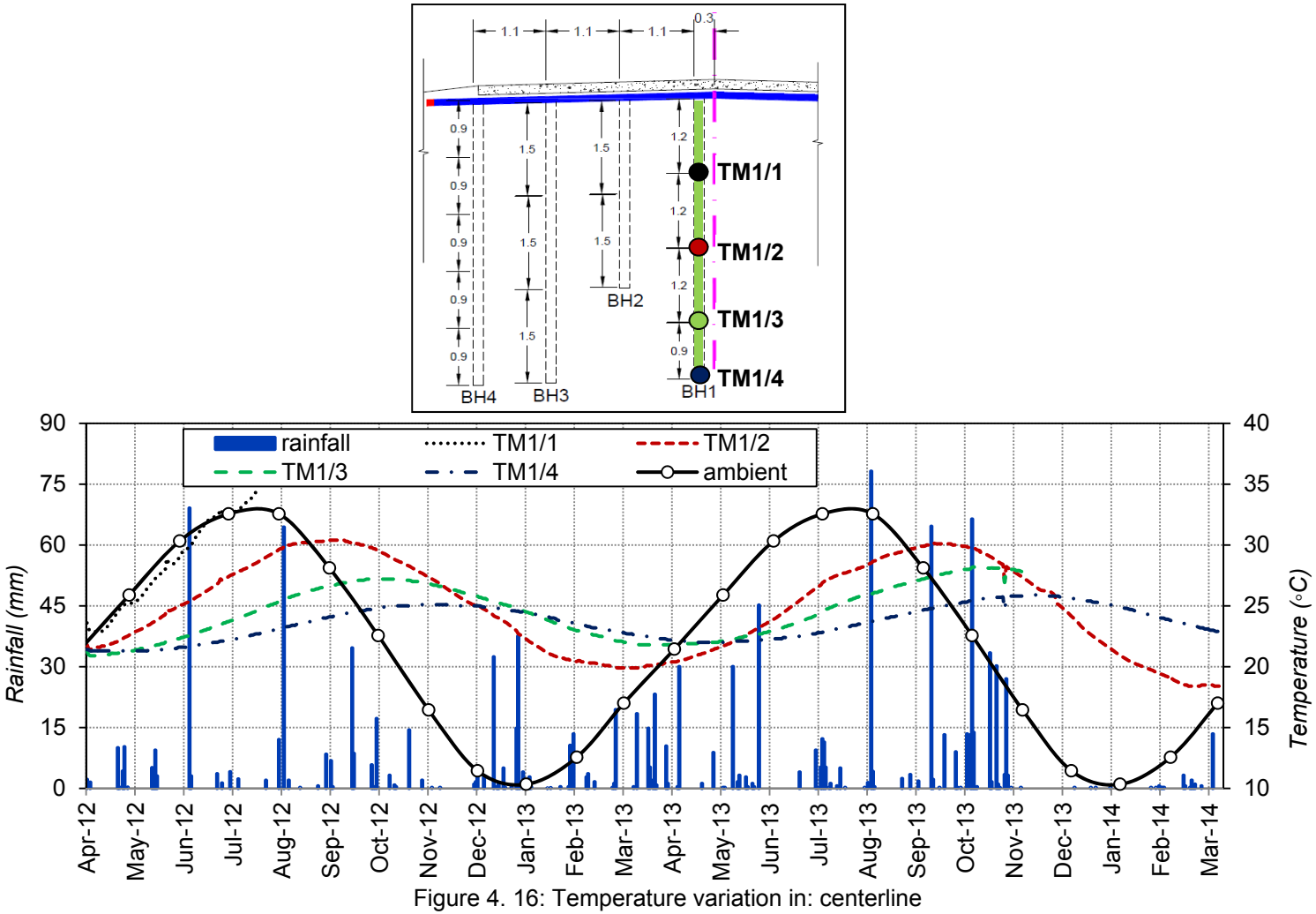

Figure 4. 16: Temperature variation in: centerline

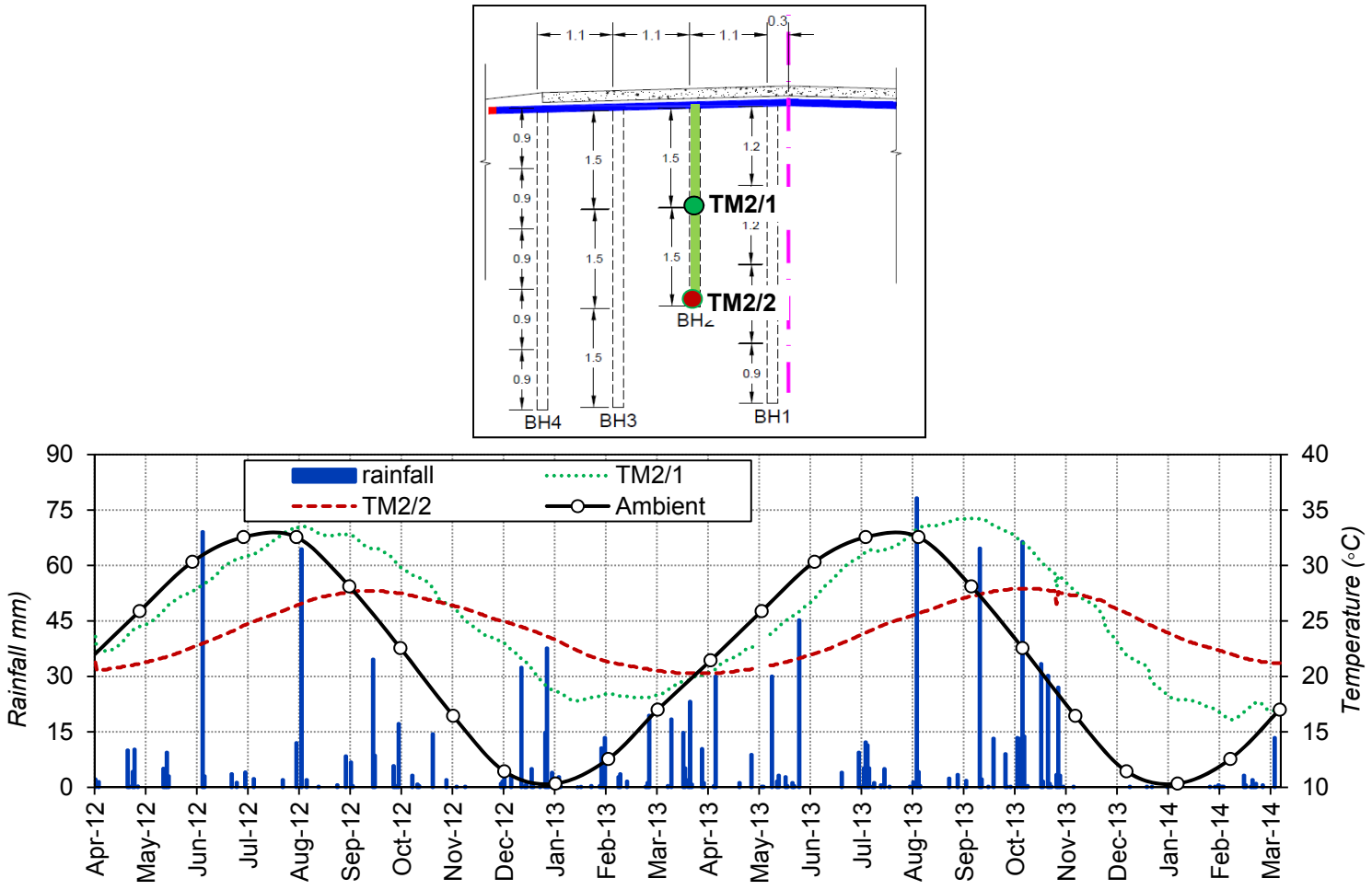

Figure 4. 17: Temperature variation in: inner wheel path

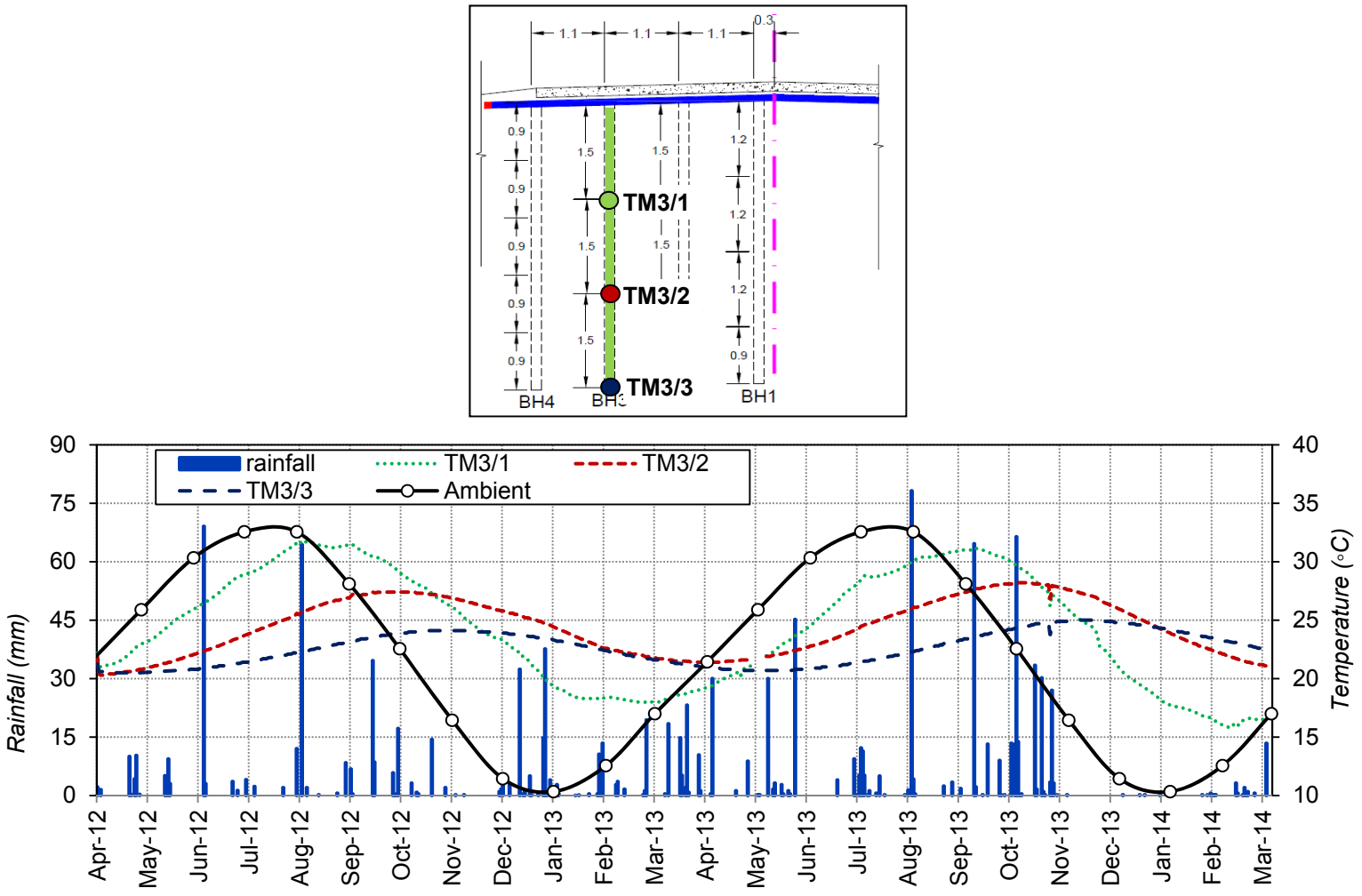

Figure 4. 18: Temperature variation in: outer wheel path

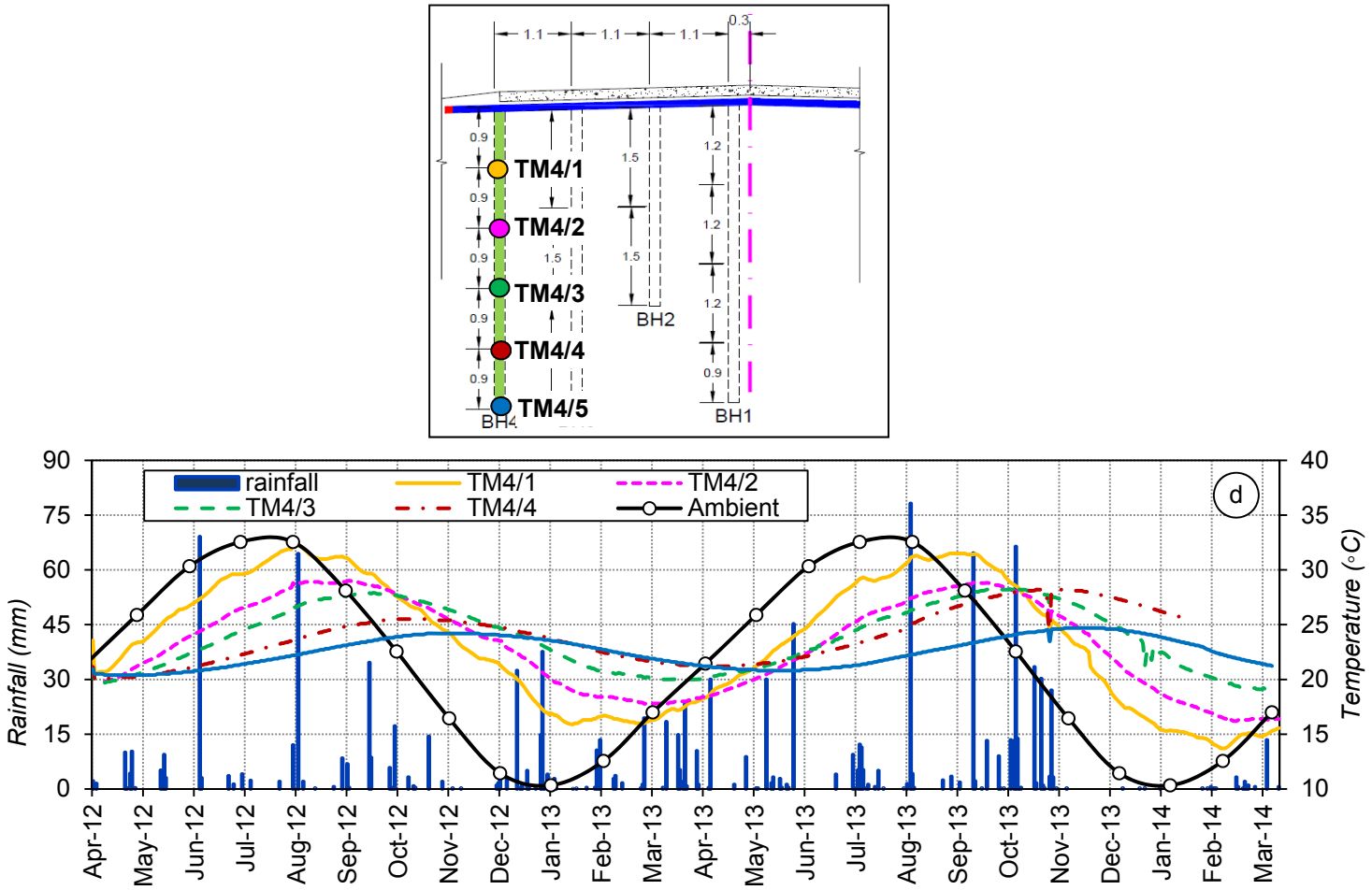

Figure 4. 19: Temperature variation in: pavement edge

TM1/2 peaked in September, almost 45 days after the peak ambient temperature. Maximum and minimum temperatures were 30 and 20 °C, respectively. Domain of variation was measured as 10°C, which was smaller than the domain of ambient temperature variation. It is evident that daily variation of temperature is dissipated and not transferred to this depth.

Records of TM1/3 and 1/4 provided the same pattern of variation with maximum/minimum values of 27.5/20.1 °C and 25/21.8; respectively. Domain of variation is reduces with depth, while the lag time increased to 72 and 101 days; respectively. Because of the high thermal inertia of the soil, the temperature fluctuations at the surface were diminished as the depth increased. Due to variable domain of variation, reverse thermal gradient was observed in winters, resulting in warmer layers at depth.

4.1.3.2. Temperature Variation at the Inner and Outer Wheel Paths (B.H.2 and 3)

Two sensors, TM2/1 and TM2/2, were installed at the inner wheel path, at 1.5 and 3 m, respectively. Peak values for TM2/1 happened in August and February, with values of 32 and 18 °C. For TM2/2, the peaks happened in September and April, with 27 and 20°C. A shift factor from the annual ambient cycle was observed with depth. TM2/1 showed sensitivity to daily temperature variation as small fluctuation around the main seasonal variation. No such sensitivity was observed in TM2/2, which was due to high inertia of the soil.

Three sensors, namely TM3/1 and TM3/2 and TM3/3, were installed in outer wheel path, at 1.5 and 3 m and 4.5m, respectively. A similar seasonal pattern was observed in all sensors. Sensors closer to the surface had more variation as opposed to deeper sensors, and lag time increased with depth, up to four months.

4.1.3.3. Temperature Variation at the Pavement Edge (B.H.4)

Five sensors were installed in this borehole which represented the variation outside the asphalt-covered portion of the road. The same pattern was repeated. Maximum variation was observed at the sensor closest to the surface (TM4/1), while the deeper sensor had the least variation. In addition to the annual cyclic behavior, TM4/1 showed daily temperature variations as well. Again due to thermal inertia of the soil, this trend diminished as the depth increased.

4.1.3.4. Evaluation and Model Development

Temperature variation at each sensor can be characterized with maximum, minimum and average temperatures, as well as the lag time and depth of the sensors, as summarized in Table 4. 4.

Table 4. 4: Summary of the behavior of the sensors with their location

Operating sensor	Dist. From CL (m)	Depth (m)	Temperature (°C)			Lag time (day)	Usage
			maximum	minimum	Average		
Ambient	---	---	32	10	21	----	----
TM1/2	0.3	2.4	30	20	25	45	D
TM1/3	0.3	3.6	27	22	24.5	72	D
TM1/4	0.3	4.5	25	23	24	101	V
TM2/1	1.4	1.5	32	17.8	24.9	23	D
TM2/2	1.4	3	28	20	24	61	V
TM3/1	2.5	1.5	31	18.3	24.65	29	V
TM3/2	2.5	3	27	21	24	66	D
TM3/3	2.5	4.5	24	22	23	110	D
TM4/1	3.6	0.9	33	15	24	31	D
TM4/2	3.6	1.8	29	18	23.5	42	D
TM4/3	3.6	2.7	28	20	24	61	V
TM4/4	3.6	3.6	25	21	23	82	D
TM4/5	3.6	4.5	24	22	23	108	D

* D: model development, V: model verification

The data was analyzed to develop a model for temperature variation. Among 13 provided data, nine were selected for model development, while four were used for verification.

Since the variation is cyclic, first degree Fourier series was used to determine the variation pattern. The generalized solution would be:

$$T(z,t) = T_0 + T_a Sin(\omega t - C_0) \quad \text{Eq. 4. 10}$$

Where:

T_0 = Average temperature at any depth *z* and time *t* (°C)

T_a = Domain of temperature at any depth *z* (°C)

ω = Frequency (day^{-1})

C_0 = Phase correction angle (lag time)

As the data are annual, the frequency is equal to 2π/365. The data were analyzed in Matlab to determine the best fitting parameters; results are summarized in Table 4. 5. The accuracy of the model is shown in Figure 4. 21 and Figure 4. 21.

Table 4. 5: Parameters of temperature variation Fourier series

	T_0	T_a	C_0	R^2 (compared to field data)
Ambient	19.3	12.35	0	0.994
TM1/2	25	5.2	56	0.997
TM1/3	24.1	2.85	93	0.992
TM2/1	25.1	7.55	33	0.996
TM3/2	23.9	3.2	89	1.000
TM3/3	22.3	1.75	119	1.000
TM4/1	23.4	7.85	29	1.000
TM4/2	23.3	5.6	51	1.000
TM4/4	22.89	2.42	101	1.000
TM4/5	22.31	1.8	119	1.000

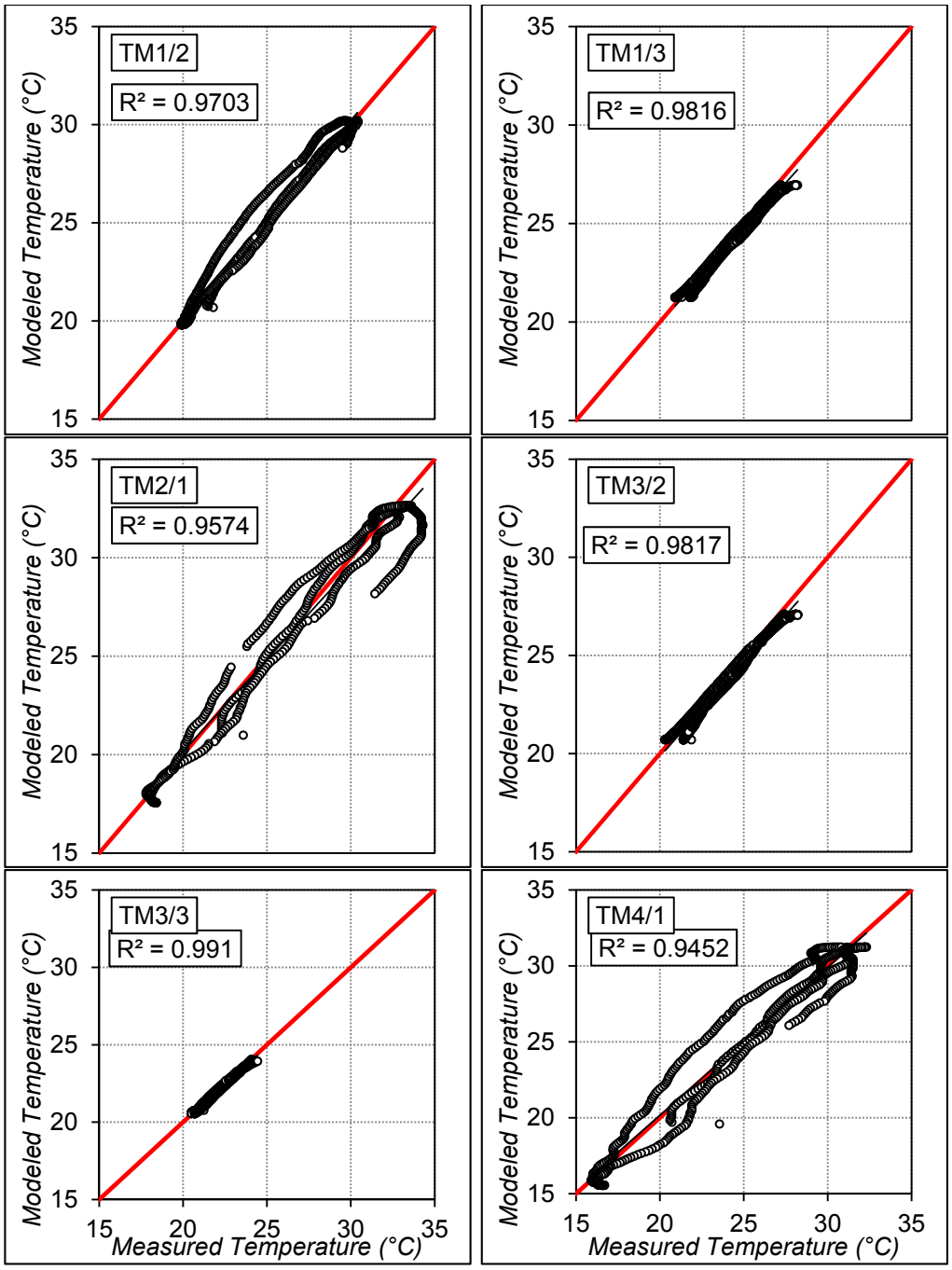

Figure 4. 20: Accuracy of the predicted model

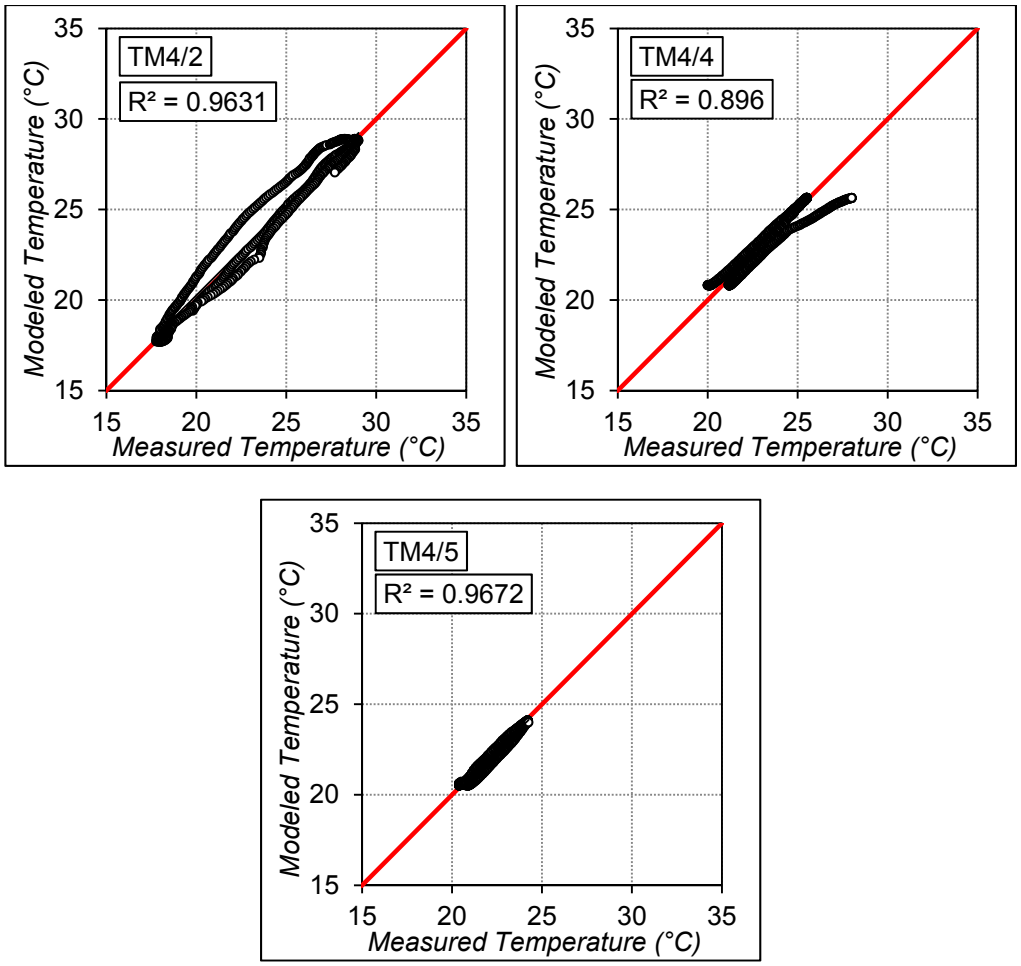

Figure 4. 21-continued: Accuracy of the predicted model

Since the soil was relatively homogenous, change of soil heat parameters, (such as thermal inertia and heat absorption capacity) could be neglected. In addition, the soil was exposed to similar loading conditions; therefore, at any defined time the only different parameter was the location of the sensors. To analyze the hypothesis, the parameters were trended against the depth of the sensor. Figure 4. 22 shows the dependency of average temperature and domain of variation on depth.

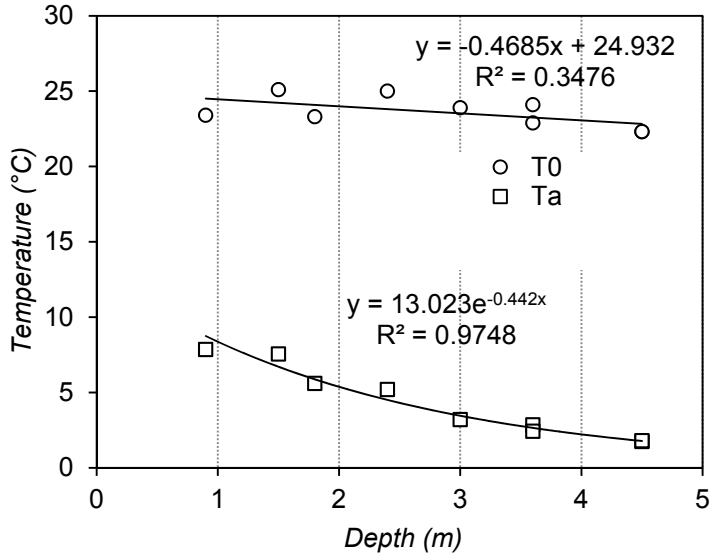

Figure 4. 22: Dependence of average temperature and domain on depth

As is clear from the graph, the average temperature of the soil layers does not significantly vary with depth and on average, remains close to 24 ºC. However, a slight decrease of 0.47 ºC/m was observed with increase of depth. On the other hand, domain of temperature variation is clearly dependent on depth. It decreases with depth, meaning the soil tends to maintain its temperature and have less variation with depth. On average, the domain of soil temperature variation with depth decreased by 1.78 ºC/m.

The soil also possesses a lag time period following the temperature variation at depth. The lag time is defined as the difference between the time of maximum ambient and maximum soil temperature, which delays soil response time (Figure 4. 23). On average, the lag time was measured to be varying with depth as 23.65day/m indicating that for every meter, the soil tends to maintain its temperature for 23 more days.

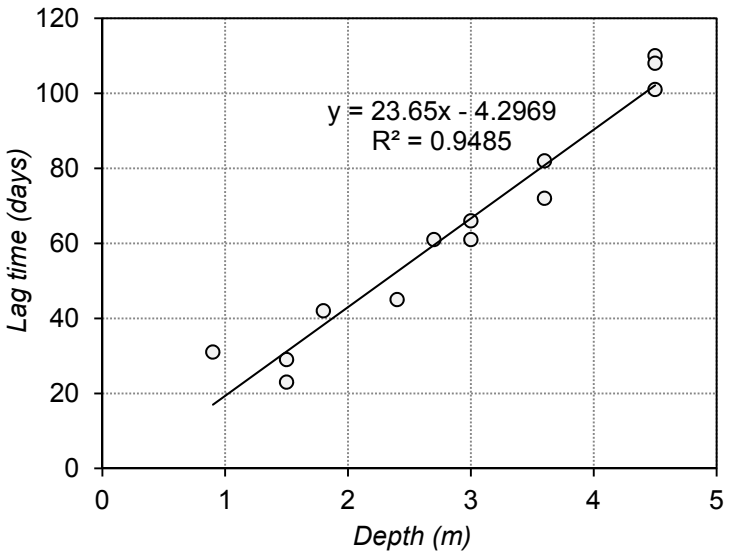

Figure 4. 23: Lag time versus depth of soil layer

Based on the overall analysis, the parameters can be summarized as below:

$$T_0(℃) = -0.4685z + 24.932 \quad \text{Eq. 4. 11}$$

$$T_a(℃) = 13.023e^{-0.442z} \quad \text{Eq. 4. 12}$$

$$C_0 = 23.65z - 4.2969 \quad \text{Eq. 4. 13}$$

Where

z = Depth from surface (m)

Therefore the overall model for temperature variation can be stated as:

$$T(℃) = (-0.4685d + 24.932) + [(13.023e^{-0.442z}) \times \sin(t - 23.65z + 4.2969)]$$

The model was validated with the calibration sensors. Time series of the obtained values and accuracy of the model are shown in Figure 4. 24 and Figure 4. 25, respectively.

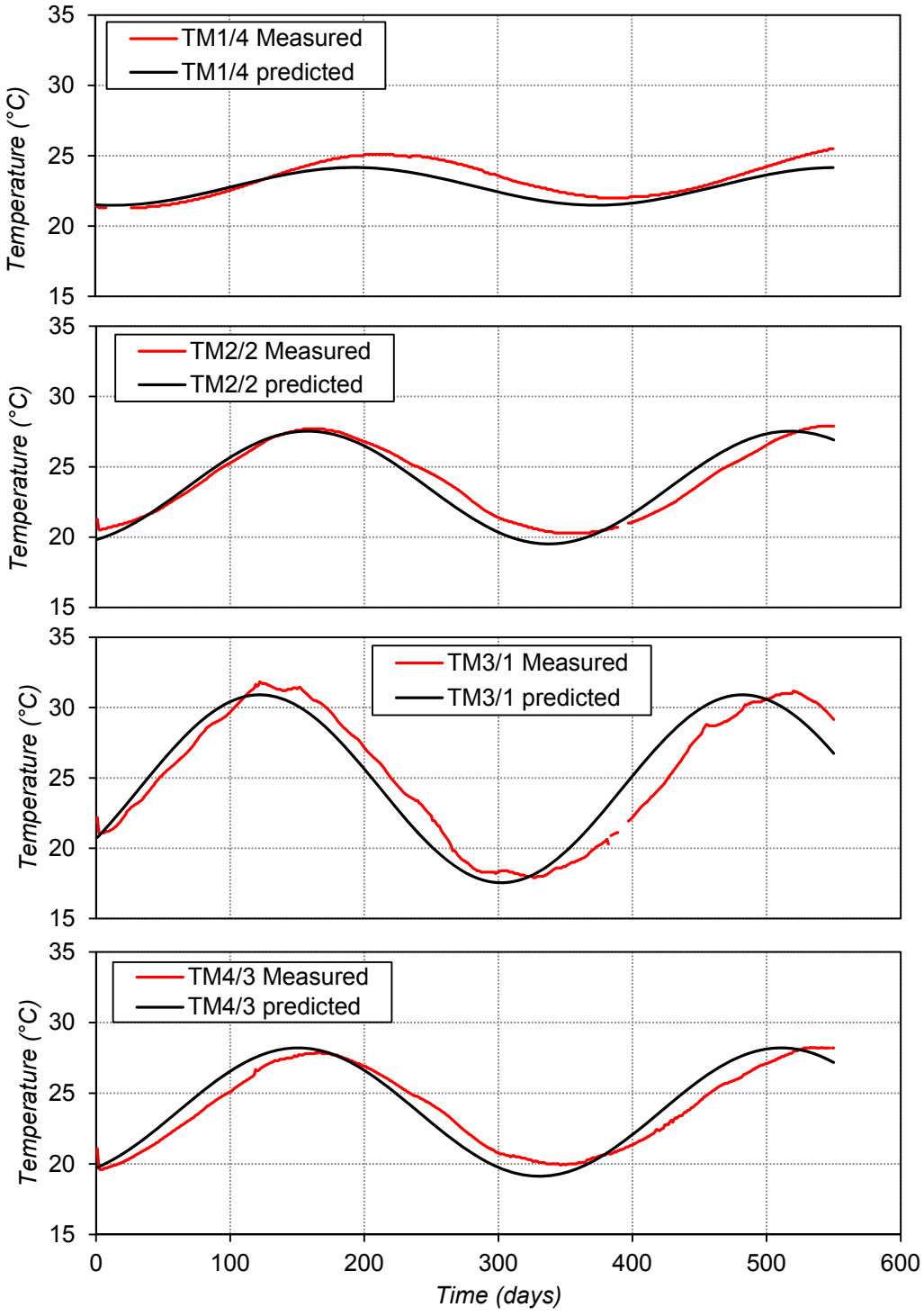

Figure 4. 24: Time series of predicted and measured vales

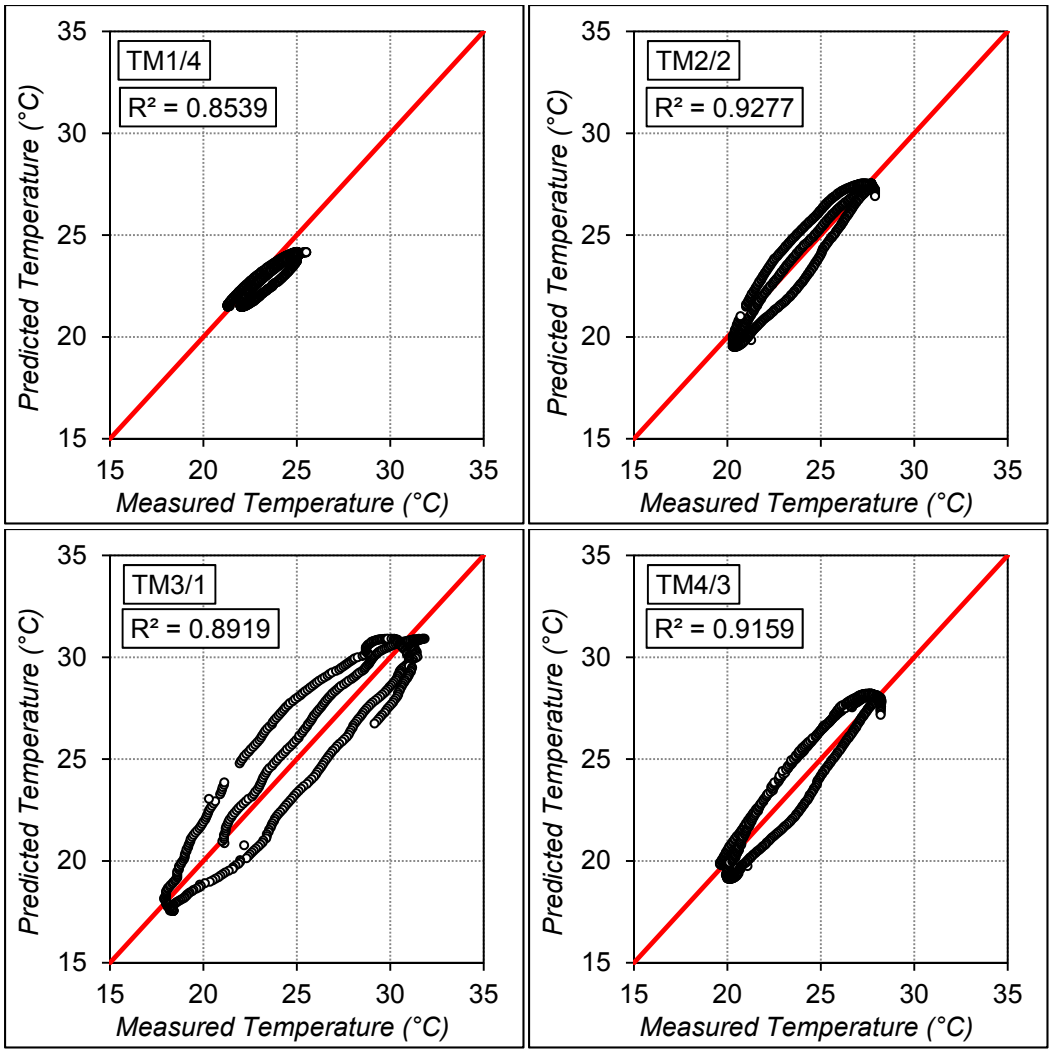

Figure 4. 25: Accuracy of the model

4.1.3.5. Analytical Solution

The sinusoidal temperature model was derived by solving the following partial differential equation (Hillel, 1982; Marshall and Holmes, 1988):

$$\frac{\partial T(z,t)}{\partial t} = D\frac{\partial^2 T(z,t)}{\partial z^2} \qquad \text{Eq. 4. 14}$$

The nonlinear equation can be solved using several assumptions, as explained in moisture variation model. The final solution can be expressed as below, which is in agreement with the developed model.

$$T(z,t) = T_0 + T_a e^{-z/d} \sin\left[\omega(t - t_0 - z/d)\right] \quad \text{Eq. 4. 15}$$

Where

T(z,t) = Soil temperature at time t (d) and depth z (m)

T_0 = Average soil temperature (°C)

T_a = Annual amplitude of the surface soil temperature (°C)

d = Damping depth (m) of annual fluctuation, d= $\sqrt{\frac{2D}{\omega}}$

where D = Soil thermal diffusivity

ω = $2\pi/365$

t_0 = Time lag (days) from an arbitrary starting date

Thermal diffusivity of the soil is the ratio of the thermal conductivity to volumetric heat capacity of the soil. For mineral soils, thermal diffusivity increases with water content at low water contents and then gradually decreases with increasing water contents at high water contents. However, for modeling purposes, it can be estimated from Table 4. 6.

Table 4. 6: Thermal diffusivity of soil (Florides and Kalogirou, 2004)

Types of soil	Thermal diffusivity of soil $\alpha=k/c_v$ (cm^2/sec)	Penetration depth of cycle (m)	
		Diurnal	Annual
Rock	0.02	1.1	20.5
Dry sand	0.001	0.3	4.5
wet sand	0.01	0.8	14.5
Dry clay	0.002	0.4	6.5
Wet Clay	0.015	0.95	18.0

4.1.3.6. Discussion

Based on the determined model, evaluation of the field results and comparison with existing literature, it was obvious that soil at all depths behaves seasonally in terms of temperature variation. The amplitude of variation decreases in depth. Florides and Kalogirou (2004) suggest z=25m as the zone of temperature stabilization. In other words, at this depth, soil becomes unresponsive to ambient temperature variation.

Variable temperature gradient was observed within the soil layers. The direction of the gradient depended on the time of year. As the surface temperature increased, the gradient became downwards. However, with decrease of surface temperature, the deeper soil maintained its temperature for an extended time, thus reversing the gradient, as shown in Figure 4. 26.

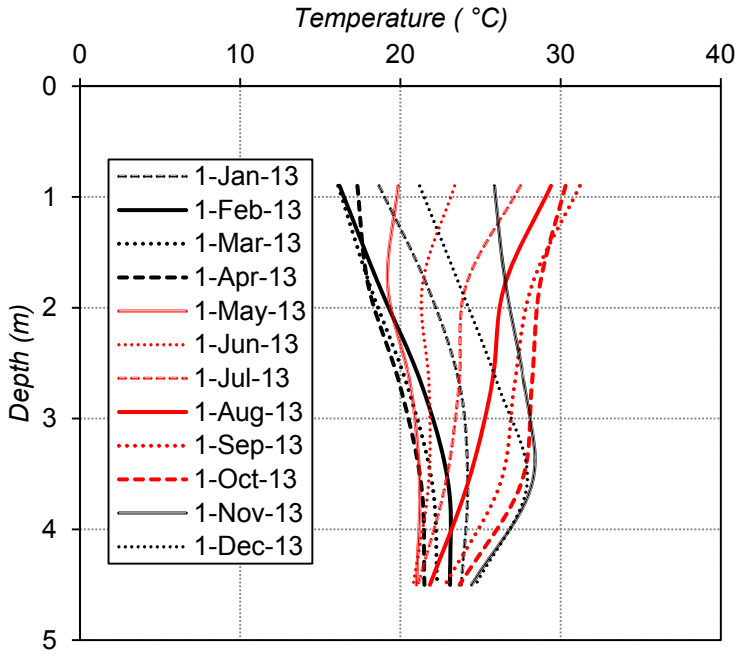

Figure 4. 26: Temperature gradient in depth (B.H.4)

Shallow soil layers showed sensitivity to daily cyclic temperatures up to 1.5 to 1.8 m depth. Due to thermal inertia of the soil, this behavior diminished in higher depths.

The developed model is in agreement with research previously performed, including Florides and Kalogirou (2004), Hillel (1982) and Marshals and Holmes (1988) and can be adequately explained in terms of a sinusoidal function.

4.1.4. Deformation Analysis of the Field

In this section, PVR of the soil was calculated and compared with survey results. A comparison was made and a model for determining elevation variation of the pavement was suggested.

4.1.4.1. Determination of PVRsite

The PVR value of the site was determined according to method TX-124-E. The site was analyzed up to 20ft (6m) in 2ft (0.6m) layers to determine the swell potential of the soil. Information of two boreholes (B.H.1 under the pavement centerline and B.H.4 under the pavement edge) were analyzed and the results are shown in Table 4. 7.

Table 4. 7: PVR results

Depth (ft.)	PVR (in)	
	Centerline	Edge
0-2	1.09	0.68
2-4	0.74	0.34
4-6	0.46	0.39
6-8	0.21	0.39
8-10	0.15	0.19
10-12	0.29	0.15
12-14	0.05	0.10
14-16	0.10	0.05
16-18	0.05	0.10
18-20	0.05	0.05
Total PVR (“)	3.2	2.44

Based on the PVR results, maximum swelling under pavement edge was estimated as 2.44" (6.2cm) while swelling deformation in the centerline of the pavement was 3.2" (8cm). The difference and greater value of PVR_{CL} with respect to PVR_{edge} is credited to smaller water content under the centerline. According to the PVR assumptions, dryer soils are subjected to more moisture absorbance; therefore, more swelling can be expected. The same pattern was observed by Nayak and Christensen (1970), in which they studied the effect of initial water content on swelling potential of expansive clays and determined that swelling potential logarithmically reduces with increase of soil water content. This evaluation is the basic theory behind many subgrade improvement technics, such as prewetting. The relation can be explained as:

$$\log(P) = 2.132 + 0.0208(LL) + 0.000665(\gamma_d) - 0.0269(w) \quad \text{Eq. 4. 16}$$

Where

LL = Liquid limit

γ_d = Dry density of soil sample in kg/m^3

w = Water content

Both PVR values of centerline and edge exceed the allowable TxDOT limit for FM roads (i.e. 2" or 5cm). Therefore, subgrade improvement methods should be exercised to reduce the PVR values, including subgrade replacement, stabilization, moisture barriers or subgrade sealing (FHWA, 2004).

4.1.4.2. Field Monitoring Results

The profile of the pavement surface and its deformation was monitored using horizontal inclinometer and monthly surveys. A survey was used to measure the overall deformation of the pavement with reference to the original survey base line. A horizontal inclinometer was used to detect the local deformation of the pavement such as crack initiation and movement of the shoulder. Figure 4. 27 reflects the time series of surveying

results over the monitoring period across the main installation line. The coordinates of the first survey were set as the zero reference, and elevations of the points in each survey were determined by subtracting the recorded elevations from the initial reading.

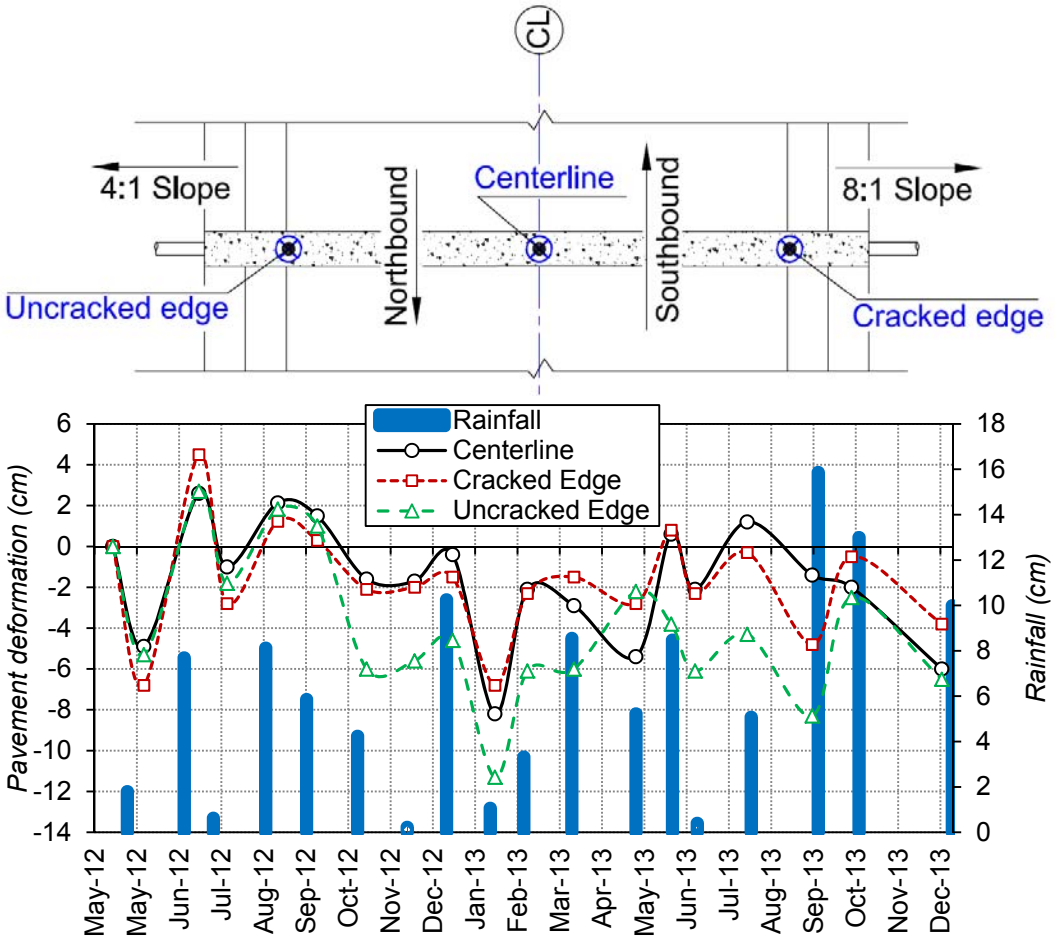

Figure 4. 27: Pavement deformation in time

The pavement elevation showed considerable sensitivity to the rainfall pattern. For instance, accumulative rainfall in the initial and second survey (May 2012) was approximately 18mm, which resulted in a downward movement of pavement profile measuring 6cm. However, the accumulative rainfall in the next month was 68mm, which caused an upward movement of approximately 8cm. The same pattern of shrinkage and

swelling was observed between surveying intervals. The overall recorded pavement deformation is summarized in Table 4. 8.

Table 4. 8: Differential movement of the pavement with rainfall

Date	Total rainfall (cm)	Relative movement in the centerline (cm)
Jun 2012	1.8288	-4.9022
Jul 2012	8.382	7.493
Aug 2012	0.635	-3.6068
Sep 2012	8.0518	3.1242
Oct 2012	5.9436	-0.635
Nov 2012	4.2418	0.889
Dec 2012	0.2286	-0.0762
Jan 2013	10.2108	1.2954
Feb 2013	1.0668	-7.7978
Mar 2013	3.3274	6.096
Apr 2013	8.5598	-0.7874
May 2013	5.2324	0.3048
Jun 2013	8.4836	3.2004
Jul 2013	0.4064	-2.6924
Aug 2013	5.4864	3.302
Sep 2013	15.875	-2.6
Oct 2013	13	-0.6
Dec 2013	10	-4
Jan 2014	0.06	0.9
Feb 2014	0.06	0.1
Mar 2014	2.3	-1.8

Several cycles of upward and downward movements were observed that appeared to be a function of moisture balance of the soil. An increased number of cycles in the pavement movement can accelerate rate of pavement deterioration and therefore needs to be modeled and considered in the design process. The movement can be described as increase of roughness index throughout the service life of the pavement.

Lytton et al. (2005) suggested estimating the rate of roughness development as a function of annual cyclic pavement deformation (Figure 4. 28). The author predicted an increase of international roughness index (IRI) to more than 200 in a 30 year life span. However, seasonal deformation and not considering the direct effect of rainfall can further accelerate pavement deterioration.

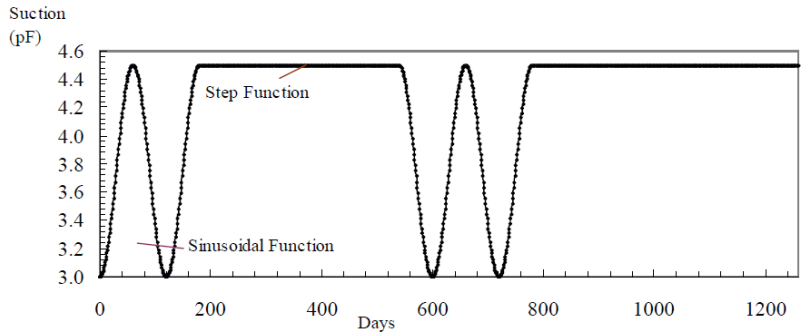

Figure 4. 28: Constructed annual suction variation in Lytton (2005) model

Similar sensitivity to rainfall was also observed by Manosuthikij (2008) as shown in Figure 4. 29. The author reported movement of soil as a function of rainfall and conculded that the crack in the pavement edge is most likely to start on the psvement surface is at it lowest vertical profile. Other researchers have also mentioned that the crack is most likely to start when the soil is at its highest shrinkage, which typically happens towards the end of dry season.

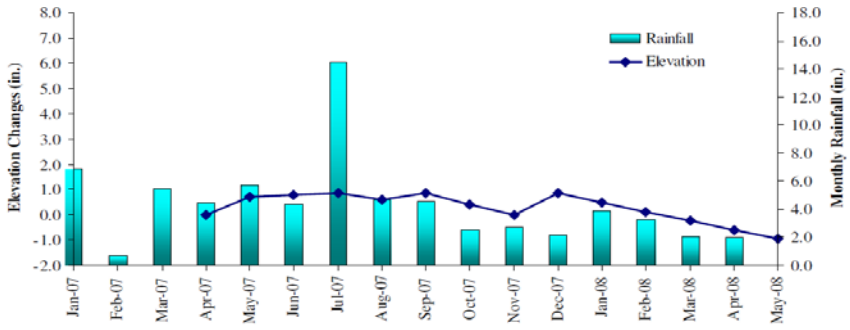

Figure 4. 29: Field surveying results observed by Manosuthikij (2008)

Results of quarterly inclinometer readings combined with survey are shown in Figure 4. 30. The survey results were used to set the elevation of the reading lines.

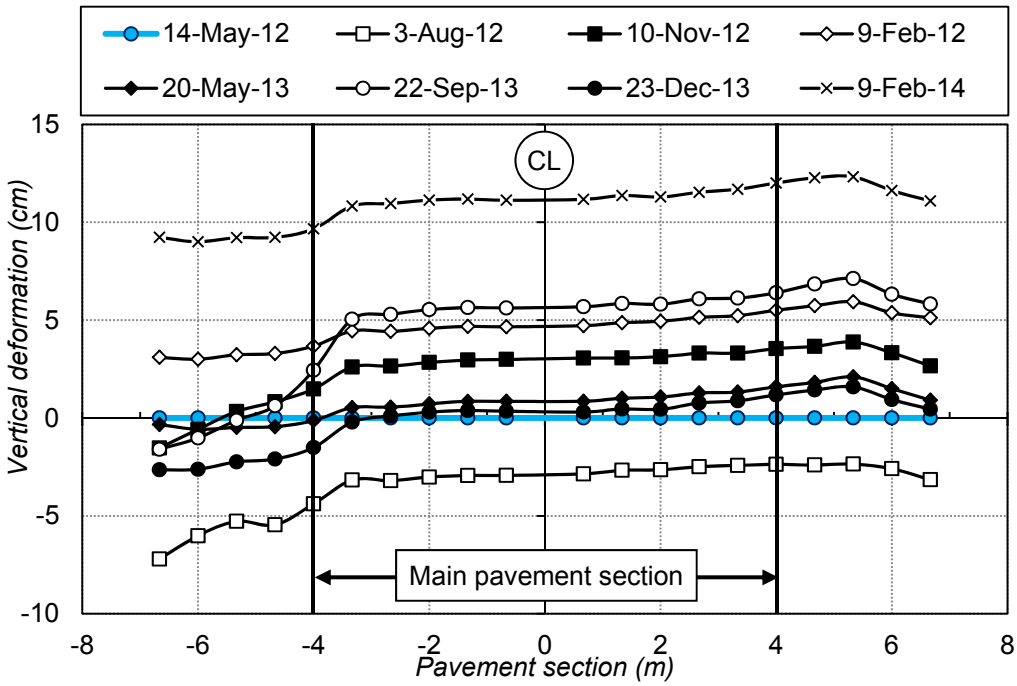

Figure 4. 30: Quarterly inclinometer readings

As can be seen, the main section of the pavement maintains a constant slope in all the readings, while severe local deformations were observed along the edge of the pavement. The most visible deformation was recorded on a survey of September 22, 2013, where the pavement edge had a drop of approximately 5cm. While reevaluating the road condition, it was determined that the pavement had suffered from edge drop (Figure 4. 31) that could have risen from two sources. The drop may have been caused by shrinking of the subgrade, which increased tensile stresses larger than failure strain of the asphalt concrete. At this point, depth and opening of the edge crack were more than 30 and 5cm; respectively. Lack of shoulder support could have intensified the issue.

Figure 4. 31: Observed edge drop

Local failure and sliding of the side slope was also observed (Figure 4. 32). Although the slope did not completely fail, shallow sliding at the crest of the slope and bulging in the mid-slope area induced differential movement in the pavement that caused cracking and was captured in the inclinometer readings.

Figure 4. 32: Shallow sliding and top crack in the pavement

4.1.4.3. Comparison of the Observed and Predicted Values

Cross sectional envelope deformation of the pavement is illustrated in Figure 4. 33. The maximum and minimum deformations of the pavement under cracked/uncracked shoulder and the centerline of the pavement was measured to be 11cm, 12cm and 14 cm, respectively. It can be seen that the movement under the cracked shoulder

happened as swelling in excess to the original surveying line (between -3.3 and +12cm). However the uncracked shoulder mostly experienced variations in shrinkage side of the volume change curve (between -9.75 and -2cm). The difference can raise form two causes; water infiltration from the crack into the subgrade which reduces the suction value and causes swelling, or steeper slope on the left side of the pavement (4:1). The deformation at the centerline of the pavement varied between -5.3 and +6.05 cm. A comparison of vertical surveyed displacement and the computed PVR values is presented in Table 4. 9.

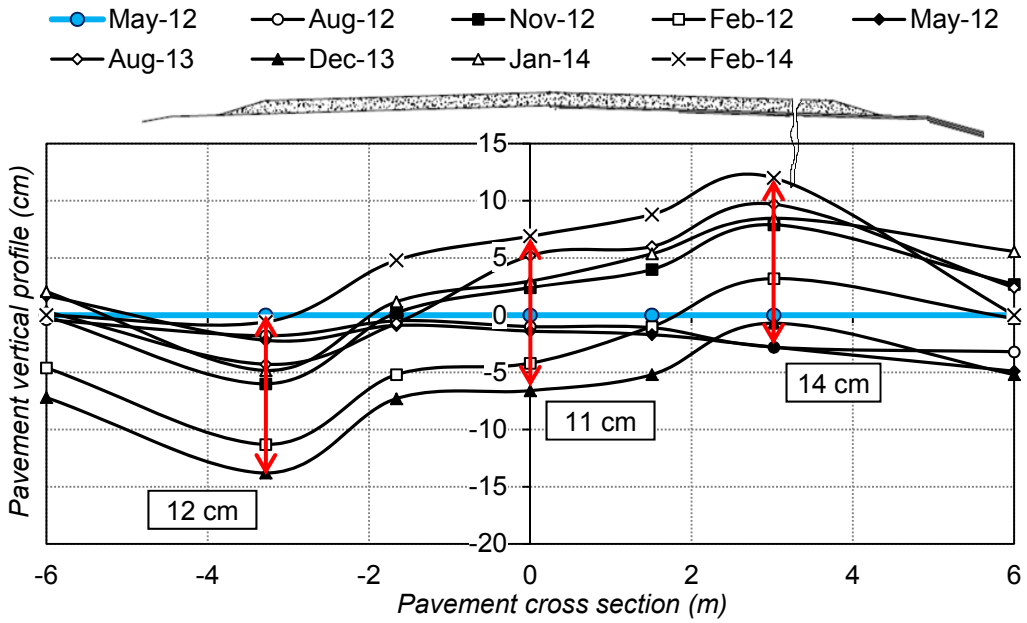

Figure 4. 33: Pavement movement with respect to the initial survey (1H:10V)

Table 4. 9: Comparison of the predicted and measure vertical movement

	Cracked Edge	Uncracked edge	Center line
Surveying	-3.3 to 12	-9.75 to -2	-5.3 to +6.05
PVR	+6.1	+6.1	+8

Comparing the PVR results with the field survey, it can be concluded that PVR alone may not accurately predict range of variation or swelling potential of the site. Not considering potential shrinkage can induce errors of up to 200% in site evaluation.

Mixed evaluations on accuracy of PVR method have been reported. Manosuthikij (2008) reported results of field observation, compared it with several predictive methods, including Snethen (1977), Hamberg (1985), PVR (2003), Lytton (2004) and concluded that the method may have limitations and increases the overall uncertainty of analysis. In addition, the outputs significantly depend on the time and place of sampling (Zhang and Briaud, 2010) and do not consider potential shrinkage of the soils. Luo (2007) analyzed the effect of shrinking soil and concluded that if there is proper adhesion between asphalt concrete and shrinking subgrade, the cracks are likely to propagate into the pavement.

4.1.4.4. Model Development

To quantify the pavement deformation based on relative moisture balance of the site, the recorded profile was non-parametrically analyzed in Matlab to determine the best possible trend. From the initial observations, it was noticed that a similar trend to moisture content variation was present. The overall trend followed a seasonal trend in addition to local deformations due to rainfall. The trending is shown in Figure 4. 34.

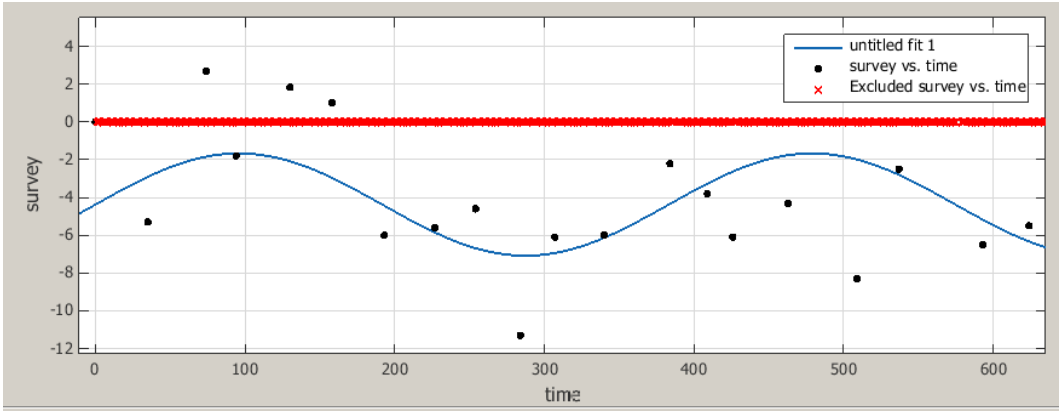

Figure 4. 34: Trending of deformation in Matlab

Since the moisture content of the soil is the major factor determining its movement, it is reasonable to expect similar elevation variations. Therefore, the analysis was conducted in two sections: determination of the main seasonal trend and additional movements due to local climatic loading.

Based on the results, the main seasonal trend peaks in summer, which can be attributed to seasonal rain and thunderstorms during the mentioned period. Such a trend resembles variation of moisture content especially in shallow depth. The formulation can be mathematically explained as a sinusoidal function:

$$\Delta h = H_0 + H_a \mathrm{Sin}(\omega t) \qquad \text{Eq. 4. 17}$$

Where:

H_0 = Average vertical profile (cm)

H_a = Domain of deformation (cm)

ω = Frequency, since the cycle is annual the frequency is equal to $2\pi/365$

t = Time from an arbitrary start date (selected as 1st May 2012) (day)

Several parameters were tried to obtain the best match and the final seasonal model was suggested as:

$$\Delta h = -4.37 + 2.7\mathrm{Sin}(0.017t) \qquad \text{Eq. 4. 18}$$

Excessive movement of pavement in addition to seasonal trend was also studied against net moisture balance of the soil at the time of survey. The net moisture balance was calculated as infiltration and exfiltration “evaporation” of water. The water evaporation was determined from evapotranspiration chart proposed by Hasenmueller and Criss (2013) and the overall water balance was determined by subtracting the provided moisture from evaporation. Figure 4. 35 shows the pavements’ excess movement against the determined net moisture balance of the site.

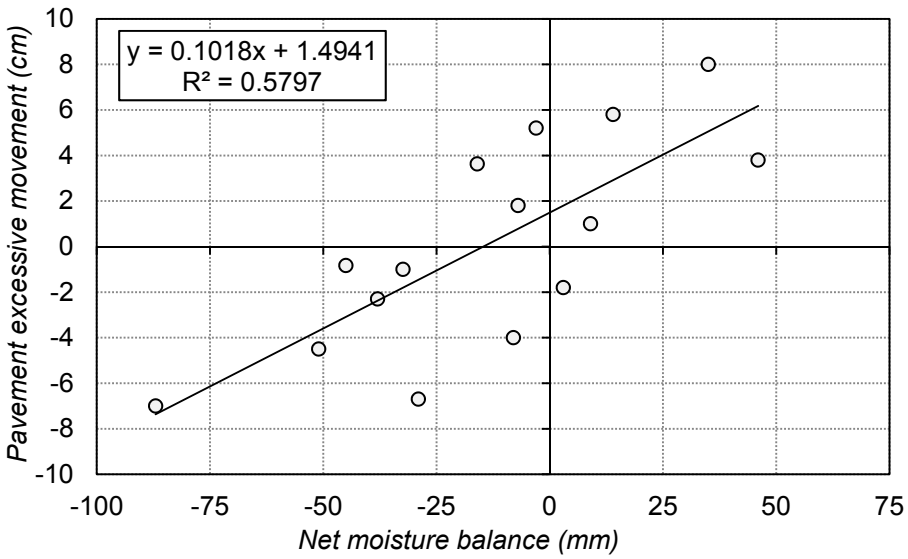

Figure 4. 35: Excessive movement of the pavement in response to rainfall

The overall deformation of the pavement can be statistically modeled as

$$\Delta h = -4.37 + 2.7\mathrm{Sin}(0.017t) + (0.1018\,Rain(t) + 1.49)$$

$$= -3.18 + 2.7\mathrm{Sin}(0.017t) + 0.1018\,Rain(t)$$

Monitoring of additional site is recommended so that the adopted equation can be validated.

4.2. Coupled Stress/Suction Evaluation of Soil Volume Change

To determine and track the pattern of volume change of expansive soils under variable net stress states, the constitutive surface of the soil was constructed. Results of different test sections and final constitutive surface are described in this section.

4.2.1. Water Content-Suction Relation under Different Normal Stresses

Results of SWCC of samples compacted wet of optimum curve (ω=29.5%) under 25, 50 and 100 kPa normal stress are shown in Figure 4. 36. The results indicated that no significant difference is observed as the normal stress on test specimen varies. The variables of the vanGenuchten equation stayed almost unaltered (Table 4. 10) and the air

entry value of the soil maintained its value of approximately 100 kPa. Therefore, it can be concluded that the SWCC of the samples wet of optimum is not strongly dependent on the applied pressure.

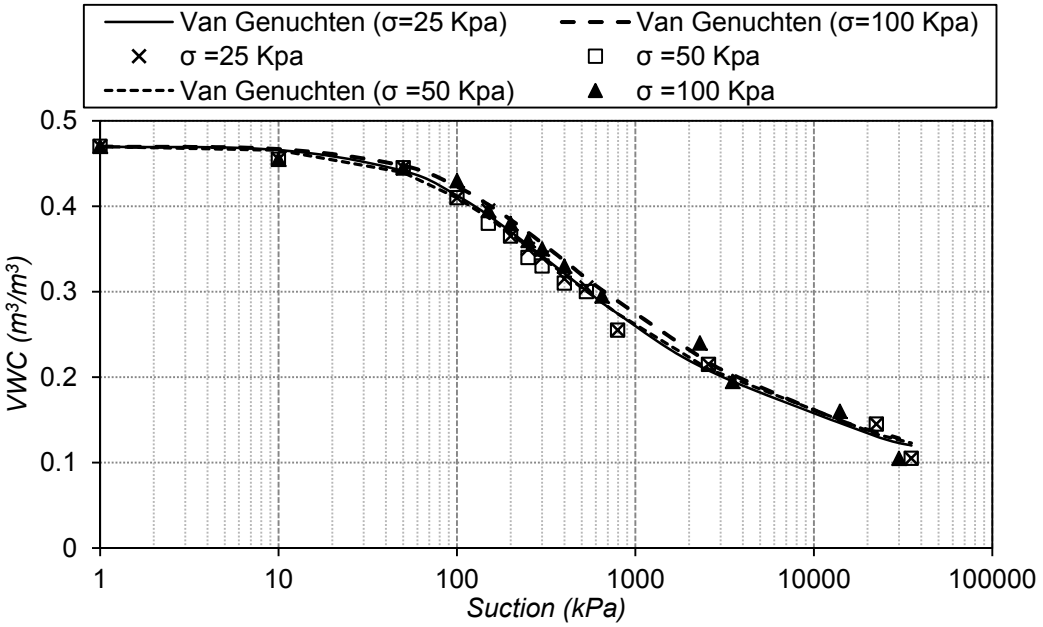

Figure 4. 36: Effect of net surcharge on SWCC (Hossain, 2013)

Table 4. 10: vanGenuchten fitting parameters (Hossain, 2013)

	Normal stress (kPa)		
	25	50	100
α	0.0064	0.0063	0.0064
n	1.2190	1.2184	1.2357
m	0.1717	0.1908	0.1792

This finding challenges conclusions of NG et al (2000), who determined that the application of normal stress increases the air entry value of the soil. The author indicated that application of net normal stress increases the small pores within the soil structure which require more suction to lose moisture. On the contrary, Hossain (2013) suggested

that the cause of unchanged air entry value is “identical micro-structure formation appearance with no interclod pores”.

The range of normal stress in the performed tests was between 25 to 100 kPa which is greater than the swelling pressure of the soil. Therefore, no additional tests of SWCC under pressure were required for coupled volume change analysis of the soil.

4.2.2. Measurement of Volume Change of the Sample

LVDT gauges were used to measure volume changes of soil samples under desaturation. The overall results of void ratio-suction relation are presented in Figure 4. 37. Since zero is not defined in the logarithmic scale, the suction axis starts from 1.

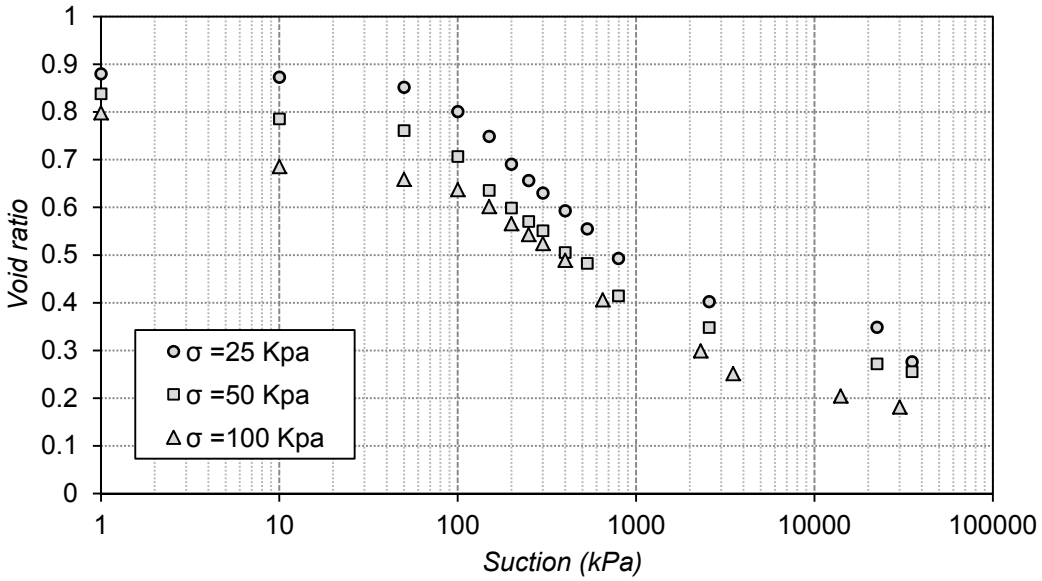

Figure 4. 37: Soil shrinkage curve under applied surcharge

As shown, the initial void ratio under 25, 50 and 100 kPa was measured as 0.88, 0.84 and 0.8, respectively, which approximately reflects consolidation of the sample under saturated state. Rate of decrease in void ratio continues with the same slope under different stresses. Once the consolidation of the sample is complete, the shrinkage rate due with suction continues at a similar slope regardless of the applied pressure.

All the obtained curves showed a similar S-shaped with two inflection points. The first one happened when a sudden increase in rate of volume change reduction was observed. In all test curves, suction at this point was approximately 100 kPa, which is close the air entry value of the soil and reflects the plastic limit of the soil (Tripathy et al., 2002; Fredlund and Houston, 2013).

In the secondary volume change phase, the decrease in void ratio happened at a faster rate compared to the previous phase. The shrinkage continued until suction value was approximately 4000 kPa. Water content at this pressure reflected residual water content. After this point, not much of shrinkage occurred with increase of suction.

Since the slopes of the curves are similar, it is apparent that the major parameter characterizing the suction-shrinkage curve is the initial void ratio or the start point of the graph. While measuring void ratio versus water content, a similar conclusion was drawn by Tripathy et al (2002), as shown in Figure 4. 38. The author observed that application of normal stress shifts the curves towards the 100% saturation line. Briaud and Zhang (2003) have also observed that swell-shrink modulus "E_w" is not influenced by applied external load.

Overall, it can be concluded that the shape and defining parameters of the soil's shrinkage curve do not vary with load application. However, variation may occur from initial consolidation of sample prior to the testing.

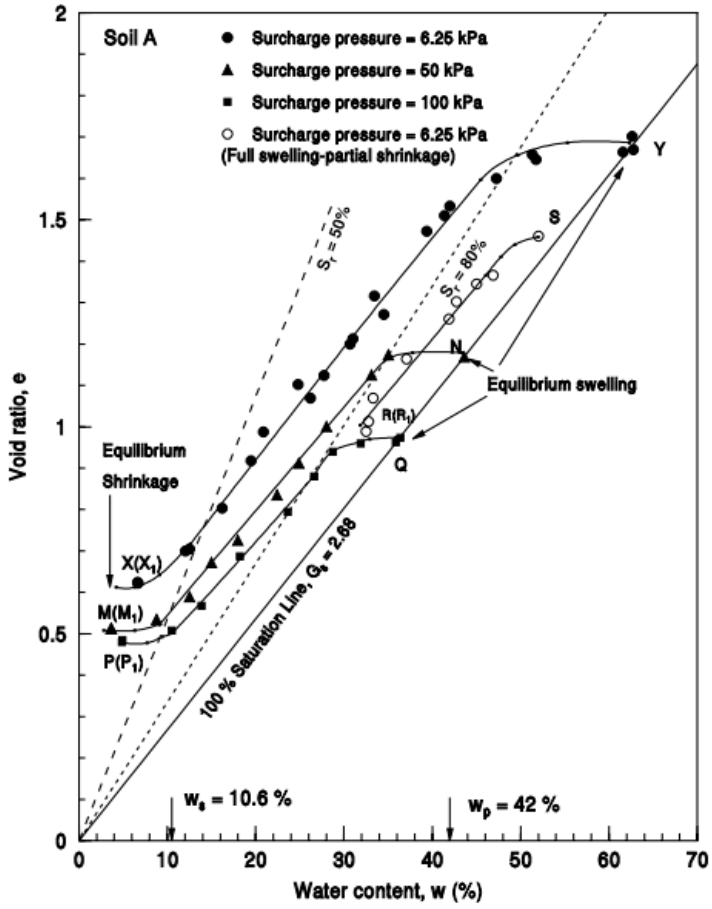

Figure 4. 38: Shrinkage curve obtained by Tripathy et al (2002)

4.2.3. Determination of the Constitutive Surface for Coupled Analysis

A void ratio-suction- normal stress constitutive surface can be obtained by plotting the above curves in a 3D space. This was performed in Matlab, as shown in Figure 4. 39. Both suction and net normal stress are in logarithmic scales. Such a surface allows users to consider effects of normal stress and moisture variation simultaneously. It is assumed that constitutive surfaces exhibit “uniqueness” (Fredlund and Rahardjo 1993), which demonstrates that there is only one relationship between the deformation and stress state variables (Chao 2007).

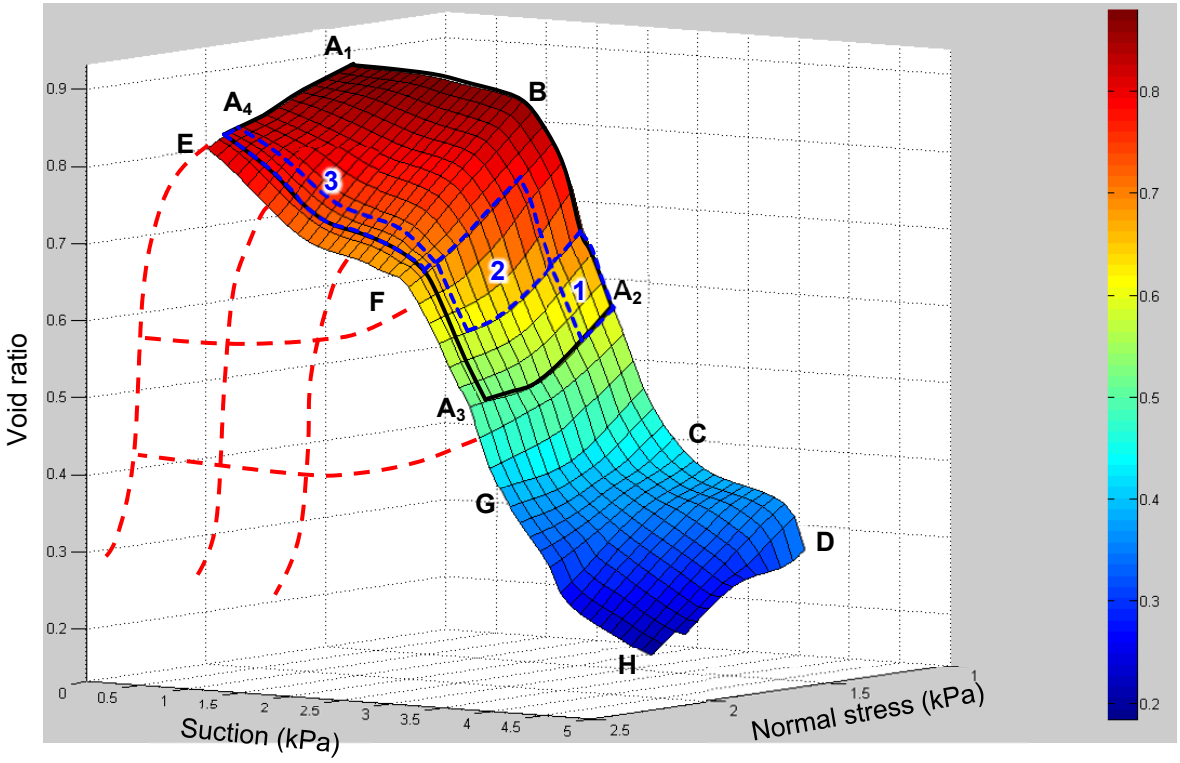

Figure 4. 39: Soil constitutive surface

Curves parallel to A_1BCD, reflect the void ratio-suction curves under different normal pressures. It is observed that the curves are moving downward as the normal stress increases, which as explained previously, is due to consolidation of the soil under increasing normal stress prior to test initiation. Segment A_1B represents the volume change before the air entry value of the soil, when the soil is drying from the saturated state towards the shrinkage limit. BC reflects the soil stress path while major changes in volume are happening. Approximately 80% of the soil volume change happens along this phase. Segment CD reflects soil transition volume change after it has passed the shrinkage limit. Therefore, no further considerable volume change is expected. In this segment, water content will decrease; however, no further volume change is observed.

Since no significant variation was detected in void ratio-suction curve under different normal stresses, similar information can be expected from the planes parallel to A_1BCD.

Segment A_1E reflects void ratio-net normal stress path (also known as one-dimensional consolidation curve), before the pressure reaches the maximum past pressure of the stress history of the soil. Curves parallel to A_1E, represent the consolidation curve under various suction values. Line BF reflects the air entry value under various normal stress, while line CG represents the void ratio at the shrinkage limit of the soil under the same condition. The corresponding water content of the points on the 3D surface can be determined by reviewing the SWCC plots. It is however, estimated that the void ratio at shrinkage limit will decrease with the applied mechanical stress, while the water contents at the shrinkage limits remain the same for different mechanical stress levels. An explanation for this phenomenon is given by Zhang (2004) who considered that the shrinkage limit is more related to microstructure of clay aggregates. For a given soil, the microstructure of the clay aggregates is the same and is not influenced by the external mechanical load (Lloret et al., 2003). As a result, the gravimetric water contents at shrinkage limit for a soil is the same for any mechanical stress level. Surface BFCG represents the range where most of the volume change occurs, and surface CGDH represents the range where there is no volume change, i.e. the zone with water content below the shrinkage limits for different total mechanical stress level.

4.2.4. Projection of Field Condition of the Constitutive Surface

Incorporation of the laboratory results and field conditions into constitutive surface space can provide an indication of overall volume change process of the soil. Based on laboratory results, the swelling pressure of the soil is estimated to be 70 kPa, equal to 1.85 in logarithmic scale and approximately 4 m of subgrade soil. In addition,

based on laboratory investigations, the samples had degrees of saturation between 100 to 85%, equivalent to suction between 0 and 100kPa (2 in log scale). Projection of the conditions on the surface can be observed as surface $A_1A_2A_3A_4$. This indicates that the possible range of variation in void ratio can be expected between 0.88 and 0.58, under highest suction and surcharge.

Layers of subgrade soil can be divided to reflect average surcharge of 25, 50 and 100, which are shown as zones 1, 2 and 3 on the constitutive surface respectively. The final volume change can be tracked as shown in Table 4. 11.

Table 4. 11: Tracking of volume change

Layer #	Layer height H_0	Initial void ratio (e_0)	Min void ratio (e_{min})	Max void ratio (e_{max})	maximum shrink (m)	maximum swell (m)
1	1.5 (0-1.5m)	0.63	0.58	0.69	0.046	0.055
2	1.5 (1.5-3m)	0.69	0.66	0.73	0.026	0.035
3	1 (3-4m)	0.73	0.71	0.75	0.012	0.0116

Therefore the maximum swelling and shrinkage of soil determined with coupled analysis is 8 and 10 cm, respectively.

4.2.5. Comparison of PVR, Field Observation and Coupled Analysis

A comparison between the predicted and observed vertical deformation in the field is shown in Figure 4. 40.

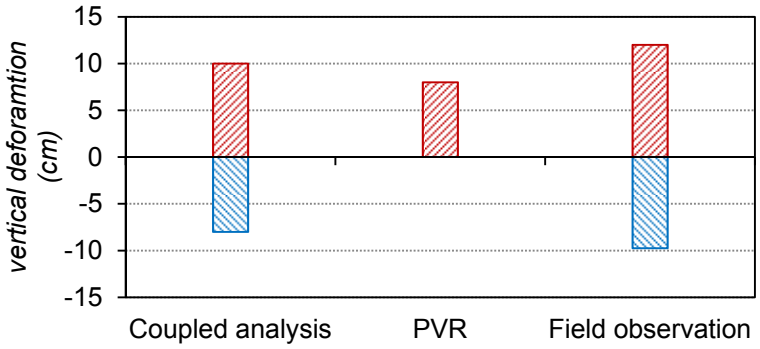

Figure 4. 40: Comparison of different prediction methods and field observation

Coupled analysis provided results close to field observation in both shrinkage and swelling. In swelling, coupled analysis and PVR provided values of 10 and 8cm, respectively. Maximum swelling observed in the field was 12cm, which is close to the value predicted by coupled analysis. In shrinkage, output of coupled analysis (8cm) was acceptably close to field observation (9.75cm) while PVR was not able to provide an estimate. This is one major shortcoming of the method.

It is evident that using a coupled analysis is a strong method to determine the real time volume change of expansive soils in the field. However, to use this method, knowledge of soil suction or moisture content variation is required. A predictive method to estimate such variations based on climatic conditions can be extremely useful.

4.3. Numerical Modeling

Three-dimensional modeling was conducted to determine the effect of swelling in stress generation and crack initiation of low volume asphalt pavements. Volume change of initially unsaturated expansive subgrade soil was investigated under various rainfall conditions. The resulting swelling and stress increase in asphalt concrete overlay was linked with possibility of crack initiation and distress development in the pavement. Abaqus was used for volumetric deformation modeling and structural analysis of the pavement.

4.3.1. Model Calibration

Before initiation of the modeling, the model needs to be calibrated. For this reason, the initial condition was calibrated for moisture variation and volumetric deformation.

4.3.1.1. Model Calibration for Moisture Content

Initially, pore water pressure was set as zero at the ground water table (4.5m depth) and the suction was let to increase linearly. A single rainfall on December 25,

2012 was selected and applied to the model. At this particular rainfall, the dry period before and after the rainfall allowed stabilization of the sensors for further comparisons. The saturated permeability of the soil was selected as the calibration parameter and varied until the results of the model became closer to field measurements. Saturated permeability was initially 10^{-7} cm/s which prevented moisture infiltration to the system. Instead, positive pore pressure was measured on model surface indicating ponding and water accumulation. Variable estimations of in-situ and laboratory measured permeability exist. Aubeny and Lytton (2003) estimated that the in-situ permeability can increase up to 10 times as result of cracks and fissures. Similarly, Zhang (2003) reported that the infiltration rate can increase on the three orders of magnitude in areas of open cracks due to rapid ingress of water through the cracked portion. This is particularly true in the case study field, where considerable crack opening is present along the edge of the pavement.

Several trials with increasing permeability functions were run, and volumetric water contents generated by the model at the location of the sensors were compared. After the results became of acceptable accuracy (Figure 4. 41), the model was considered calibrated.

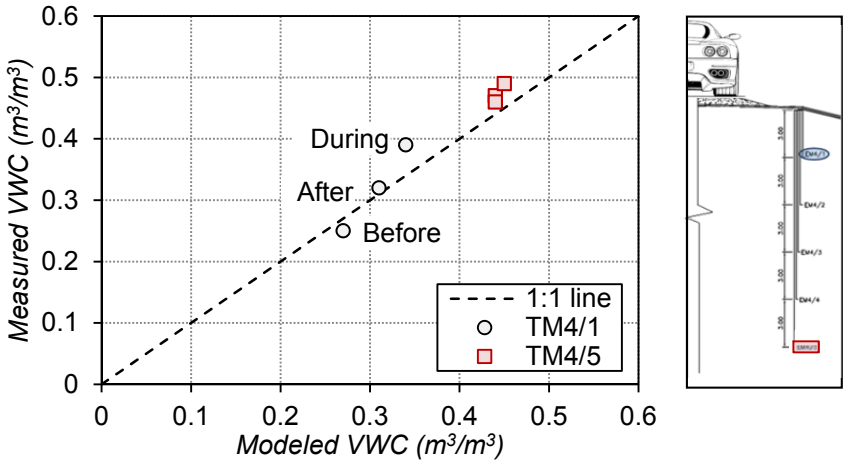

Figure 4. 41: Measured and modeled VWC before, during and after rainfall

In both model and field measurements, it was evident that the moisture content at deeper layers did not experience considerable moisture variation and stayed at approximately saturated state. However in shallow depths, moisture content variation of approximately 0.15 m^3/m^3 was observed. The model outputs generally produced values within 95% accuracy during all modeling stages and therefore, was considered acceptable.

4.3.1.2. Model Calibration for Volume Change

The model was also calibrated against volume change. Time integration of the model was controlled with UTOL parameter, which specifies the allowable pore water pressure variation in the model. In this case, UTOL was increased to a large value so that the nonlinear volume change of the model could be adjusted (Abaqus user manual). In addition, confining pressure on the model was set using fixed boundary conditions to prevent lateral bulging of the sample under normal pressure. The overall reported graph is shown as Figure 4. 42.

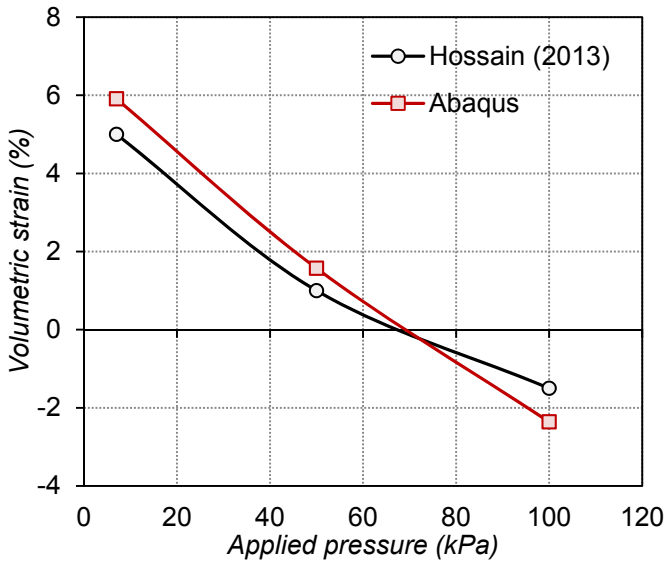

Figure 4. 42: Volume change calibration results

The calibrated material model predicted the volume change of the sample under applied load with acceptable accuracy. Under 7 kPa pressure, the measured and modeled values were 5 and 5.91%, respectively. Swelling of the samples under 50 kPa was 1 and 1.57% for measurement and model. In addition, swelling pressure of the sample was accurately modeled. Good assumptions for confining pressure and nonlinearity in the model along acceptable pore water pressure change during load applications are key factors in unsaturated modeling in Abaqus.

4.3.2. Initial Preparation

Prior to simulation of the model, the geostatic stress was run to distribute the stress inside the model body and ensure that no extra displacement occurred prior to modeling. The final stress and displacement contours are shown in Figure 4. 43.

It can be observed that the stress varied between -71500 Pa at the bottom boundary to -25130 Pa at the top. Based on the theory of soil mechanics, the stress distribution, considering suction, can be estimated from:

$$\sigma = \sigma' + u$$

Which will yield $\sigma_{top} = -29.4$ while σ_{bot} remains -71.5kPa, as suction at the groundwater table remains zero. It was observed that the model had a difference of approximately 15% with theoretical value; however this difference is to be expected in finite element stress analysis. The displacement of the model was maintained at 10^{-4} order, which is acceptable for modeling purposes.

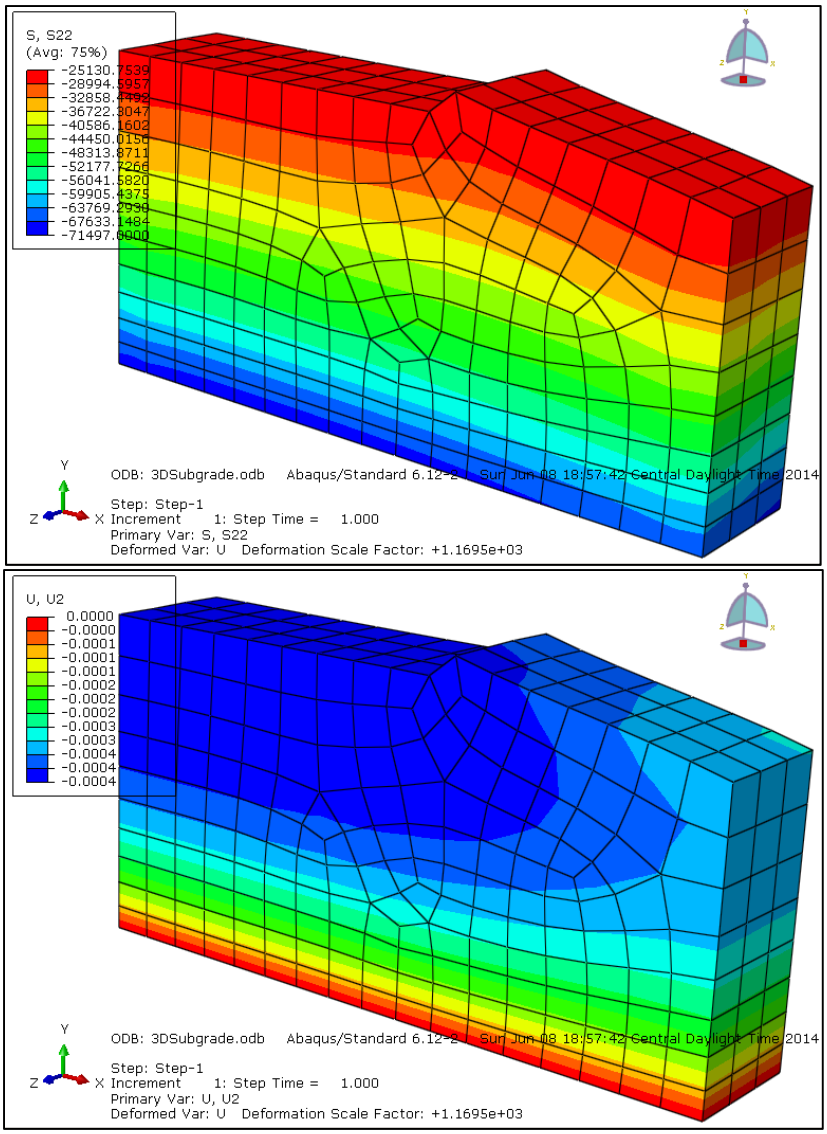

Figure 4. 43: Displacement (top) and stress distribution (bot) contours

The net normal stress at the bottom of the model remained close to the soil's swelling pressure. Therefore, if the moisture content variation was present, this depth could have contributed to the overall volume change; however it would be minimal.

4.3.3. Comparison with Field Output Data

The instrumented pavement site was used to compare transient field moisture content with numerical simulation. In addition, transient volume change of the site was

also modeled and compared. Later, the time factor was omitted, and single rainfalls were induced for parametric study.

4.3.3.1. Moisture Variation Time Series

After model calibration, a time period between February and May 2013, was selected for comparing the results with field instrumentation outputs. Considerable accumulative rainfall of 165mm was observed during this short period, which provided good readings in the sensors.

Outputs of the model at two points along the edge of the pavement corresponding to sensors TM4/1 and TM4/5 are shown in Figure 4. 44. It was observed that the FE results are close to actual recordings in the field.

In location corresponding to TM4/1, the FE was able to predict the average moisture content as well as the increase in water content as a result of rainfall. In addition, the rate of desaturation and time period of saturation was modeled with acceptable accuracy. Limited discrepancies and larger variations of field observations compared to FE output may be related to formation of cracks and fissures that can redirect moisture flow through the unsaturated media, causing an anomaly in the reading. The average moisture content in sensors and model was approximately 0.28 m^3/m^3 and 0.29m^3/m^3. The average increase in moisture content after rainfall events was approximately 0.03-0.04 m^3/m^3.

The FE output at TM4/5 location followed a similar trend. Neither field nor FE output showed considerable variations due to rainfall and maintained a constant value of 0.53 and 0.5 m^3/m^3. It appears that the accuracy of the model increased with increase of depth and decrease of moisture variation pattern.

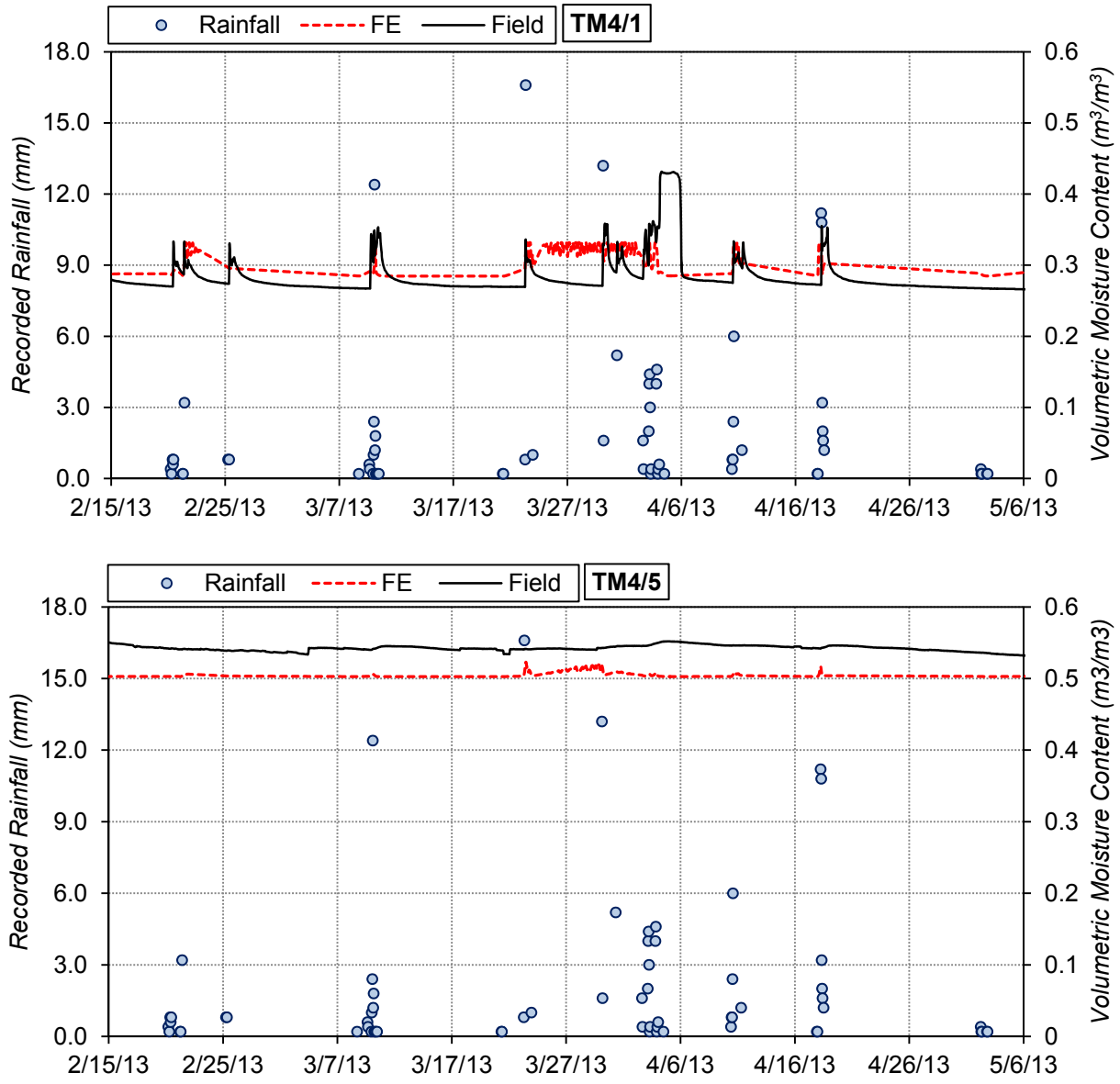

Figure 4. 44: Moisture content comparison between field and finite element outputs;

Top: TM4/1 at 0.9m depth, bot: TM4/5 at 4.5 m depth

In addition, a pattern of suction variations in the pavement subgrade, as a result of rainfall infiltration. Figure 4. 45, shows the suction variation as a result of rainfall application on the model. Suction along the pavement centerline and edge was

compared before and after rainfall. Based on numerical modeling results, it can be seen that the pavement edge experienced reduction in suction from the surface down to 2.7m depth. At the surface, suction reduced from 30 to 17 kPa, which continued to approximately 1.8m depth from surface. Afterwards, suction reduced similar to a cubic function of the depth until no variation was seen at 2.7m. Projection of this suction reduction, on the coupled analysis surface, indicates that the soil might experience variation in void ration of 0.1 (between 0.8 and 0.9), which will produce approximately 8cm of swelling.

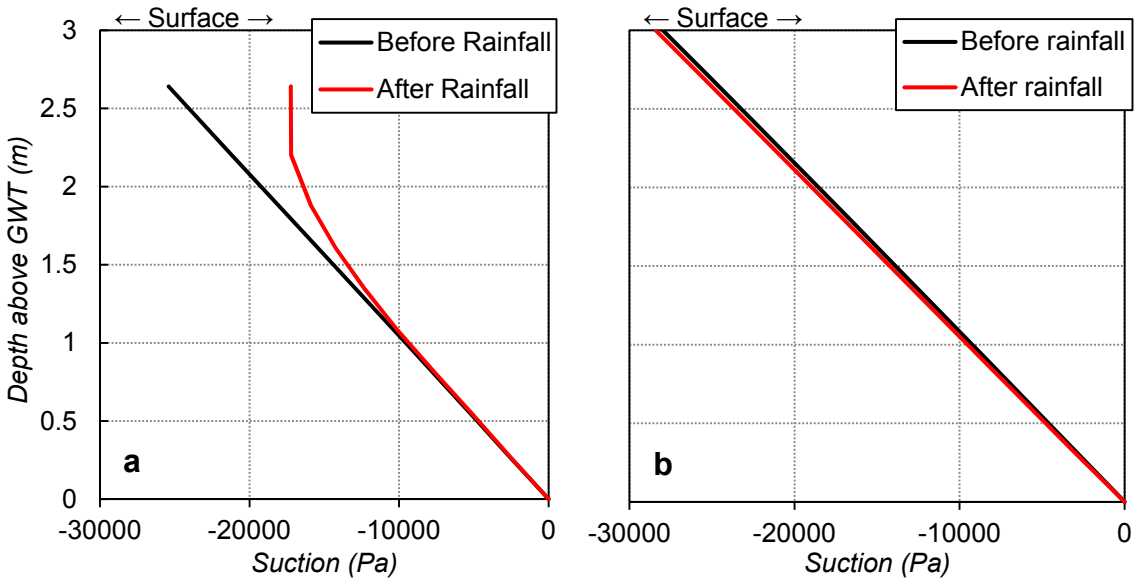

Figure 4. 45: Subgrade suction variation at a: pavement edge, b: pavement centerline

On the other hand, no considerable variation was noticed as a result of rainfall along the pavement centerline. This was expected since the pavement was defined as an impermeable cover. No suction variation indicates that no considerable volume change should be expected. However this finding challenges field observations, as centerline vertical movement was also recorded. The suction variation at the centerline may have

resulted from two sources that were not captured in numerical modeling: first, cracks and fissures of the surface and second, horizontal transfer of water from sides into pavement subgrade. The first can be achieved through discrete elementing the pavement model, and the second can be addressed by measurement and increasing the horizontal permeability of the soil and increasing the analysis time.

4.3.3.2. Vertical Deformation Modeling

The model was loaded with the rainfall pattern recorded at the field. In addition, a seasonal pattern of evaporation was applied to the model based on a method introduced by Hasenmueller and Criss (2013). The results of modeled versus surveyed time series is shown in Figure 4. 46. To be compatible with the survey timeline, the modeling zero time was May 2012.

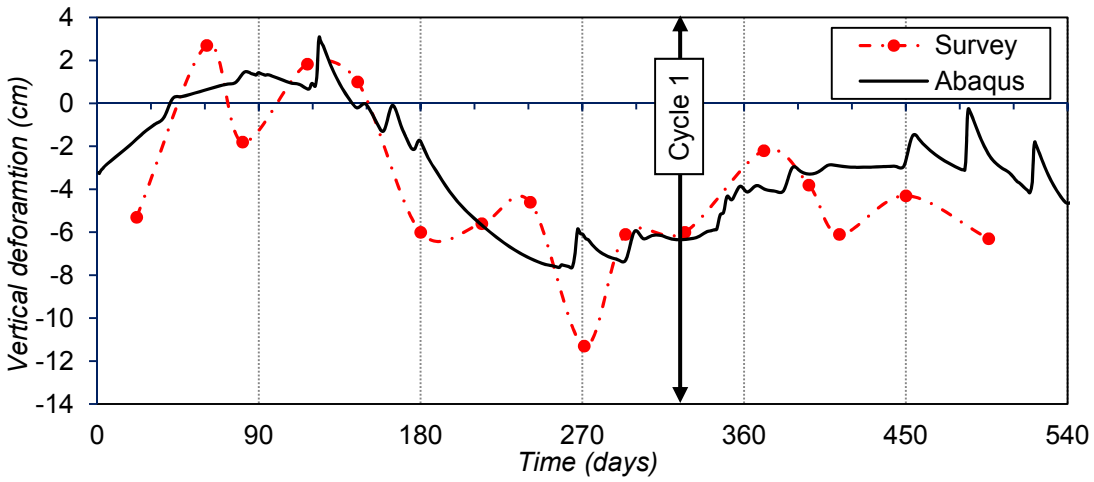

Figure 4. 46: Measured and modeled vertical deformation time series

It was observed that the model was able to replicate the seasonal trends of variation. The envelope of vertical deformation was +3/-12 in the survey and +3/-8 in the numerical modeling. However, additional movements in excess of the trend were observed due to individual rainfalls that were not captured in the main survey. Since surveying is a discrete point data collection method, by default, it overlooks some extra

variations that happen within intervals. The additional movements ranged between 0.5 to 5cm, which caused major stresses on the pavement structure. Not considering the deformations in modeling and design would significantly reduce the accuracy of the model.

4.3.4. Parametric Study

To study the effect of environmental loading on pavement performance and stress distribution, a parametric study was performed

1. Swelling of soil due to individual rainfall was determined. Different combinations of rainfall intensity and duration were considered.
2. Effects of swelling on stress distribution in the pavement structure were modeled. This analysis was performed under three different temperatures usually encountered in Texas.
3. The resulting stress was compared with the tensile cracking strain to determine the crack initiation threshold of the pavement
4. Based on the return period of the rainfall, design rainfall and design life of the pavement were determined.

Individual parts mentioned above are described

4.3.4.1. Swelling Caused by Individual Rainfall Events

Rainfalls with three different return periods were selected according to Texas rainfall data collected from the National Oceanic and Atmospheric Administration (NOAA), as shown in Table 4. 12. However, the overall value was modeled as different combinations of rainfall intensity (cm/min) and durations (min). All rainfall intensities were continued until the overall provided moisture exceeded the 100 return period (22.4cm). For this purpose, rainfall intensities were selected ranging from 0.1 mm/min to 1 mm/min.

This range was inspired by the actual rainfall data recorded at the field. The selected rainfall intensities were applied to the model for various times between 10 to 1440mins.

Table 4. 12: Rainfall overall volume and return period

return period (Yr.)	Rainfall (cm)
2	6.75
5	12.5
10	15
25	17.5
50	20
100	22.5

After running of the model, the overall vertical swelling of the pavement edge was measured as shown in Figure 4. 47.

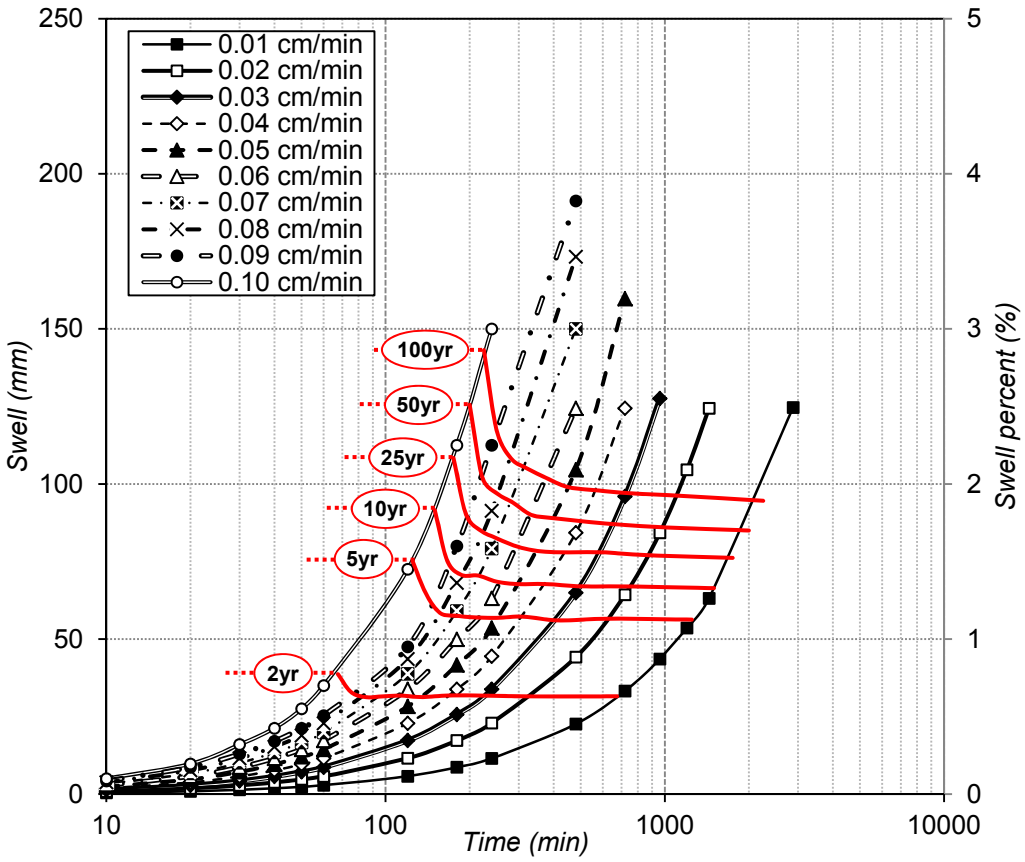

Figure 4. 47: Swelling of the pavement edge in time

As observed from the graph, the time-swelling relation can be presented as a rectangular hyperbola function. Sridharan and Gurtug (2004) (Figure 4. 48) suggested a full swelling path to occur in three distinct phases, initial, primary and secondary swelling. The percent of swelling completed in each of the stages depends on many parameters, including swell potential and microstructure of the soil (Dakshamurthy, 1978). During initial swelling, swollen clay particles rearrange within the internal voids of clay structure. Therefore, not much volume change is observed, while primary swelling occurs when the voids can no longer accommodate the swollen particles. Therefore, at this stage, swelling

happens at a faster rate. Researchers suggest that approximately 80% of overall swelling happens during the primary stage.

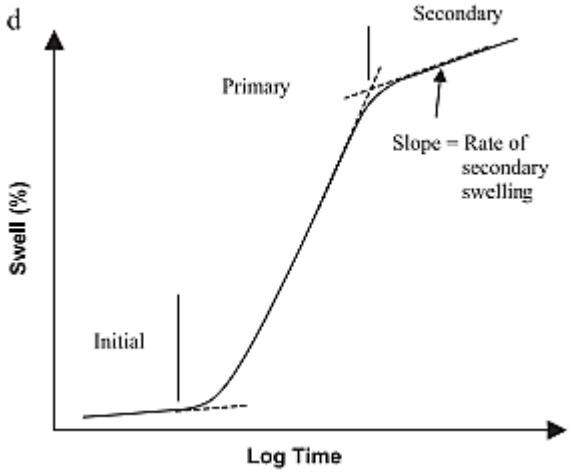

Figure 4. 48: Schematic swelling process (Sridharan and Gurtug, 2004)

By comparing the determined trend with the behavior observed by Sivapullaiah et al (1996) it can be concluded that most of the swelling in the field occurs in the primary stage. The reason may be that not enough moisture is available for soil to complete its complete swelling phase and enter the secondary swelling phase. Therefore the swelling path of the soil does not complete. and considering full swelling for design purposes may be conservative. This finding itself confirms Lytton et al's (1995) disagreement with PVR method assumptions regarding availability of free capillary water for soil at all depths to perform full swelling. Therefore, the PVR method may provide over predictive results.

Upon completion of a swelling path, the soil may swell up to 80% (Dakshamurthy, 1978; Suvalliaha,1996) also observed the same trend on samples measured in the laboratory (Figure 4. 49). In subgrade swelling, the presence of high overburden pressure, especially at high depths, prevents excessive swelling and limits it to 3 or 4 percent. In-situ swelling of 3 to 4 % was also reported by Manosuthikij (2008) who reported maximum movement of 61.7mm (equal to 3.43% swelling) for a 4m model.

However, the author allowed swlling of the model from the sides of the model and did not consider confining pressure effects of the side walls, which can introduce errors in the overall calculations.

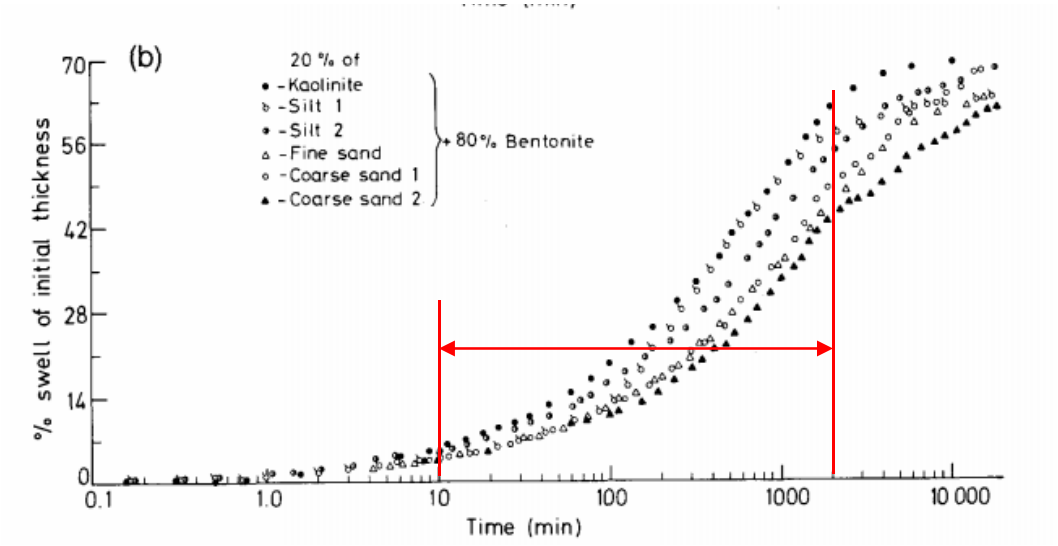

Figure 4. 49: Time percent swell of samples with 80% bentonite (Sivapullaiah et al, 1996)

Based on the overall provided moisture (equal to rainfall intensity times the duration), the return period of each swelling occurrence can be determined, as shown in Figure 4. 50. This provides an idea of the overall swelling percent and its return period which can be used for structural design of the asphalt concrete.

The overall determined swelling, with respect to provided moisture (rainfall intensity times its duration), is provided in Figure 4. 50. It was observed that for the conditions encountered in the site of monitoring, the swell-rainfall relation can be best expressed as a linear function. With R^2=0.9805, the linear equation can be used to estimate the overall swelling as a result of rainfall, with their return period.

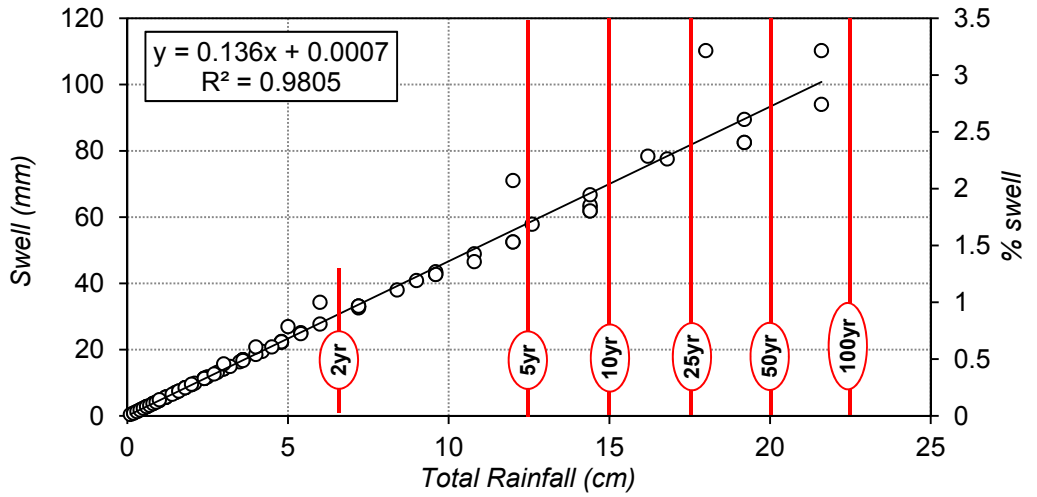

Figure 4. 50: Total rainfall versus swell percent and total swell

The higher return period indicates larger overall rainfall provided. Ng et al. (2001) suggested that there should be a critical rainfall return period above which no significant increase in pore water pressure will be induced. Based on the graph findings, most of the rainfall events produced swelling that fall within the 2years return period. This means that for a pavement to endure the effects of rainfall within two years of construction, the structural strength should be strong enough to withstand approximately 3cm of differential swelling.

4.3.4.2. Stress Strain Analysis and Effect of Temperature

The swelling can cause internal strains inside the pavement asphalt layer. Due to temperature sensitivity of the asphalt mix, identical deformation can cause various stress distributions that may cause failure. To parametrically study the effect of stress and strain, the stress strain curve of asphalt concrete mix, under three different temperatures, was extracted from the FHWA and LTPP database and used to define the asphalt material. By applying variable swelling on the edge due to rainfall, internal strains in

pavement structures were captured, as shown in Figure 4. 51. The size of the elements is 5cm.

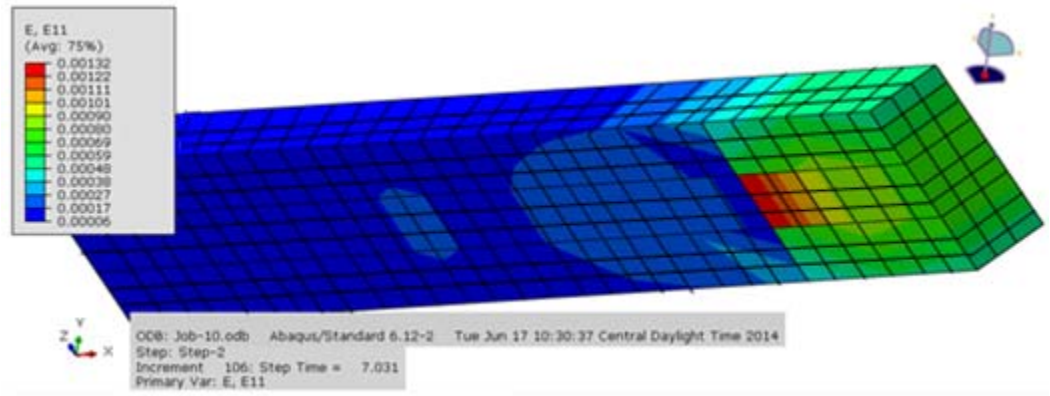

Figure 4. 51: Internal stress increase in pavement structure

E11 defines the strain along the x axis and positive value notifies tensile strain. It can be seen than an applied swelling causes the maximum tensile strain at approximately 30cm from the edge of the pavement. Considering pure mechanics, if a material is stiff (such as HMA) an upward movement on a cantilever beam should have the most moment and strain at the fixture (Figure 4. 52).

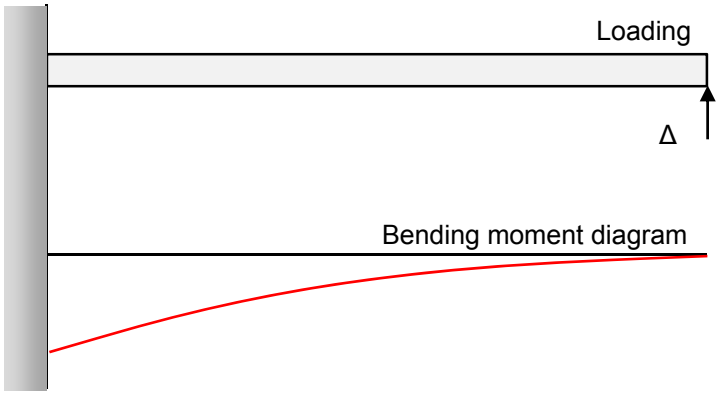

Figure 4. 52: Strain development in a cantilever beam

However, since tire loads are being applied, the zone of strain development is refrained within the loading area. Therefore, although in case of farm to market roads the tensile cracks are not load initiated, loading contributes to the location and propagation of the crack. The maximum strain and its value is a function of loading and swelling and can be defined by structural analysis of the pavement. Multiple analyses under various stress strain curves and edge swelling were performed; however, in all models, the zone of maximum strain was confined to the load application area, approximately 30cm from the edge. This phenomenon is in line with reports of area engineers in North Texas area.

Critical behavior of asphalt concrete is defined in tension. Therefore, the asphalt was loaded with different edge swelling, and the resulting maximum tensile strain was compared with critical tensile strain of the material. The resulting strains for different temperatures are shown in Figure 4. 53, Figure 4. 54 and Figure 4. 55.

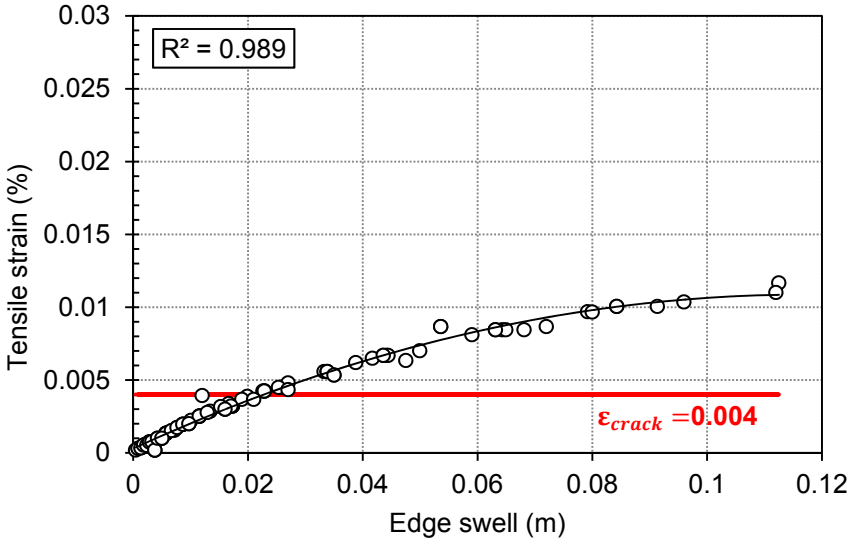

Figure 4. 53: Swell/strain T=5°C

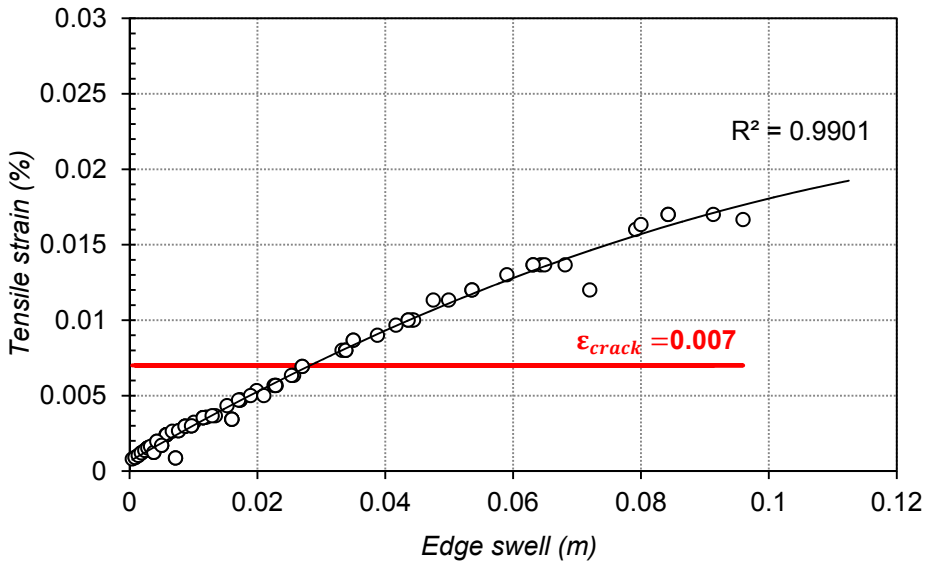

Figure 4. 54: Swell/strain T=25°C

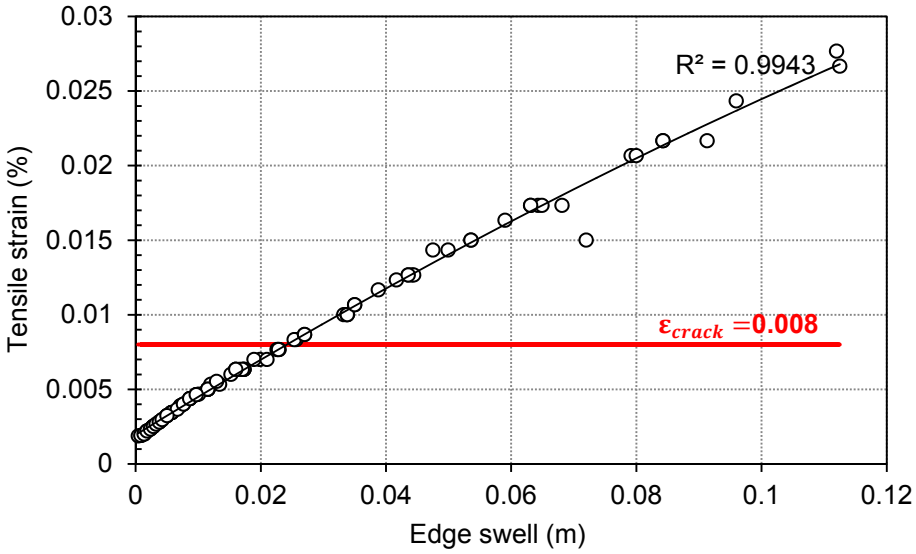

Figure 4. 55: Swell/strain T=40°C

As determined by the outputs of numerical analysis, the strain developed inside the pavement structure can be most properly expressed as a power function of the induced displacement. The function trends more toward a linear shape as the

temperature increases. The amounts of swelling which produce cracking strain are summarized in Table 4. 13.

Table 4. 13: Summary of the outputs

	ε_{crack}	edge swell (cm)	equivalent rain (cm)	return period (Yr.)
T= 5°C	0.004	2.26	5	< 2
T= 25°C	0.007	2.6	5.2	< 2
T= 40°C	0.008	2.4	5.1	< 2

It was observed that although the material became softer with an increase of temperature, the amount of swelling, which caused ultimate cracking of the structure, was approximately constant. This observation was attributed to increased elasticity of the material, as it is capable of bearing more strain before cracking begins.

It can also be observed that, with respect to current stress strain behavior, the asphalt will most probably begin to crack within two years of construction, which is compatible with current observations of area engineers in North Texas. Therefore, increasing the cracking threshold of the asphalt concrete or strengthening the pavement in the critical zone can improve the performance significantly.

Chapter 5

Conclusions and Recommendations

Volumetric deformations of expansive subgrade soils induce major construction and maintenance challenges on structures and in particular, pavements. The stresses within the pavement structure cause many surficial distresses including cracking, roughness and uneven profile. Due to light weight and low structural stiffness, farm to market roads are more prone to destruction caused by expansive subgrades. The distresses can be better controlled or maintained through an accurate understanding of volume change, subgrade moisture variation and stress distribution inside the pavement structure.

The overall objective of this research was to study the real time effect of environmental loading on pavement performance. To conduct such a research, the in-situ variation of the subgrade moisture content and temperature, as a result of environmental loading was studied, monitored and modeled. The vertical movement of the pavement was observed and the distresses on a test pavement section were controlled. The moisture and temperature variations were analyzed in Matlab and a trend to capture both seasonal and temporary variations was proposed. The deformation of the pavement as a result of environmental loading was modeled and numerical analysis was used to quantify effects of moisture infiltration on pavement cracking. The modeling was performed at several temperatures that usually occur in Texas and critical rainfall to initiate crack was determined.

In this chapter the conclusions of the conducted activities are summarized and recommendations for future studies are made.

5.1. Summary of Conclusions

Based on the current study, main results and conclusions can be summarized as below:

5.1.1. Moisture Variation

1. Survival rate of moisture sensors in the field can be determined as 70% and needs to be considered for instrumentation planning and design.
2. Results obtained from field instrumentation indicate that variations of moisture content were different at different depths. Shallower sensors showed responses in form of peaks, which temporarily increased the moisture content of the soil by 10-20%. Average moisture content recorded by the sensors varied between 0.25-0.38 m^3/m^3.
3. Moisture variations recorded by deep sensors were largely dominated by presence of groundwater table and were maintained at an approximate constant value of 0.4 to 0.5 m^3/m^3.
4. Depth of active zone based on moisture variation was extended to 4.5m, as traces of moisture variation were still observed in sensors located at this depth. However, based on swelling tests, the swell pressure was measured as 70 kPa, which is approximately equal to 4m of in-situ soil.
5. Definition of active zone, as a sole function of moisture variation or swell pressure is inaccurate. It was concluded that true definition should be depth limited by moisture variation or the swell pressure of the soil, whichever is smaller.
6. The overall trend of moisture variation could be explained as a combination of seasonal variations and temporary increase in moisture content. The seasonal trend peaks in wet season, where intense consecutive rainfall

events prevent dissipation of moisture. The lowest peaks happen toward the end of the dry season.

7. Existence of an asphalt cover did not prevent moisture from infiltrating the system. The reason was determined to be presence of cracks and fissures on the surface, which acted as a conduit for moisture infiltration.

5.1.2. Temperature Variation

1. Survival rate of temperature sensors was more than 90%, which showed a good and durable trend for future instrumentations.
2. Perfect seasonal temperature variations were observed in all sensors; however, the amplitude of variation and the peak time depended on the depth at which the sensor was installed.
3. The sensors closer to ground surface showed faster response to ambient temperatures and were accompanied by larger amplitude. Traces of cyclic daily variations were observed in shallow sensors.
4. The deeper sensors had smaller amplitude, while increasingly lagging behind the annual ambient cycle. A trace of daily variations had already been dissipated due to thermal inertia of the soil.
5. Average temperature of soil at all depths stayed close to average ambient temperature (24°C) and did not show any variation with depth.
6. Amplitude of temperature variation dramatically decreased with depth and varied between 10°C at 1m depth to less than 5°C at 4.5m depth.
7. Lag time increased through the depth of the soil, from 45 days close-to-surface to approximately 150 days at deeper layers.

5.1.3. Vertical Deformation

1. The surveying activity was performed every month to record the vertical deformation of the pavement with respect to the initial survey baseline.
2. Maximum and minimum recorded values under the cracked shoulder were between -3.3 and +12cm, while the uncracked shoulder primarily experienced variations in the shrinkage side of the volume change curve (between -9.75 and -2cm). The deformation at the centerline of the pavement varied between -5.3 and +6.05 cm.
3. The PVR values for the site were determined as +8 for the centerline and +6.1 for the edge. The difference and greater value of PVR_{CL} with respect to PVR_{edge}, is credited to smaller water content under the centerline.
4. Comparison of survey values with PVR showed that the PVR values are not accurate indications of pavement swelling, nor does it predict shrinkage as well. Consequently, it incorporates inaccuracy especially in case of pavement design.
5. A main seasonal trend was observed in the vertical deformation of the pavement. Additional movements were detected that caused swelling or shrinkage, which were functions of climatic loading.

5.1.4. Non Parametric Analysis

1. Non-parametric analysis in Matlab proved to be an adequate tool to use in analyzing unpredictable field variations.
2. The analysis method was capable of detecting both seasonal and temporary variations of moisture with acceptable accuracy. The model was developed based on recordings of four sensors and validated against two other ones.

Accuracy of the predicted model was R^2=0.5, which advances current predictive methods considerably.

3. The determined model was most accurate and captured variations of temperature lag time and amplitude with depth. Nine sensors were used for model development and four were used for validation. Accuracy of the predicted model was R^2=0.98.
4. A model was also developed for deformation, which was a sinusoidal function with the addition of net moisture balance of the soil. Although the method showed good compatibility with site observations, another set of data were required for validation.

5.1.5. Coupled Analysis of Volume Change

1. SWCC compacted wet of optimum is not strongly dependent on the applied normal stress.
2. Volume change of samples with suction happen along the same slope during initial, primary and secondary shrinkage. The difference between the curves happened due to decrease of initial void ratio under load application rather than suction variation.
3. Coupled analyses of stress and suction variations were capable of tracing volume changes in both shrinkage and swelling and provided continuous measurements of void ratio in response to changes of either normal stress or suction.
4. Prediction of soil volume change in swelling and shrinkage provided close numbers to values recorded at the field. In swelling, predicted and measured values were 10 and 12 cm, while in shrinkage the values were 8 and 9.75, respectively.

5.1.6. Numerical Modeling

1. Results of numerical modeling in Abaqus provided acceptable results in both moisture variation and volume change. In moisture variation analysis, the analysis results showed convergence of approximately 95%. In volumetric deformation analysis, the model output successfully predicted the volumetric strain with load application.
2. According to the volume change analysis, the course of swelling in pavements happens in the initial and partly primary stages. This indicates that the swelling path is not fully completed. Therefore, assuming full swelling in design and analysis may be conservative.
3. Overall swelling strain was measured as 3.5%, which is compatible with observations over the active zone (12cm/400cm of active zone).
4. Based on stress strain analysis, swelling of approximately 2cm causes strains large enough to initiate crack within the pavement structure. After that, due to reduction in pavement net area, propagation of crack happens at greater pace.
5. The 2cm swell can be caused by any combination of rainfall intensity and duration that produces 5cm of rainfall. This value falls within the 2-year return period of rainfall. This indicates that with current structural performance of the pavement, cracks are most likely to occur within the first two years of construction.
6. Temperature was not found to be an important factor in determining the critical swelling/rainfall for design. Due to increased elasticity, the pavement endures greater strain before crack initiation; however, it is neutralized by increased cracking strain of the pavement.

5.2. Recommendations for Future Work

1. The proposed models have been verified for the performance of the monitored site and provide more accurate results than previously obtained. However, it is recommended that the theories be tested in additional fields for further validation.
2. Elevation monitoring and smaller intervals provide more data points for volume change analysis.
3. For model development, it is recommended that various mix properties of asphalt concrete and evaluate efficiency of stronger mix design properties be considered. Modeling of rigid and flexible pavements would be extremely useful.
4. It is recommended to model enhanced and stabilized subgrade materials to determine the efficiency of current performed technics.
5. Pavement section optimization can be performed to determine the most acceptable pavement section for farm to market roads.
6. Performance of various types of highways, including state and interstate highways on expansive soil would provide valuable information regarding enhanced design of roadways on problematic soils.

Appendix I

Borehole log: FM2757

LOGO UT Arlington

BORING NUMBER BH1

CLIENT Texas Department of Transportation
PROJECT NUMBER
DATE STARTED 4/19/12 COMPLETED
DRILLING CONTRACTOR Alpha TEsting
DRILLING METHOD
LOGGED BY M.H CHECKED BY
NOTES

PROJECT NAME
PROJECT LOCATION
GROUND ELEVATION 0 ft HOLE SIZE 4 inches
GROUND WATER LEVELS:
AT TIME OF DRILLING 14.00 ft / Elev -14.00 ft
AT END OF DRILLING —
AFTER DRILLING —

DEPTH (ft)	SAMPLE TYPE NUMBER	TESTS	U.S.C.S.	GRAPHIC LOG	MATERIAL DESCRIPTION
0			CH		FAT CLAY WITH GRAVEL, SANDY CLAY, (CH) 11 % gravel, 8 % sand, 80 % fines, light tannish gray
3.0					-3.0
					FAT CLAY, CLAYEY CLAY, (CH) 0 % gravel, 3 % sand, 97 % fines, dark blackish gray
5	SH BH1-4	PP = 2.75 tsf MC = 17% DD = 104 pcf	CH		
	GB BH1-5	MC = 19% LL = 61 PL = 22			
7.0					-7.0
	GB BH1-7	MC = 21% LL = 57 PL = 19			FAT CLAY, (CH) 0 % gravel, 2 % sand, 98 % fines, dark blackish gray
10			CH		
	GB BH1-12	MC = 26% LL = 59 PL = 21			
15	SH BH1-14	PP = 2.73 tsf MC = 20% DD = 101 pcf			
15.0					-15.0

LOGO UT Arlington

BORING NUMBER BH2

CLIENT Texas Department of Transportation
PROJECT NAME
PROJECT NUMBER
PROJECT LOCATION
DATE STARTED 4/19/12 COMPLETED
GROUND ELEVATION 0 ft HOLE SIZE 4 inches
DRILLING CONTRACTOR Alpha TEsting
GROUND WATER LEVELS:
DRILLING METHOD
AT TIME OF DRILLING —
LOGGED BY M.H CHECKED BY
AT END OF DRILLING —
NOTES
AFTER DRILLING —

DEPTH (ft)	SAMPLE TYPE NUMBER	TESTS	U.S.C.S.	GRAPHIC LOG	MATERIAL DESCRIPTION
0					FAT CLAY, SILTY CLAY, (CH) 4 % sand, 96 % fines
5	SH	PP = 2.5 tsf MC = 21% DD = 94 pcf	CH		
	GB	MC = 25% LL = 52 PL = 20			
10				10.0	-10.0
	GB	MC = 28% LL = 64 PL = 22			Bottom of borehole at 10.0 feet.

LOGO UT Arlington

BORING NUMBER BH3

CLIENT Texas Department of Transportation
PROJECT NUMBER
DATE STARTED 4/19/12 COMPLETED
DRILLING CONTRACTOR Alpha TEsting
DRILLING METHOD
LOGGED BY M.H CHECKED BY
NOTES

PROJECT NAME
PROJECT LOCATION
GROUND ELEVATION 0 ft HOLE SIZE 4 Inches
GROUND WATER LEVELS:
AT TIME OF DRILLING 14.50 ft / Elev -14.50 ft
AT END OF DRILLING —
AFTER DRILLING —

DEPTH (ft)	SAMPLE TYPE NUMBER	TESTS	U.S.C.S.	GRAPHIC LOG	MATERIAL DESCRIPTION
0			CH		FAT CLAY, (CH) 4 % sand, 96 % fines
5	SH	PP = 2.6 tsf MC = 22% DD = 100 pcf			
	GB	MC = 23% LL = 65 PL = 19			
10	GB	MC = 24% LL = 57 PL = 23			
15				15.0	-15.0
	GB	MC = 22% LL = 56 PL = 22			Bottom of borehole at 15.0 feet.

LOGO UT Arlington

BORING NUMBER BH4

CLIENT Texas Department of Transportation
PROJECT NAME
PROJECT NUMBER
PROJECT LOCATION
DATE STARTED 4/19/12 COMPLETED
GROUND ELEVATION 0 ft HOLE SIZE 4 Inches
DRILLING CONTRACTOR Alpha TEsting
GROUND WATER LEVELS:
DRILLING METHOD
AT TIME OF DRILLING —
LOGGED BY M.H CHECKED BY
AT END OF DRILLING —
NOTES
AFTER DRILLING —

DEPTH (ft)	SAMPLE TYPE NUMBER	TESTS	U.S.C.S.	GRAPHIC LOG	MATERIAL DESCRIPTION
0			CH		FAT CLAY, (CH) 6 % sand, 94 % fines
5	SH	PP = 2.57 tsf MC = 26% DD = 91 pcf			
	GB	MC = 21% LL = 60 PL = 22			
10	SH	MC = 27% DD = 92 pcf			
	GB	MC = 20% LL = 59 PL = 19			
15	SH	MC = 27% DD = 88 pcf			
	GB	MC = 24% LL = 51 PL = 20			15.0 -15.0 Bottom of borehole at 15.0 feet.

References

AASHTO. *Guide for Mechanistic Empirical Design of New and Rehabilitated Pavement Structures.* Washington, D.C.: NCHRP Project 1-37A,Transportation Research Board of the National Academies, 2004.

Abed, A. "Numerical simulation of a trial wall on expansive soil in Sudan." *Plaxis Bulletin*, 2007: 21, 14-18.

Adem, H H, and S K Vanapalli. "Constitutive modeling approach for estimating 1-D heave with respect to time for expansive soils." *International Journal of Geotechnical Engineering*, 2013: 7(2), 199-204.

Aitchison, G D, and B G Richards. "A Broad-Scale Study of Moisture Conditions in Pavement Subgrades Throughout Australia: The Selection of Design Values for Soil Suction Equilibria and Soil Suction Changes in Pavement Subgrades. ." In *In Moisture Equilibria and Moisture Changes in Soils Beneath Covered Areas: A Symposium in Print*, by G D Aitchison, 226–232. Butterworths, Sydney, Australia, 1965.

Aitchison, GD. "The quantitative description of the stress-deformation behavior of expansive soils-preface to set of papers." *3rd International Conference on Expansive Soils.* 1973. 2, 79 – 82.

Akbulut, H., and K. Aslantas. "Finite element analysis of stress distribution on bituminous pavement and failure mechanism." *Materials & design*, 2005: 26(4), 383-387.

Ali, HA, and A Lopez. "Statistical analyses of temperature and moisture effects on pavement structural properties based on seasonal monitoring data." *Journal of the Transportation Research Board*, 1996: 1540(1), 48-55.

Alonso, E. E., J. Vaunat, and A. Gens. "Modelling the mechanical behaviour of expansive clays." *Engineering geology*, 1999: 54(1), 173-183.

Ambassa, Z, F Allou, C Petit, and R M Eko. "Top-down and bottom-up fatigue cracking of bituminous pavements subjected to tangential moving load." *7th RILEM international conference on cracking in pavements.* Delft, Netherlands: Springer, 2012. 675-685.

Aouad, M F, K H Stoke, and J M R Vinuesa. *Evaluation of flexible pavements and subgrades using the spectral-analysis-of-surface-waves (SASW) method.* Austin, TX: Center for Transportation Research, Bureau of Engineering Research, University of Texas at Austin, 1993.

ASTM. *Standard test method for one-dimensional swell or collapse of cohesive soils (ASTM D4546).* American Society of Testing and Materials, 2008.

Aubeny, C, and R Lytton. *Long-term strength of compacted high-PI clays .* No. FHWA/TX-03/2100-1, FHWA, 2003.

Basma, A A, and T I Al-Suleiman. "Climatic Consideration in New AASHTO Flexible Pavement Design." *Journal of Transportation Engineering*, 1991: 117 (2), 210-223.

Bayomy, F., and H. Salem. *Monitoring and Modeling Subgrade Soil Moisture for Pavement Design and Rehabilitation in Idaho Phase III: Data Collection and Analysis.* Boise, ID: Idaho Transportation Department, 2004.

Briaud, J. L., X. Zhang, and S. Moon. "Shrink test-water content method for shrink and swell predictions." *Journal of geotechnical and geoenvironmental engineering*, 2003: 129(7), 590-600.

Brooks, RJ, and AT Corey. "Hydraulic properties of porous media." *Journal of Hydrology*, 1964.

Buhler, R.L., and A.B. Cerato. *Stabilization of Oklahoma expansive soils using lime and Class C fly ash.* 162, 1-10: ASCE Geotechnical Special Publication, 2007.

Burmister, DM. "The theory of stresses and displacements in layered systems and applications to the design of airport runways." *Highway research board annual meeting.* Washington, DC, 1943. (23), 126–144.

Chao, K C, D D Overton, and J D Nelson. "The effects of site conditions on the predicted time rate of heave." *Unsaturated Soils .* ASCE, 2006 . pp. 2086-2097.

Chao, KC. *Design principles for foundations on expansive soils.* Fort Collins, CO: PhD dissertation, Colorado State University, 2007.

Chen, Fu Hua. *Foundations on Expansive Soils.* Amsterdam: Elsevier, 2012.

Cobos, D R, and C Chambers. *Calibrating ECH2O Soil Moisture Sensors .* Pullman, WA : Decagon Devices, 2010.

Dafalla, M A, and M A Shamrani. "Road Damage Due to Expansive Soils : Survey of the Phenomenon and Measures for Improvement." *GeoHunan International Conference .* Hunan, China: TRB, 2011. 73-80.

Dakshanamuthy, V. "A new method to predict swelling using a hyperbolic equation." *Geotechnical Engineering*, 1978: 79-87.

Das, SK, P Samui, AK Sabat, and TG Sitharam. "Prediction of swelling pressure of soil using artificial intelligence techniques." *Environmental Earth Sciences*, 2010: 61(2), 393-403.

Dhowian, AW. "Field performance of expansive shale formation." *Journal of King Abdulaziz University (Engineering Sciences)*, 1990: 2, 165–82.

Driscoll, R, and M Crilly. *Subsidence damage to domestic buildings. Lessons learned and questions asked.* London, UK: Building Research Establishment, 2000.

Estakhri, Cindy K, and Shiva Ramakrishnan. *Guidelines for the use of underseals as a pavement moisture barrier.* College Station: TTI Texas A&M, 2006.

Fityus, S, and DW Smith. "A simple model for the prediction of free surface movements in swelling clay profiles." *2nd International Conference on Unsaturated Soils.* Beijing, China: ASCE, 1998. 473-478.

Fleureau, J. M., S. Kheirbek-Saoud, R. Soemitro, and S. Taibi. "Behavior of clayey soils on drying-wetting paths." *Canadian Geotechnical Journal*, 1993: 30(2), 287-296.

Florides, G, and S Kalogirou. "Measurements of ground temperature at various depths." *3rd International Conference on Sustainable Energy Technologies.* Nottingham, UK, 2004.

Fredlund, D G, and S L Houston. "Interpretation of soil-water characteristic curves when volume change occurs as soil suction is changed." In *Advances in Unsaturated Soils*, by B Caicedo, C Murillo, L Hoyos, J E Colmenares and I R Berdugo, 15-31. London, UK: Taylor and Francis, 2013.

Fredlund, D G, H Rahardjo, and M D Fredlund. *Unsaturated soil mechanics in engineering practice.* Hoboken, NJ: John Wiley & Sons, 2012.

Fredlund, D. G., H. Rahardjo, and M. D. Fredulund. *Unsaturated soil mechanics in engineering practice.* Hoboken, NJ: John Wiley & Sons, 2012.

Fredlund, DG. "Prediction of ground movements in swelling clays." *31st Annual Soil Mechanics and Found Engineering Conference.* Minneapolis, MN: University of Minnesota, 1983.

Fredlund, DG, and A Xing. "Equations for the soil-water characteristic curve." *Canadian Geotechnical Journal*, 1994: 31(4), 521-532.

Fredlund, DG, and NR Morgenstern. "Stress state variables for unsaturated soils." *Journal of Geotechnical and Geoenvironmental Engineering*, 1977: 447-466.

Fredlund, M.D., J.R. Stianson, D.G. Fredlund, H. Vu, and R.C. Thode. "Numerical Modeling of Slab-On-Grade Foundations." *Unsaturated soils.* Carefree, AZ: ASCE, 2006. 2121-2132.

Fredlund, MD, DG Fredlund, and GW Wilson. "Estimation of volume change functions for unsaturated soils." *UNSAT-ASIA.* Singapore, 2000. 18-19.

Fredlund, MD, GW Wilson, and DG Fredlund. "Representation and estimation of the shrinkage curve." *3rd Int. Conf. on Unsaturated Soils.* 2002. 145-149.

Freeman, TJ, and DN Little. *Maintenance Strategies for Pavements with Chemically Stabilized Layers.* FHWA/TX-01/1722-6, College station, Tx: Texas Transportation Institute, Texas A & M University, 2002.

Gardner, WR. "Some steady-state solutions of the unsaturated moisture flow equation with application to evaporation from a water table." *Soil science*, 1958: 85(4), 228-232.

Gay, D.A. *Development of a predictive model for pavement roughness on expansive clay.* College Station, Texas: Doctoral Dissertation, Texas A&M University, 1994.

Gibson, N. H., C. W. Schwartz, R. A. Schapery, and M. W. Witczak. "Viscoelastic, viscoplastic, and damage modeling of asphalt concrete in unconfined compression." *Journal of the Transportation Research Board*, 2003: 1860(1), 3-15.

Hamberg, DJ, and JD Nelson. "Prediction of floor slab heave." *5th International Conference on Expansive Soils.* Adelaide, South Australia, 1984. 137-140.

Harris, P. *Evaluation of Stabilization of Sulfate Soils in Texas.* FHWA/TX-08/5-4240-01-1, College station, TX: Texas Transportation Institute, Texas A & M University, 2008.

Hasenmueller, E A, and R E Criss. "Water Balance Estimates of Evapotranspiration Rates in Areas with Varying Land Use." In *Evapotranspiration - An Overview*, by S G Alexandris, 1-22. InTech, 2013.

Hearn, G J, T Hunt, J Aubert, and J Howell. "Landslide impacts on the road network of Lao PDR and the feasibility of implementing a slope management programme." *International conference on management of landslide hazard in the Asia.* 2008.

Heath, W, B S Saros, and J W F Dowling. *Highway Slope Problems in Indonesia.* London, Uk: Transport & Road Research Laboratory, 1990.

Hedayati, M, M Hossain, A Mehdibeigi, and B Thian. "Real-Time Modeling of Moisture Distribution in Subgrade Soil." *Geo-Congress 2014 Technical Papers.* Atlanta, GA: ASCE, 2014. 3015-3024.

Hensen, Emiel J.M., and Brend Smit. "Why Clays Swell." *Journal of Physical Chemistry B*, 2002: 12664-12667.

Holland, JE, and DA Cameron. "Seasonal Heave of Clay Soils." *Civil Engineering Transactions*, 1981: 55-67.

Hossain, J. *Geohazard Potential of Rainfall Induced Slope Failure on Expansive Clay.* Arlington, Tx: Doctoral Thesis, University of Texas at Arlington, 2013.

Houston, S. L., H. B. Dye, C. E. Zapata, K. D. Walsh, and W. N. Houston. "Study of expansive soils and residential foundations on expansive soils in Arizona." *Journal of performance of constructed facilities,*, 2011: 25 (1), 31- 44.

Huang, S, DG Fredlund, and SL Barbour. "“Measurement of the coefficient of permeability for a deformable unsaturated soil using a triaxial permeameter." *Canadian Geotechnical Journal*, 1998: 35:426-432.

Huang, YH. *Pavement Analysis and Design.* NewJersey: Prentice-Hall, 1993.

Hung, V. Q., D. G. Fredlund, and J. Pereira. "Coupled solution for the prediction of volume change in expansive soils." *Third international conference on unsaturated soils.* Recife, Brazil: ASCE, 2002. pp. 181-186.

Hussein, EA. "Viscoplastic Finite Element Model for Expansive Soils." *EJGE*, 2001: Paper#2001-0122.

Intharasombat, N, AJ Puppala, and R Williammee. "Compost amended soil treatment for mitigating highway shoulder desiccation cracks." *Journal of Infrastructure Systems*, 2007: 13(4), 287-298.

Jayatilaka, R. *A model to predict expansive clay roughness in pavements with vertical moisture barriers.* College station, Texas: Doctoral Dissertation, Texas A&M University, 1999.

Jones, L. D., and I. Jefferson. "Expansive soils." In *CE Manual of Geotechnical Engineering Volume 1: Geotechnical Engineering Principles, Problematic Soils and Site Investigation*, 413-441. 2012.

Kandhal, PS, and RB Mallick. "Longitudinal joint construction techniques for asphalt pavements." *Eighth International Conference on Asphalt Pavements.* 1997. (1), 363-379.

Kim, H., and W. G. Buttlar. "Discrete fracture modeling of asphalt concrete." *International Journal of Solids and Structures*, 2009a: 46(13), 2593-2604.

Kodikara, J, P Rajeev, D C C Chan, and C Gallage. "Soil Moisture Monitoring at the Field Scale Using Neutron Probe." *Canadian Geotechnical Journal*, 2014: 51, 332–345.

Kuo, C, and C Huang. "Three-dimensional pavement analysis with nonlinear subgrade materials." *Journal of Materials in Civil Engineering*, 2006: 18(4), 537-544.

Kutilek, M. "Some theoretical and practical aspects of infiltration in clays with D-constant." *In Proc. ISSS Symp. on Water and Solute Movement in Heavy Clay Soils.* 1984. (37), 114-128.

Lloret, A, MV Villar, M Sanchez, A Gens, X Pintado, and EE Alonso. "Mechanical behaviour of heavily compacted bentonite under high suction changes." *Géotechnique*, 2003: 53(1), 27-40.

Lu, Y., and P. J. Wright. "Numerical approach of visco-elastoplastic analysis for asphalt mixtures." *Computers & structures*, 1998: 69(2), 139-147.

Luo, R, and JA Prozzi. "Development of Longitudinal Cracks on Pavement over Shrinking Expansive Subgrade." *Road Materials and Pavement Design*, 2010: 11(4), 807-832.

Lytton, R. L. *The Characterization of Expansive Soils in Engineering.* American Geophysical Union, San Francisco, California: Presentation at the Symposium on Water Movement and Equilibria in Swelling Soils, 1977.

Lytton, R., C. Aubeny, and R. Bulut. *Design procedure for pavements on expansive soils.* Austin, TX: Texas Department of Transportation, 2005.

Machan, G, and V G Bennett. *Use of inclinometers for geotechnical instrumentation on transportation projects: State of the practice.* Washington, DC: ransportation Research E-Circular (E-C129), 2008.

Manosuthikij, T. *Studies on volume change movements in high PI clays for better design of low volume pavements.* Arlington, TX: University of Texas at Arlington, 2008.

Manosuthkij, T, AJ Puppala, S Nazarian, and Y Wanyan. "Comparisons between Measured and Predicted Swell Strains Using PVR and Suction Based Models." *Problematic soils and rocks and in situ characterization.* Denver, CO: ASCE, 2007. 1-11.

Marks, BD, and TA Haliburton. "Subgrade Moisture Variations Studied with Nuclear Depth Gages." *Highway Research Record*, 1969: 276,14-24.

McDowell, C. "Interrelationship of load, volume change, and layer thickness of soils to the behavior of engineering structures." *Highway Research Board.* 1956. No. 35, 754-772.

Mulungye, R. M., P. M. O. Owende, and K. Mellon. "Finite element modelling of flexible pavements on soft soil subgrades." *Materials & design*, 2007: 28(3), 739-756.

Nayak, NV, and RW Christensen. "Swell characteristics of compacted expansive soils." *Clay and Clay Minerals*, 1971: 19(4), 251–261.

Nelson, J D, D K Reichler, and J M Cumbers. "Parameters for heave prediction by oedometer tests." *4th International Conference on Unsaturated Soils.* Carefree, Arizona, 2006.

Nelson, J. D., and D. J. Miller. *Expansive soils, problems and practices in foundation and pavement engineering.* New York: Wiley, 1992.

Nelson, J.D., D.D. Overton, and K. Chao. "An Empirical Method for Predicting Foundation Heave Rate in Expansive Soil." *GeoShanghai 2010 International Conference.* Shanghai: ASCE, 2010. 190-196.

Nelson, JD, D D Overton, and DB Durkee. "Depth of wetting and the active zone." *Geotechnical special publication*, 2001: 95-109.

Nguyen, Q., D. G. Fredlund, L. Samarasekera, and B. L. Marjerison. "Seasonal pattern of matric suctions in highway subgrades." *Canadian Geotechnical Journal*, 2010: 47(3), 267-280.

Oh, J H, et al. *Pavement Repair Strategies for Selected Distresses in FM Roadways.* San Antonio : No. FHWA/TX-11/0-6589-1, The University of Texas at San Antonio , 2012.

Osman, M A, and A M.E Sharief. "Field and laboratory observations of expansive soil heave." *6th International Conference of Expansive Soils.* New Delhi, India, 1987.

Park, SW, Y Richard Kim, and RA Schapery. "A viscoelastic continuum damage model and its application to uniaxial behavior of asphalt concrete." *Mechanics of Materials*, 1996: 24(4), 241-255.

Petry, T M, and D N Little. "Review of stabilization of clays and expansive soils in pavements and lightly loaded structures-history, practice, and future. ." *Journal of Materials in Civil Engineering*, 2002: 14(6), 447-460.

Pham, H. Q. *Volume-mass constitutive relations for unsaturated soils.* Saskatoon, Canada: Doctoral dissertation, Unversity of Saskatchewan, 2005.

Puppala, A J, T Manosuthkij, S Nazarian, L Hoyos, and B Chittoori. "In Situ Matric Suction and Moisture Content Measurements in Expansive Clay during Seasonal Fluctuations., ." *Geotechnical Testing Journal*, 2012: 35(1), 1-9.

Puppala, A. J., T. Manosuthikij, and B. Chittoori. "Swell and shrinkage strain prediction models for expansive clay." *Engineering Geology*, 2014: 168, 1-8.

Puppala, A. J., T. Manosuthkij, S. Nazarian, and L. R. Hoyos. "Threshold moisture content and matric suction potentials in expansive clays prior to initiation of cracking in pavements." *Canadian Geotechnical Journal*, 2011: 48, 519–531.

Rada, GR, SP Engineer, DR Smith, and MW Witczak. "Structural design of interlocking concrete pavements." *Transportation association of Canada conference.* 1991.

Ramadhan, R H, and H I Al-Abdul Wahhab. "Temperature variation of flexible and rigid pavements in Eastern Saudi Arabia." *Building and environment*, 1997: 32(4), 367-373.

Rao, R. R., H. Rahardjo, and D. G. Fredlund. "Closed-form heave solutions for expansive soils." *Journal of Geotechnical Engineering*, 1988: 114 (5), 573- 588.

Rauhut, J B, A Eltahan, and A L Simpson. *Common characteristics of good and poorly performing AC pavements.* FHWA, Report number FHWA-RD-99-193, 1999.

Richards, B G. "An Analysis of Subgrade Conditions at the Horsham Experiment Road Site Using the Two-Dimensional Diffusion Equation on a High-Speed Digital Computer." In *Moisture Equilibria and Moisture Changes in Soils Beneath Covered Areas: A Symposium in Print (*, by G D Aitchison, 243–258. Butterworths, Sydney, Australia, 1965.

Schwartz, CW, and RL Carvalho. "Distribution of permanent deformations within HMA layers." *Airfield & Highway Pavements Conference.* ASCE, 2008. 86-98.

Scullion, T, S Sebesta, and J Harris. *Identifying the benefits of nonstandard stabilizers in high sulfate clay soils.* A status report: Research Rep. No. 408330, 1, College station, Tx: Texas Transportation Institute, 2001.

Sebesta, S. *Investigaation of maintenace base repairs over expansive soils:year 1 report.* Austin, Tx: Texas Department of Transportation, 2002.

Snethen, DR. *An evaluation of methodology for prediction and minimization of detrimental volume change of expansive soils in highway subgrades.* volume ii (no. Fhwa-rd-79-50 final rpt), 1979.

Sou, Z. *Evaluation of asphalt concrete pavement service life using 3D nonlinear finite element analysis and nonlinear fatigue damage model.* Hong Kong: Doctoral Dissertation, The Hong Kong Polytechnic University, 2012.

Sridharan, A, and Y Gurtug. "Swelling behaviour of compacted fine-grained soils." *Engineering geology*, 2004: 72(1), 9-18.

Talluri, N., V. Puljan, T. Manosuthikij, A. J. Puppala, and S. Saride. "Prediction of Swell-Shrink Movements of Pavement Infrastructure." *Geo-Frontiers Congress.* Dallas: ASCE, 2011. 2740-2749.

Tripathy, S, K S Rao, and D G Fredlund. "Water content-void ratio swell-shrink paths of compacted expansive soils." *Canadian geotechnical journal*, 2002: 39(4), 938-959.

TxDOT. *Test Procedure for determination of potential vertical rise.* Austin: TxDOT, 1999.

Van Genuchten, MT. "A closed-form equation for predicting the hydraulic conductivity of unsaturated soils." *Soil Science Society of America Journal*, 1980: 44(5), 892-898.

Vanapalli, S, and L Lu. "A state-of-the art review of 1-D heave prediction methods for expansive soils." *International Journal of Geotechnical Engineering*, 2012: 6(1), 15-41.

Walsh, Kenneth D, Craig A Colby, William N Houston, and Sandra L Houston. "Method for Evaluation of Depth of Wetting in Residential Areas." *ASCE Journal of Geotechnical and Geoenvironmental Engineering*, 2009: 135(2), 169–176.

Wang, B. R., Y. J. Hu, and X. Qiu. "SWCC based prediction model of equilibrium moisture of clay subgrade with high groundwater table." *Key Engineering Materials*, 2014: 579, 906-910.

Wang, M W, J Li, S Ge, and S T Li. "Moisture migration tests on unsaturated expansive clays in Hefei, China." *Applied Clay Science*, 2013: 79, 30-35.

Wanyan, Y., I. Abdallah, S. Nazarian, and A. J. Puppala. "Expert System for Design of Low-Volume Roads over Expansive Soils." *Transportation Research Record: Journal of the Transportation Research Board* 2154, no. 1 (2010): 81-90.

Weston, DJ. "Expansive roadbed, treatment for Southern Africa." *4th International Conference on Expansive Soils.* 1980. 1: 339-360.

Wolfe, W., T. Butalia, and J. Howdyshell. *Long Term Monitoring of Moisture Under Pavements.* Columbus, OH: Ohio Department of Transportation , 2010.

Yi, J, S Shen, B Muhunthan, and D Feng. "Viscoelastic–plastic damage model for porous asphalt mixtures: Application to uniaxial compression and freeze–thaw damage." *Mechanics of Materials*, 2014: 70, 67-75.

Young, R. *Soil properties and behaviour.* Elsevier, 2012.

Zapata, C. E., W. N. Houston, S. L. Houston, and K. Walsh. "Soil–Water Characteristic Curve Variability." *Advances in Unsaturated Geotechnics.* Denver: American Society of Civil Engineers, 2000. 84-124.

Zapata, C.E., and W.N. Houston. *Calibration and validation of enhanced integration climatic model for pavement design.* Washington, D.C.: Transportation Research Board, 2008.

Zhang, X. *Consolidation theories for saturated-unsaturated soils and numerical simulation of residential buildings on expansive soils.* College Station, TX: PhD dissertation, Texas A&M university, 2004.

Zhang, X, and J L Briaud. "Coupled water content method for shrink and swell predictions." *International Journal of Pavement Engineering*, 2010: 11(1), 13-23.

Zhang, X, and RL Lytton. "Modified state-surface approach to the study of unsaturated soil behavior. Part I: Basic concept." *Canadian Geotechnical Journal*, 2009: 46(5), 536-552.

Zheng, J., and R. Zhang. "Prediction and Application of Equilibrium Water Content of Expansive Soil Subgrade." *Second International Conference on Geotechnical and Earthquake Engineering.* Chengdu, China: ASCE, 2013. 754-761.

Zornberg, J G, and R Gupta. "Reinforcement of pavements over expansive clay subgrades." *17th International Conference on Soil Mechanics and Geotechnical Engineering.* Cairo, Egypt: ICSMGE , 2009. 765-768.

Zornberg, JG, J Kuhn, and S Wright. *Determination of Field Suction Values Hydraulic Properties and Shear Strength in High PI Clays.* Rep. 0-5202-1, Austin, Tx: Center for Transportation Research, University of Texas at Austin, 2007.

Biographical Information

Mahsa Hedayati was born in Rasht, Iran. She initiated her Bachelor's Degree in Civil Engineering in 2003 at Amirkabir University of Technology (Tehran Polytechnic). She pursued her education in GeoEnvironmental engineering at Tehran University and graduated with her Master of Science in 2010. Meanwhile, she gained more professional experience as a structural/geotechnical engineer while working in oil and gas industry at Sazeh® consultants, Tehran, Iran. In 2011, she was admitted to the civil engineering doctoral program at University of Texas at Arlington where she got the opportunity to work under supervision of Dr. Sahadat Hossain as a graduate research assistant. During her research, she has focused on unsaturated soil mechanics, expansive soil behavior, pavement distress development, real time data analysis and finite element numerical modeling. She has won multiple awards, including best technical paper at ASCE Texas fall conference (Dallas, September, 2013), GeoInstitute travel grant for GeoCongress 2014 (Atlanta, March 2014) and Dean of Engineering graduate fellowship (May 2014).